Bar-Ilan University

Quantum Effects in Superconducting Nano-Loops and Networks

OMRI J. SHARON

Department of Physics

Ph.D Thesis

Submitted to the Senate of Bar-Ilan University

Ramat-Gan, Israel   October 2018

This work was carried out under the supervision of

Prof. Yosef Yeshurun and Prof. Avner Shaulov

Department of Physics

Bar-Ilan University

Acknowledgments

I wish to thank **Prof. Yosef Yeshurun** and **Prof. Avner Shaulov**, for their great amount of patience, support, perspective and wisdom. As my advisors, they supported many of my ideas and let me execute them. They took off me most of the work I enjoy the least and managed to take beautiful unexplainable results and show them in a light of incredible discoveries. They made me see things in my data that I would normally miss. I must remind them that we still have plenty of unpublished, unexplained data that is waiting for their magic touch.

I deeply thank **Prof. Dr. Elke Scheer** for having me in her group for six months, I wish to thank her students **Julian Broun** and **Dr. Christopher Espy** whom I worked with and the rest of the people in Scheer's working group who made my research period in Germany so educative and enjoyable. I would also like to thank **Matthias Hagner** from the nano-lab in Konstanz University, who was very patience and nice and taught me handling the machines in the nano-lab. Matthias always smiled and spread joy to the people surrounding him while teaching and it was a pleasure to know him and work beside him.

I came to the superconductivity lab thanks to **Dr. Doron Barness** who was my **T.A.** in Shaulov's course. I think I mainly wanted to spend more time with Doron in the lab, yet he finished soon after I joined.

I would like to thank **Dr. Ilya Sochnikov** who was my mentor when I joined the lab. He taught me everything he knew and my entire doctorate period I tried to make things better than the best, better than Ilya. I continued the interesting research Ilya has started investigating and found great joy and satisfaction in this field.

In the more applied electronics and mechanical part, I wish to thank the two people who helped me and taught me the most important things I could learn in my doctorate. I thank **Eli Perel** for helping me, teaching me and filling many gaps in my electronics knowledge, I could not have enough gratitude to show my appreciation. I also thank **Dov Friedman**, from the mechanics workshop who helped me with everything I needed right away and especially taught me how to use some of the workshop equipment myself- which brought me real joy.

I truly thank **Dr. Amos Sharoni**, his group and especially his student **Naor Vardi**. Amos gave me so many good tips, insights and directions considering my research and projects I had in mind. Naor was as much as a technical advisor and helped with Keithley instruments, thin film sputtering, PPMS guidance and much more. I cannot thank Naor enough.

Table of Contents

Abstract

Understanding superconductivity on the nano-scale is of both fundamental interest and practical importance. The fundamental interest aims at understanding many novel phenomena manifested by nano-scale superconductors and not seen in the bulk. The practical importance stems from the potential of nano-superconducting structures to be used in innovative devices and systems including quantum computers. This work focuses on investigation of the quantum behavior of nano-size superconducting single loops and networks. It consists of four studies: (a) an experimental study of the current dependence of the magnetoresistance (MR) oscillations in a linear array of Nb nano-loops near the critical temperature, (b) an experimental study of the MR oscillations of Nb *single* nano-loops measured at high currents close to the depairing current, (c) a search for an experimental evidence for the theoretically predicted *hc/e* flux periodicity in nano size aluminum superconducting networks - a work done in collaboration with Scheer's group in Konstanz university, Germany, (d) a theoretical study of fluxoids configurations in finite superconducting networks. These studies revealed novel phenomena and insights in the behavior of superconducting nano-loops and networks.

Our first study demonstrated current-induced SQUID behavior of superconducting Nb nano-loops without Josephson junctions. MR measurements in such loops showed that as the bias current increases, the parabolic Little-Parks magnetoresistance oscillations become sinusoidal and eventually transform into oscillations typical for a SQUID. We associated this phenomenon with the flux-induced non-uniformity of the order parameter along a superconducting nano-ring, arising from the superconducting leads ('arms') attached to it. Current enhanced phase slip rates at the points with minimal order parameter create effective Josephson junctions in the ring, switching it into a SQUID.

In the second study, we measured single granular Nb nano-rings in an extended range of bias-currents. Our measurements revealed current-induced crossover between two distinct quantum coherence effects. At low bias currents, Cooper-pairs coherence is manifested by Little-Parks oscillations with flux periodicity of *hc/2e*. At high bias currents, magnetoresistance oscillations with flux period of *hc/e* are observed and

interpreted as Aharonov-Bohm oscillations, reflecting phase coherence of individual quasi-particles. We explained these data viewing the ring as a chain of superconducting grains weakly coupled by tunnel junctions. Low bias currents allow coherent tunneling of Cooper pairs between the grains. Increasing the current above the critical current of all the junctions creates a quasi-particles conduction channel along the ring, allowing for quantum interference of quasi-particles.

The *hc/2e* magnetic-flux periodicity observed in the magnetoresistance of superconducting rings has been considered as a hallmark for electronic pairing in superconductors, manifesting the existence of Cooper pairs. However, several theoretical works have shown that the existence of Cooper pairs does not necessarily imply an *hc/2e* periodicity. For example, an *hc/e* flux periodicity was predicted for s-wave nano-rings with size smaller than the coherence length, ξ_0. In an attempt to confirm this prediction experimentally, we combined efforts with Scheer's group from Konstanz University in fabrication and measurements of Al nano-networks. The choice of Al was based on its large ξ_0. In this third study, we participated in fabrication, measurements and interpretation of the data. An indication for a crossover to *hc/e* periodicity was observed in one sample in the waveform of the first period which was consistent with the theoretical prediction. Observation of more than one period was impeded by the relatively low value of the critical field in Al.

Fluxoid quantization effects have been previously studied extensively, both theoretically and experimentally, in a variety of superconducting networks. However, most of these studies focus on the phase boundary between the superconducting and the normal states, paying less attention to the fluxoids configuration in the networks as a function of the applied magnetic field. The limited number of studies considering fluxoids configurations present results of experimentally measured or theoretically calculated configurations in various networks, providing no intuitive understanding of the underlying physics. In our fourth study, we theoretically analyzed fluxoids configurations in superconducting finite networks using the "current squared" model (known as the "J^2 model"). Our analysis yielded an Ising like expression for the total energy of the network as a function of the loops vorticities and the applied magnetic field. This expression

provided an intuitive understanding of the mechanism governing the fluxoid configurations in finite networks. Specifically, it showed that fluxoids can be treated as repulsively interacting objects driven toward the network center by the applied field. Based on this analysis, we illustrated different configurations of fluxoids in different types of networks by simulations.

Our studies shed light on the different mechanisms underlying the various flux periodicities and fluxoid configurations in superconducting nano-loops and networks. Understanding the physics behind these phenomena may lead to the development of new concepts in the growing research area aiming at exploiting superconductors in nano-circuits.

1 Introduction

In this chapter, I explain briefly concepts that appear in the dissertation. In addition, I mention relevant previous studies and emphasize our contribution to the discussed subjects.

1.1 Fluxoid Quantization and Magnetoresistance Oscillations in Superconducting Loops

London introduced the concept of *fluxoid* [1] in multiply connected superconductors as the sum of the flux through a superconducting loop and the integral of the screening currents over the circumference of the loop:

$$\Phi' = \Phi + \frac{4\pi}{c} \oint_c \lambda^2 \vec{J_s}\, d\vec{l}$$
(1)

where Φ is the magnetic flux through the loop, c is the speed of light and λ is London's penetration depth. London's calculations showed that in a multiply connected superconductor, the fluxoid (and not the flux) is quantized:

$$\Phi' = n\Phi_0 = n\frac{hc}{2e}$$
(2)

where n is an integer, h is the Plank constant and $2e$ is the charge of a Cooper pair. Note: all the calculations in the Introduction chapter were done in CGS units. In several of our papers we used MKS units where $\Phi_0 = h/2e$ rather than $\Phi_0 = hc/2e$.

Measuring resistance in a superconducting state is usually possible only near the superconductor's critical temperature, current or field (T_c, I_c, H_c in type I superconductors, H_{c2} in type II superconductors) where the screening current density, J_s, is extremely small. In this limit, the flux through the loop approximately equals to the external magnetic flux and the supercurrent density in a superconducting loop with a radius r and circumference L may be derived from Equations (1) and (2)

$$J_s = \frac{c\Phi_0}{4\pi\lambda^2 L}\left(n - \frac{\Phi}{\Phi_0}\right) = \frac{c\Phi_0}{8\pi^2\lambda^2 r}\left(n - \frac{\Phi}{\Phi_0}\right)$$
(3)

The integer number, n, is called the winding number, and it counts the number of fluxoids trapped inside the loop. As is clear from Equation (3), the supercurrent density is linear with the flux, exhibiting a periodic behavior with a period Φ_0, as described in Figure 1(a). The periodic behavior is a consequence of the requirement for minimum energy described below.

Due to the induced supercurrent, the kinetic energy of the circulating Cooper pairs – which is proportional to the square of the supercurrent density – increases by

$$E_k = \frac{4\pi\lambda^2}{c^2}J_s^2 = \frac{\Phi_0^2}{4\pi\lambda^2 L^2}\left(n - \frac{\Phi}{\Phi_0}\right)^2 = \frac{\Phi_0^2}{16\pi^3\lambda^2 r^2}\left(n - \frac{\Phi}{\Phi_0}\right)^2. \tag{4}$$

Figure 1(b) exhibits the parabolic dependence of E on Φ predicted by Equation (4). The requirement for minimum energy determines the winding number n, as shown in Figure 1(c). This minimum energy is described by the solid red line in Figure 1(b).

Fluxoid quantization effects have been demonstrated in numerous experimental works. Most relevant to this dissertation are magnetoresistance experiments which showed oscillatory behavior with a period of Φ_0 in single loops [2-11], networks [12-15], arrays of Josephson junctions [16-18], and other complex structures [19, 20]. These magnetoresistance oscillations are usually associated with the Little-Parks effect discussed in Section 1.3 below. In the next Section 1.2 we discuss fluxoid quantization in coupled loops and point to one of the topics that compose the present dissertation.
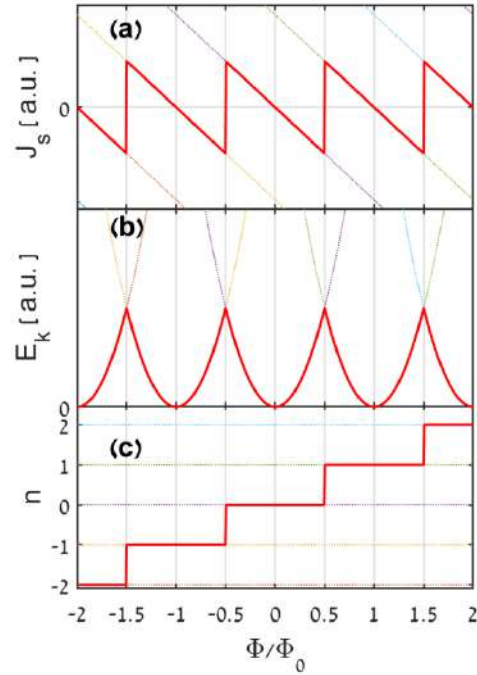
Figure 1. (a) Supercurrent density in a superconducting loop for different winding numbers. (b) Energy of a superconducting pairs corresponding to the square of the supercurrent density for different winding numbers is plotted as dotted lines. (c) Population of fluxons in a superconducting loop, as a function of magnetic flux piercing the loop, expressed in units of the flux quantum.

1.2 Fluxoid Quantization in Coupled Loops

Fluxoid quantization effects have been studied extensively, both theoretically and experimentally, in a variety of superconducting networks [7, 12, 13, 21-32]. However, most of these studies focus on the phase boundary between the superconducting and the normal states, paying less attention to the fluxoids configuration in the networks as a function of the applied magnetic field. The limited number of studies considering fluxoids configurations present results of experimentally measured or theoretically calculated configurations in various networks, providing no intuitive understanding of the underlying physics [13, 32-34]. In this dissertation (Chapters 3.1 and 3.2) we elucidated the mechanism governing the fluxoid configuration in finite superconducting networks as a function of the applied field.
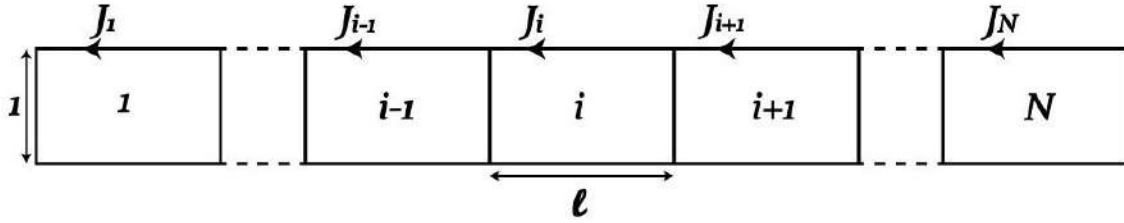
Figure 2. A superconducting ladder with N cells/loops, and sides' ratio of 1:l.

In Equation (1) we introduced the fluxoid in a single superconducting loop. When two loops have a common side, these loops are effectively coupled. In Chapter 33.1 we focused on a 1D finite network ('ladder') illustrated in Figure 2. Our analysis of such superconducting ladders yielded an Ising-like expression for the total energy of the ladders as a function of the loops vorticities and the applied magnetic field. This expression shows that fluxoids can be treated as repulsively interacting objects driven towards the ladder center by the applied field. A 'short range' and a 'long range' interactions give rise to remarkably different fluxoid configurations that are illustrated by simulations. Some of these configurations include the same number of fluxoids arranged in different positions, some of which are incommensurate to the ladder symmetry. These results are demonstrated in Figure 3. The figure describes the fluxoids arrangements as a function of field for ladders with 7, 8 and 9 loops. An empty loop is colored blue, and occupied loop is colored yellow or green. The green color indicates degenerated configurations which are incommensurate with the symmetry of the ladder. The ladders with 7 and 9 loops demonstrate the general rule that when the number of loops is odd, the first fluxoid always occupies the loop at the ladder's center. In ladders with an even number of loops, the first fluxoid occupies a degenerated state on either side of the center, as demonstrated by the ladder with 8 loops. As the field increases, a second fluxoid enters the ladder, pushing the first one out of its position and both fluxoids arrange themselves in an optimum configuration, keeping apart from each other and away from the network edges. In the ladder with 9 loops, this configuration conforms the symmetry of the ladder, however, this is not the case in the ladders with 7 and 8 elements. As more fluxoids enter the ladder with increasing field, rearrangement of fluxoids continues until the last fluxoid enters the ladder's center completing one period in which

each loop is occupied with one fluxoid. Occupation of the loops in the following periods follows the same pattern.

Figure 3. Fluxoid configuration as a function of magnetic flux in ladders with 7, 8 and 9 loops, in the first period. An empty loop is colored dark blue, and occupied loop is colored yellow or green. The green color indicates degenerated configurations which are incommensurate with the symmetry of the ladder.

The conclusions drawn from the analysis for 1D networks are also valid for 2D networks. Namely, fluxoids in 2D networks repel each other and are driven to the center by the applied field. This was demonstrated in Chapter 3.2 for small (3x3) networks, as shown here in Figure 4. The figure shows that the first fluxoid appears in the central loop of the network, as in a ladder. Note that the number of different configurations (11) exceeds the number of loops in the network, due to rearrangement of the same number of fluxoids as the field increases. This situation occurs in configurations of 3 and 6 fluxoids. Among the 11 different configurations, there are 6 degenerated states that are incommensurate to the network symmetry (marked in green in Figure 4).

This theoretical study gives a strong motivation for future experimental work. The fluxoid occupation in a ladder can be verified using, e.g., a scanning SQUID. Since the

scanning SQUID's measurements are very sensitive to magnetic field, it can measure the currents induced in the sides of the loops and detect the position of fluxoids in the ladder.
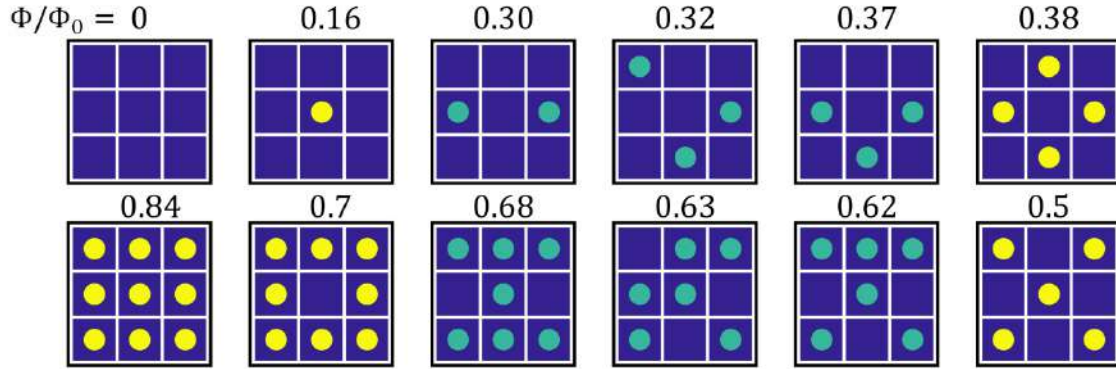
Figure 4. Fluxoid configurations in 3x3 square network calculated in the framework of the $'J^2$ model'. An empty loop is colored dark blue, and occupied loop is colored yellow or green. The green color indicates degenerated configurations which are incommensurate with the symmetry of the ladder.

1.3 The Little-Parks Effect

The additional energy, E_k, of the fluxoid's current defined in (4) suppresses the critical temperature, T_c, periodically. This effect was first observed experimentally by Little and Parks [35, 36]. They demonstrated that a thin-walled superconducting tin cylinder pierced by a magnetic flux shows magnetoresistance oscillations with a period equals to the superconducting flux quantum $\Phi_0 = hc/2e$ (see Figure 5(a)). Little and Parks associated the resistance oscillations $\Delta R(H)$ with periodic changes in ΔT_c (Figure 5(b)) in the superconducting transition temperature: $\Delta R = \Delta T_c \frac{dR}{dT}$. The amplitude of the oscillations, ΔT_c, scales with $\left(\frac{\xi_0}{r}\right)^2$, where ξ_0 is the zero-temperature coherence length, and r the radius of the cylinder.
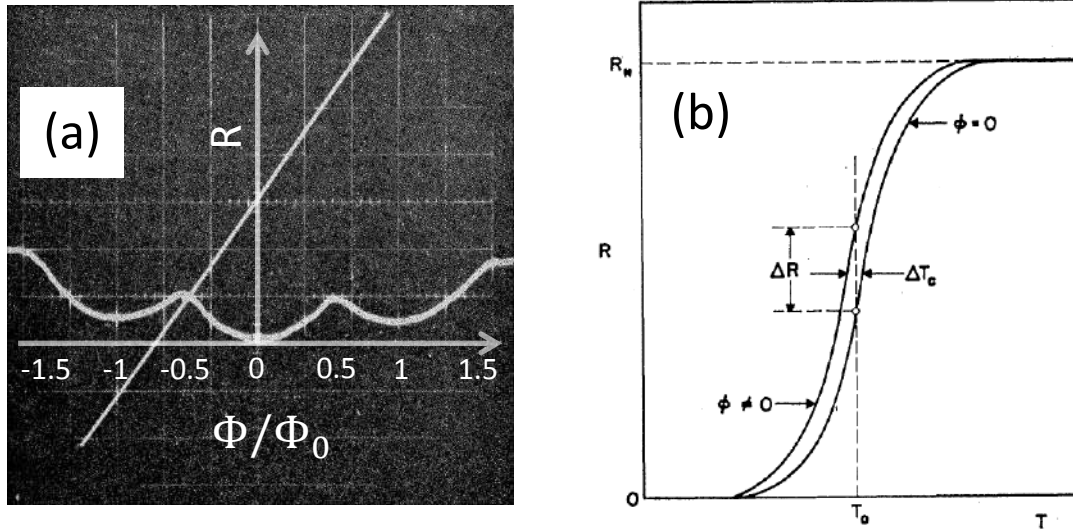
Figure 5. (a) Resistance of the tin cylinder as function of magnetic flux depicted from the original paper by Little and Parks [35] . (b) Schematic plot of resistance vs. temperature: interpretation of the change in T_c reflected as change in the resistance.

The Little-Parks magnetoresistance oscillations are usually demonstrated with relatively small bias currents. The bias current, I_b, contributes a constant term $\propto I_b^2$, to the total energy and it is therefore expected that the waveform of the magnetoresistance oscillations should not be affected by the current. In reality, however, the situation is much different as elaborated on in Sections 1.4 and 1.5 below and in Chapters 3.3, 3.5 and 3.6. For example, even at relatively small bias currents, the observed waveform of the magnetoresistance oscillations deviates quite frequently from the predicted parabolic behavior, Equation (4), exhibiting sinusoidal-like oscillations, see e.g.[28, 37, 38]. Such deviations were related to a distribution of the ratio ξ/r in a wide ring [37] (ξ is the coherence length and r is the radius of the ring), or to a size distribution of rings in a network [28]. In Chapter 3.4 we propose an alternative explanation associated with the existence of Josephson junctions (JJ) in the ring. The existence of such junctions is highly probable in superconducting nano-rings with superconducting leads ('arms') attached to them, as elaborated in the next Section (Section 1.4).

1.4 Nano-Rings with 'Arms'

De Gennes [39] considered a superconducting 'lasso', namely a superconducting ring (radius R) with an attached arm (length L) (Figure 6(a)). To obtain the order parameter of the lasso under an external field H perpendicular to the ring, he used the linearized Ginzburg–Landau equation (LGL),

$$\left(i\frac{\partial}{\partial s} - \frac{2eA_{||}}{\hbar}\right)^2 \Delta(s) - \frac{1}{\xi^2}\Delta(s) = 0, \tag{5}$$

where s is a coordinate along the ring's rim, Δ is the superconducor's order parameter and $A_{||}$ is the magnetic vector potential parallel to the superconducting wires composing the loop. At a 'node', namely where the arm and the ring are connected, the order parameter satisfies the following conditions

$$\sum_p \left(\frac{\partial}{\partial s} + i\frac{2eA_{||p}}{\hbar}\right)\Delta(s_p) = 0, \tag{6}$$

where the summation is taken over superconductor wires (p) that are connected to the node. The gauge of the vector potential is taken as $A_{||} = \frac{HR}{2}$ on the ring and $A_{||} = 0$ on the arm.

Figure 6. (a) An illustration of a superconducting 'lasso': a ring with radius R attached with an arm with length of L. (b) An illustration of a superconducting ring with two arms.

From Equation (5), the spatial dependence of the order parameter on the arm is:

$$\Delta(x) = \Delta_0 \frac{\cos\left(\frac{x}{\xi}\right)}{\cos\left(\frac{L}{\xi}\right)}, \tag{7}$$

where Δ_0 is the order parameter at the node and x the coordinate from the endpoint of the arm. On the ring, the order parameter is:

$$\Delta(s) = e^{-i\frac{s}{R}\frac{\Phi}{\Phi_0}}\left(\alpha e^{i\frac{s}{\xi}} + \beta e^{-i\frac{s}{\xi}}\right). \tag{8}$$

Here Φ is the magnetic flux through the ring and α, β are coefficients to be determined from the boundary conditions:

$$\Delta(0) = \alpha + \beta = \Delta_0, \tag{9}$$

$$\Delta(s = 2\pi R) = e^{-i\frac{2\pi R}{R}\frac{\Phi}{\Phi_0}}\left(2\alpha i \sin\left(\frac{2\pi R}{\xi}\right) + e^{-i\frac{2\pi R}{\xi}}\right) = \Delta_0, \tag{10}$$

From Equations (9) and (10) we can derive the coefficients α and $(= \Delta_0 - \alpha)$:

$$\alpha = \frac{e^{i2\pi\frac{\Phi}{\Phi_0}} - e^{-i\frac{2\pi R}{\xi}}}{2i\sin\left(\frac{2\pi R}{\xi}\right)}. \tag{11}$$

Since not only the order parameter but also its derivative has to be continuous along the rim, we should solve the following equation as well:

$$\left(\frac{d}{dx}\Delta(x)\right)\Big|_{x=L} - \left(\frac{d}{ds}\Delta(s) + i\frac{1}{R}\frac{\Phi}{\Phi_0}\Delta(s)\right)\Big|_{s=0} + \left(\frac{d}{ds}\Delta(s) + i\frac{1}{R}\frac{\Phi}{\Phi_0}\Delta(s)\right)\Big|_{s=2\pi R} = 0. \tag{12}$$

Equations (9), (10) and (12) form a set of coupled equations. For non-trivial solutions of $\{\alpha, \beta, \Delta_0\}$, $\xi(\Phi)$ should satisfy the following transcendental equation:

$$\cos\left(2\pi\frac{\Phi}{\Phi_0}\right) = \cos\left(2\pi\frac{R}{\xi}\right) - \frac{1}{2}\sin\left(2\pi\frac{R}{\xi}\right)\tan\left(\frac{L}{\xi}\right). \tag{13}$$

Equation (8) for the order parameter contains the coefficients $\alpha(\Phi), \beta(\Phi)$ and the parameter $\xi(\Phi)$ as a function of the magnetic flux through the ring. When analyzing this solution, de-Gennes found that the order parameter in the antipodal point of the ring, $\Delta(s = \pi R)$ (see Figure 6(a)), goes to 0 as Φ approaches $\Phi_0/2$.

Alexander [40] extended this work of de-Gennes to the general case of a superconducting ring with multiple arms. In the special case of two arms (see Figure 6(b)), Alexander found that in the mid-points between the arms (marked as anti-podal points in Figure 6(b)), the order parameter decreases as Φ approaches $\Phi_0/2$, reaching a minimum (though a non-zero value).

Based on de-Gennes and Alexander's calculations, Fink et al.[41] suggested that the minimum order parameter in the antipodal points should effectively create Josephson junctions. Therefore, a nano-ring with two arms should behave as a SQUID. In the

present dissertation (Chapter 3.3) we provide an experimental demonstration of such a SQUID behavior. Our magnetoresistance measurements showed a current induced crossover from the parabolic Little-Parks oscillations at low bias currents into $|\sin \pi \, \Phi/ \Phi_0|$ oscillations typical of a SQUID behavior. This crossover is demonstrated in Figure 7. The formation of a SQUID behavior is attributed to the combined effects of current induced phase slips and non-uniform order parameter along the loop caused by the superconducting arms.

Future experiments using tunnel junctions connected to a superconducting loop with one and two arms can verify the above model and give a fundamental physical understanding for the mechanism governing this current-induced effect.

Figure 7. Magnetoresistance of a single ring for different bias currents. Measurements performed at T = 7.1 K with currents between 1 µA and 4 µA are described as a function of the magnetic flux, Φ, normalized to the quantum flux, Φ_0, taking the ring area as $1.2 \cdot 10^{-9}$ cm^2. The guide to the eye solid curves through the data points describe classical Little-Parks parabolic oscillations (1 µA curve), Little-Parks sinusoidal oscillations in a SQUID (2 and 3 µA curves) and typical SQUID oscillations (4 µA curve).

1.5 *hc/e*-Periodicity in Superconducting Loops

In a multiply connected superconductor, the fluxoid is quantized in units of $\Phi_0 = h/2e$, where the 2e is a hallmark of electron pairing in the superconductor.

Theoretical studies [42-47] have predicted that in superconducting nano-loops with a length-scale a $< \xi$ the dominant periodicity is *hc/e* rather than *hc/2e*. The same theories predict that for high-Tc superconductors (HTS) with d-wave symmetry, the *hc/e* periodicity is also expected for a $\gtrsim \xi$. Recent experiments [28, 37] failed to identify the *hc/e* component in HTS. We associated this failure with the small coherence length, ξ_0, (~2 nm) typical to HTS resulting in a $>> \xi$ rather than the required a $\gtrsim \xi$. To bypass this problem we focused on aluminum, a low-T_c superconductor with a relatively large bulk coherence length (ξ_0 = 1.6 μm). We note, however, that in nanostructures made of thin films the coherence length is reduced due to the finite mean free path, and simultaneously the penetration depth λ_L is enhanced. Typical values of ξ in these aluminum nanostructures are in the range of 100 to 200 nm. Close to Tc, the coherence length $\xi(T)$ diverges, allowing in principle to meet the criterion a $< \xi$ in nanostructures with circumferences in the order of several hundred nanometres. On the other hand, the critical field of bulk Al amounts to only 10 mT, giving a strong limitation for the number of Little-Parks oscillations (LPO) that can be observed. Taking these considerations together, we fabricated aluminum 'double-networks' [28] and measured their magnetoresistance. One of the intriguing findings of these measurements is described in Figure 8(a) and Figure 8(b). In Figure 8(a) we plotted the differential MR (differential resistance vs. magnetic field) of an aluminum double network near T_c with bias currents of 0 and 2.1 μA. Figure 8(b) predicts the total energy (E(Φ)-E(0))/E(0) for a square loop. There is a clear difference between states with an even and an odd number of winding number, q, reflected in the deformation of the parabola in q=0. The overall flux periodicity for E is *hc/e*. The mapping between the energy to the resistance is through a monotonic function (usually $R \propto e^{-E/k_B T}$ [48]), thus maintaining the overall shape of the function. The similarity between the experimental plots and the theoretical plot is clear: the minima in the odd and even winding number have different shapes. We elaborate on consequences of these measurements in Chapter 3.5.
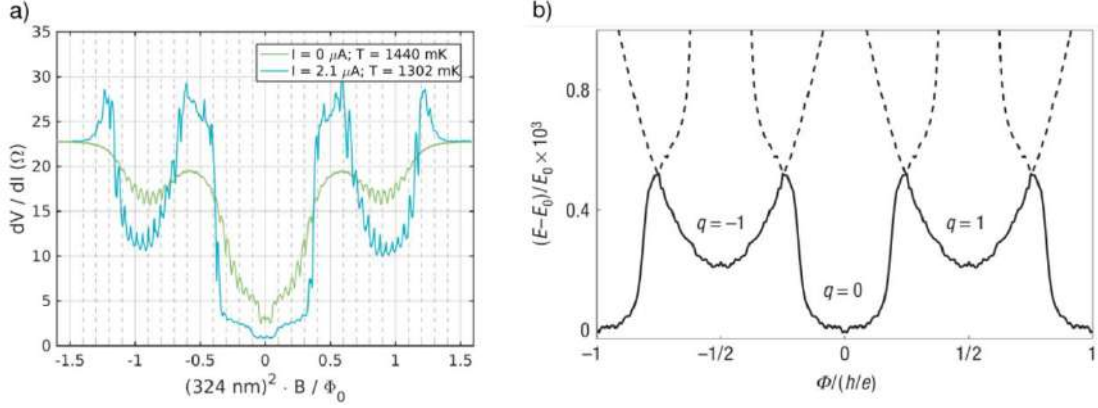
Figure 8. (a) Comparison of differential magnetoresistance of an aluminum double network with zero DC bias current and with 2.1 μA DC bias current close to T_c, (b) Theoretical plot of energy vs. flux for a superconducting loop with a < ξ, showing the modulation of the odd Little-Parks oscillations [44]. In the right figure Φ is described in units of $\Phi_0 = hc/e$.

1.6 The Aharonov-Bohm Effect

Magnetoresistance oscillations with *hc/e* flux periodicity are observed in mesoscopic metallic rings [49], demonstrating the Aharonov-Bohm (AB) effect [50] in solid state systems. In the AB effect, an electron wavepacket is coherently split into two wavepackets passing opposing sides of the ring. The wavepackets accumulate phase shifts of opposite signs along their paths. The two packets are recombined, and the resulting interference signal depends on the total magnetic flux enclosed by the two paths. The AB phase shift accumulated along points *a* and *b* is

$$\varphi = -\frac{e}{\hbar c}\int_a^b A \cdot dx \tag{14}$$

where A is the vector potential $B = \nabla \times A$. For the effect to be experimentally observed, it is essential that the ring size will be of the order or smaller than the 'phase coherent length', $L_\phi = \sqrt{D\tau_\phi}$ [51], where D is the diffusion coefficient and τ_ϕ is the time between inelastic collisions. L_ϕ at low temperatures is, typically, of order several micrometers, hence the need for a mesoscopic ring.
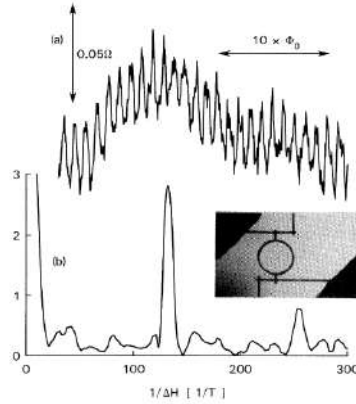
Figure 9. (a) Magnetoresistance of Au ring measured at T = 10 mK. (b) Fourier power spectrum in arbitrary units containing peaks at *hc/e* (and *hc/2e*). The inset is photograph of the measured ring. The inside diameter of the loop is 784 nm, and the width of the wires is 41 nm. From Webb *et al.* [49].

Webb *et al.* [49] were the first to report clear Aharonov-Bohm oscillations in mesoscopic metallic rings (Figure 9). Since then, the effect was demonstrated not only in metals [52] but also in many other non-metallic systems, see e.g. [53-60].

In this dissertation (Chapter 3.6 below), we demonstrate AB effect resulting from phase coherence of quasi-particles in a granular superconducting ring, essentially composed of a chain of superconducting Josephson junctions. To the best of our knowledge, this is the first demonstration of phase coherence in such a system. Moreover, the data indicates an enhancement of the AB effect as compared to the effect in metallic rings. Interestingly, the effect was observed only at high bias currents, see Figure 10. At low bias the magnetoresistance exhibits the LP effect with *hc/2e* flux periodicity. A crossover to the AB effect, with *hc/e* periodicity, is observed at relatively large currents in a range below the depairing current. At these high currents the AB effect arises from phase coherence of quasi-particles flowing in the resistive channel created by the Josephson junctions in the voltage state.
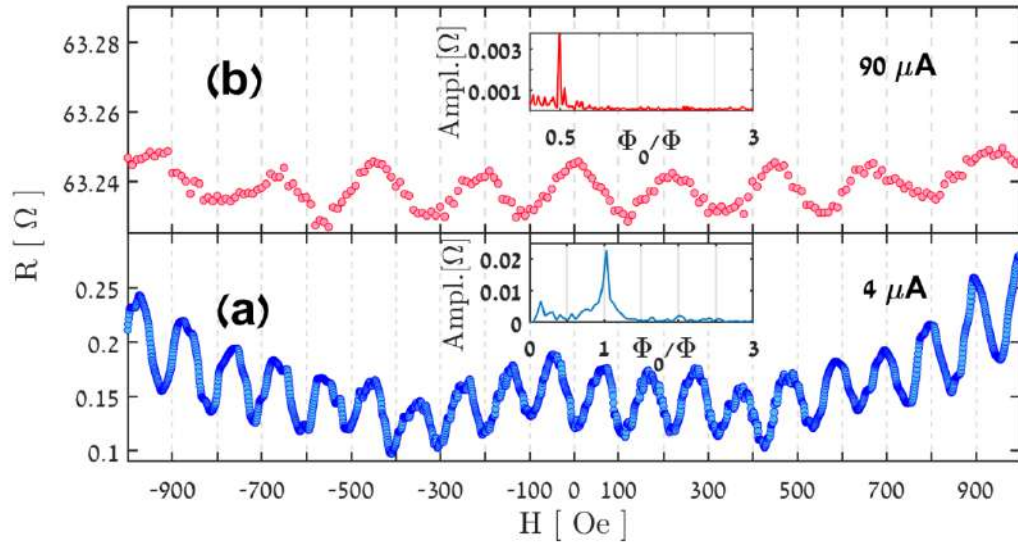
Figure 10. Magnetoresistance oscillations in the Nb ring at 3.5 K, for bias currents of 4 and 90 μA, lower and upper panels, respectively. Note the doubling of the flux periodicity from 105 to 210 Oe, corresponding to crossover of the flux periodicity from *hc/2e* to *hc/e*, respectively.

2 Experimental Methods

The experimental work described in this dissertation required fabrication of nano-structures, material characterization and transport measurements. These requirements are challenging when entering the nano-scale domain. Nano-scale features are extremely fragile and aspect ratio between width and thickness plays a significant role. The relevant methods are briefly described in the following Sections.

2.1 Fabrication

2.1.1 Magnetron Sputtering

Sputtering is a physical vapor deposition (PVD) technique in which plasma ions (usually Argon) are accelerated towards a negatively biased desired material which called target. Under a certain pressure of gas, the atoms collide, and release electrons, then the ions are accelerated while during the acceleration they ionized more atoms causing avalanches and amplifying the plasma. When the ions hit the target, they release aggregates of multiple atoms from the target, those aggregates are sputtered into all directions, and to the substrate holder that usually is localized few cm away from the target. A set of magnets is set under the target in order to focus the ions to the target. There are 2 main modes, DC and AC sputtering, used depending on the target material, whether it conducts or insulates. Since we deposit conducting metals, the target is biased with a DC voltage, which can enable a high deposition rate.

Sputter deposition is a well-established technique for deposition of high quality transition metal oxides. The desired phase can be deposited directly from a target with the correct stoichiometric ratio or can be achieved by reactive sputtering, where reactive gases (such as oxygen or nitrogen) are added during the deposition. Reactive processes are, in general, harder to control, since they include "target poisoning", a phenomenon that arises from the formation of a compound layer on the target surface, which is a result of chemical reaction of the reactive gas with the surface of the sputtering target. The poisoning can change the deposition rate, which can increase the poisoning further. Hence, for efficient reactive sputtering it is important to find a set of parameters that is relatively stable to small perturbations, and that results in a reproducible sample quality.

We sputtered niobium on SiO_2 substrate, in room temperature. We used a 99.95% purity Nb target. Working pressure was 2 mTorr, flowing 28 SCCM of argon to the chamber. Deposition rate was ~1.8 Å/s achieving T_c of 7.4K. Since this growth was not done on epitaxial substrate, XRD measurements characterized the films as polycrystalline.

We also deposited NbN. We found a good protocol for our NbN 5nm thin film: 1) Heat the chamber with the sample to 800°C in high vacuum, and leave it for two hours. 2) Lower the temperature to 750°C and leave it for two hours. 3) Begin sputtering at 2 mTorr. Since the target is Nb 99.95% pure, we need nitrogen atmosphere to make the sputtered Nb a thin NbN film. We used 26.1 SCCM of argon and 2.9 SCCM of N_2, which gives us partial pressure of 10% nitrogen. Sputtering rate was 0.9 Å/s. This method combined with R-cut sapphire as a substrate helped us achieving amorphic stoichiometry. T_c of this extremely thin sample was 11.5 K.

2.1.2 Nano-Patterning

A high resolution electron beam (e-beam) lithography system was exploited for nano-patterning the films. The e-beam system installed at the Bar-Ilan Institute of Nanotechnology and Advanced Materials is the CRESTEC-9000C. The electron beam lithography is based on 'writing' with a focused electron beam in a thin layer of a material sensitive to the accelerated electrons (electron beam resist). The main advantage of electron beam lithography is that it is a very effective way to go beyond the diffraction limit of light and make features of few tens of nanometers or even less. In some cases, the exposed parts of the resist become highly soluble and can be removed by liquid developers (positive tone resists). In other cases, the exposed parts of the resist become unsolvable and the un-exposed parts can be removed by developers (negative tone resists).

We used Poly(methyl methacrylate) (PMMA) as a negative tone resist. Although, in typical conditions PMMA functions as a positive resist, at increased exposure times PMMA may crosslink and become unsolvable in typical organic developers [61]. We

observed that a cross-linked negative tone PMMA ensures a much higher contrast, resolution, and aspect ratio. In a layer of ~70 nm, we could reach a feature size of 17 nm with a gap 7nm. Cross-linked PMMA are also very stable during ion milling, probably due to the enhanced stiffness of the crosslinked polymer. Step 1: A layer of PMMA resist was spun-off on top of film. We used AR-P which is a special kind of PMMA with a molecular weight of 200,000 to produce a film of ~120 nm after spincoating at the speed of 5,000 RPM. The AR-P 200K gave the best results in terms of contrast, resolution, aspect ratio and resistant to the destructive chlorine etching process (discussed in Chapter 2.1.3). The sample with the resist layer was 'baked' on a hot plate for 2 min at 180 °C. Step 2: Then the desired patterns of the loops were exposed using a CRESTEC Cable-9000C high resolution e-beam lithography system with an acceleration voltage of 50 keV and typical beam current of 500 pA. Step 3: We used relatively high doses of electron beam exposure to produce a negative tone image of the loops and contacts design in the layer of resist. Using high resolution of 240,000 dots in a field of 600 μm makes the electron beam to divert 2.5 nm each step (grid spacing is 2.5 nm). Since the spot size of the beam is larger than the grid size (distance between adjacent grid cells), each grid cell has an effective exposure which is ~6.8 times larger than using sparse dots/low resolution. This method reduced the exposure time by a factor of 2. Step 4: Development of the exposed sample was done in the standard method: 40-60 seconds in MIBK (methyl isobutyl ketone), diluted 3:1 with Isopropyl alcohol, then 20 seconds in IPA (Isopropyl alcohol) which is the stopper for the MIBK developer. In this step, parts of the resist near the negative unsolvable (cross-linked) parts are removed. Step 5: To remove the remains of the unexposed parts of the resist, we developed the samples for 4-10 minutes in acetone (the longer the better), using IPA as a stopper for at least 1 minute. This 'negative' resist pattern served as a mask for transferring the pattern to the superconducting film by chemical etching.

2.1.3 Reactive Ion Etching

Etching was done using an RIE/ICP (Reactive Ion Etching / Inductively Coupled Plasma) system. We used an interferometer to determine the etching state of the sample. We stopped the etching two seconds after the interferometer indicated that the niobium

layer was fully etched. A mixture of Cl_2 and BCl_3 produced the finest results thus used for the main part of my work.

Etching was performed in room temperature, under a pressure of 5 mTorr and a gas flow of 20 SCCM for the Cl_2 and 5 SCCM for the BCl_3. RIE Bias forward power was 50W. No ICP was used. We did use a stabilization step before the etching step, but its parameters did not affect the etching procedure. Etching was not linear and an interferometer was used to determine when the etching step was done. A long stabilization step allowed us to calibrate the interferometer for each sample we etched.

2.2 Transport Measurements

We measured the resistance of the different rings as a function of temperature, magnetic field and bias currents. The measurements were done using a commercial Physical Properties Measurement System (PPMS, Quantum Design Inc.) that provides a temperature range of 2-400 K and magnetic field up to 9 T to measure R vs. T and R vs H curves. To communicate, program, automate and control the system, we used MATLAB computing environment.

The aluminum network measurements were performed at Konstanz University in a HelioxVL helium-3 cryostats from Oxford Instruments. Four-point resistance measurements were performed with a bias current below 500 nA, using SR830 lock-in amplifiers. A Yokogawa 7651 served as the DC voltage and current bias. A custom-built adder combined the DC signal from the Yokogawa and the AC signal of 4 mV at 117.17 Hz, which was then fed into the cryostat on the bias input lead. The signal passed through the sample and was amplified by a Femto DLPCA-200 current amplifier, from which it was then read by one of the lock-in amplifiers. To accomplish the four-point measurements, two additional electrical leads, above and below the sample in the electrical potential landscape, lead to a Femto DLPVA-100 voltage amplifier, from which the voltage signal was then fed into the other lock-in amplifier. The outputs from both lock-in amplifiers were then fed into an ADWin Gold data acquisition system, where they were digitized and passed on to the computer to be saved.

The Heliox cryostats each came outfitted with an Allen-Bradley thermal element at the helium-3 sorption pump, two 2.2 kW (RuO_2) thermal elements at the 1.5 K plate and helium-3 pot, and heaters at the helium-3 sorption pump and the helium-3 pot. These five elements were controlled through the Oxford Instruments ITC 503 temperature controllers that were delivered with each cryostat.

2.2.1   Resistance Measurements

Resistivity measurements were conducted using 4-probe and delta mode method to eliminate contact resistance and parasitic voltage offset.

2.2.2   I-V Characteristics Measurements

I-V characteristics was measured using 4-probe in 5 quarters: measuring the voltage while increasing the bias current to the maximum current, then decreasing the bias current to the negative minimum current, and then increasing the current again to the maximum current. This method was used to detect if hysteresis in the I-V characteristics exists.

3   Publications

The following 6 publications summarize the research work done in the framework of this dissertation:

3.1   **Fluxoids configurations in finite superconducting networks**

Omri J. Sharon, Noam Haham, Avner A. Shaulov, and Yosef Yeshurun
Physica C **543**, 46-51 (2017).

3.2   **Fluxoids behavior in superconducting ladders**

Omri J. Sharon, Noam Haham, Avner Shaulov and Yosef Yeshurun
Journal of Physics: Conf. Series **969** 012048-012054, (2018).

3.3   **Current-induced SQUID behavior of superconducting Nb nano-rings**

Omri J. Sharon, Avner Shaulov, Jorge Berger, Amos Sharoni, and Yosef Yeshurun
Scientific Reports **6**, 28320-28325 (2016).

3.4   **Little-Parks oscillations in superconducting ring with Josephson junctions**

Omri J. Sharon, Amos Sharoni, Jorge Berger, Avner Shaulov, and Yosef Yeshurun
Journal of Physics: Conf. Series **969** 012047-012053, (2018).

3.5   **Flux-periodicity crossover from *h/2e* to *h/e* in aluminium nano-loops**

C. Espy, O. J. Sharon, J. Braun, R. Garreis, F. Strigl, A. Shaulov, P. Leiderer, E. Scheer, Y. Yeshurun
Journal of Physics: Conf. Series **969**, 012045-012051 (2018).

3.6   **Current-Induced Crossover of Flux Periodicity from *h/2e* to *h/e* in Superconducting Nb Nano-Ring**

Omri J. Sharon, Avner Shaulov, Jorge Berger, Amos Sharoni, Richard Berkovits and Yosef Yeshurun
Nano Letters **18**, 7851–7855 (2018).

The first two publications establish a solid ground for understanding the interaction between fluxoids and the physics behind their arrangements in superconducting networks.

The third and fourth publications reveal novel phenomena associated with the influence of bias current on the behavior of superconducting nano-loops.

The last two report on experimental discovery of *hc/e* (rather than the conventional *hc/2e*) flux periodicity in nano- and meso-scopic superconducting loops, induced by size-effect and bias-current, respectively.

3.1 Fluxoids configurations in finite superconducting networks

Omri J. Sharon, Noam Haham, Avner A. Shaulov, and Yosef Yeshurun
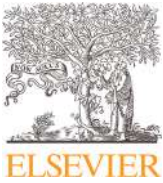
Fluxoids configurations in finite superconducting networks

Omri J. Sharon, Noam Haham, Avner A. Shaulov, Yosef Yeshurun*

Department of Physics and Institute of Nano Technology and Advanced Materials, Bar-Ilan University, 5290002 Ramat-Gan, Israel

A R T I C L E   I N F O

A B S T R A C T

Analysis of superconducting ladders consisting of rectangular loops, yields an Ising like expression for the total energy of the ladders as a function of the loops vorticities and the applied magnetic field. This expression shows that fluxoids can be treated as repulsively interacting objects driven towards the ladder center by the applied field. Distinctive repulsive interactions between fluxoids are obtained depending on the ratio l between the loops length and the common width of adjacent loops. A 'short range' and a 'long range' interactions obtained for $l \gtrsim 1$ and $l \ll 1$, respectively, give rise to remarkably different fluxoid configurations. The different configurations of fluxoids in different types of ladders are illustrated by simulations.

1. Introduction

Macroscopic quantum phenomena continue to attract attention since the early days of quantum mechanics [1]. A prominent example of a macroscopic quantum phenomenon is exhibited by loops and networks made of thin superconducting wires. The quantity quantized in these multiply-connected systems is the fluxoid defined as: $(4\pi\lambda^2/c)\oint \vec{J}\cdot\overrightarrow{dl} + \phi$, where $\vec{J}$ is the density of the shielding current in a loop, λ is the penetration depth, and ϕ is the magnetic flux threading the loop. In each and every loop of a network the fluxoid must be an integer multiple of the flux quantum ϕ_0 [2]. The requirement of minimum energy determines the number and arrangement of fluxoids in the network giving rise to periodic changes in the energy as a function of the external field.

Fluxoid quantization effects have been studied extensively, both theoretically and experimentally, in a variety of superconducting networks [3-17]. However, most of these studies focus on the phase boundary between the superconducting and the normal states, paying less attention to the fluxoids configuration in networks as a function of the applied magnetic field. The limited number of studies considering fluxoids configurations present results of experimentally measured or theoretically calculated configurations in various networks, providing no intuitive understanding of the underlying physics [6,17-19]. The purpose of the present work is to elucidate the mechanism governing the fluxoid configuration in finite superconducting networks as a function of the applied field. Understanding the physics behind the different fluxoid configurations may lead to the development of new concepts in

'fluxonics' – a growing research area aiming at exploiting superconductors in digital circuits [20-23].

We theoretically analyze the simplest case of a superconducting 1D network ('ladder') using the "current squared" model (known as the "J² model") [6,18,24]. In this model the kinetic energy of the network is calculated as the sum of the squared currents over all the network wires, and the number and arrangement of the fluxoids are determined by the requirement of minimum energy. Our analysis yields an Ising like expression for the total energy of the network as a function of the loops' vorticities and the applied magnetic field. This expression shows that fluxoids can be treated as repulsively interacting objects subjected to an additional interaction with the applied field. The field tends to direct the fluxoids towards the network center while fluxoids repel each other tending to keep themselves apart. Competition between these two interactions determines the equilibrium arrangement of fluxoids in the network as a function of the applied field.

We distinguish between three types of ladders depending on the ratio l between the loops' length and the common width of adjacent loops in the ladder. For $l \gg 1$, the interaction between fluxoids is negligible and the ladder can essentially be considered as a collection of separate, non-interacting loops. As the ratio l decreases toward 1, 'short range' repulsive interactions arise, decreasing exponentially with the relative positions of the fluxoids. Ladders with $l \ll 1$ are characterized by a 'long range' interaction, which depends on the product of the fluxoids' locations relative to the ladder's edges. The different configurations of fluxoids in these different types of ladders are illustrated by simulations.

* Corresponding author.
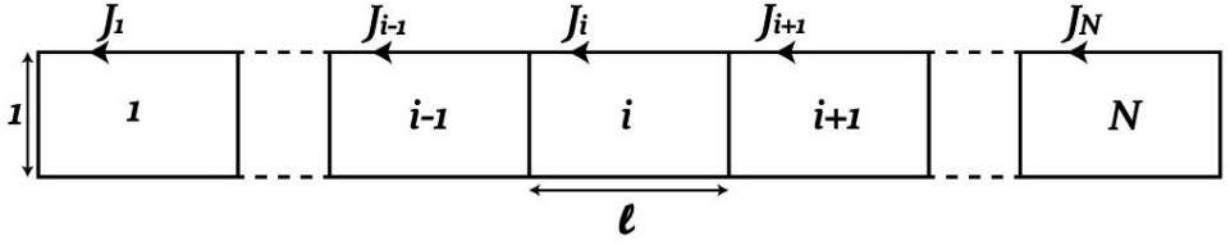*E-mail address:* yeshurun@mail.biu.ac.il (Y. Yeshurun).

Fig. 1. Finite rectangular ladder consisting of *N* loops.

2. Analysis

Consider a superconducting ladder of finite length, consisting of *N* rectangular loops of unit width and length *l*, as shown in Fig. 1.

The fluxoid quantization equation for loop *i* reads:

$$2(l+1)J_i - J_{i-1} - J_{i+1} = n_i - \frac{\phi}{\phi_0}, \qquad (1)$$

where n_i is the vorticity of the loop *i*, ϕ is the flux threading this loop, and by definition $J_i = 0$ for $i < 0$ or $i > N$. For simplicity, the coefficient $4\pi\lambda^2/c$ is taken as 1. According to Eq. (1), the set of the fluxoid quantization equations for all the loops can be written as a matrix equation:

$$\hat{A} \cdot \vec{J} = \vec{n} - \frac{\vec{\phi}}{\phi_0}, \qquad (2)$$

where the elements of the matrix $\hat{A}$:

$$A_{ij} = 2(l+1)\delta_{i,j} - \delta_{i,j-1} - \delta_{i,j+1},$$

$\delta_{i,j}$ being the Kronecker δ.

The current vector $\vec{J}$ can be calculated from Eq. (2) by inversion:

$$\vec{J} = \hat{A}^{-1}\left(\vec{n} - \frac{\vec{\phi}}{\phi_0}\right) \qquad (3)$$

Denoting the matrix $\hat{A}^{-1}$ as $\hat{B}$, Eq. (3) can be written as a set of equations:

$$J_i = \sum_{j=1}^{N} B_{ij}\left(n_j - \frac{\phi}{\phi_0}\right), \quad i = 1..N. \qquad (4)$$

Using the J^2 model, knowledge of J_i allows calculation of the energy E_i of the loop *i*:

$$E_i = 2lJ_i^2 + \frac{1}{2}(J_i - J_{i-1})^2 + \frac{1}{2}(J_i - J_{i+1})^2 + \frac{1}{2}J_1^2\delta_{1,i} + \frac{1}{2}J_N^2\delta_{N,i}$$

$$= J_i[(2l+1)J_i - J_{i-1} - J_{i+1}] + \frac{1}{2}J_{i-1}^2 + \frac{1}{2}J_{i+1}^2 + \frac{1}{2}J_1^2\delta_{1,i} + \frac{1}{2}J_N^2\delta_{N,i},$$

and the total energy *E* of the network:

$$E = \sum_{i=1}^{N} E_i = \sum_{i=1}^{N}\left\{J_i(-J_i + 2(l+1)J_i - J_{i-1} - J_{i+1}) + \frac{1}{2}J_{i-1}^2 + \frac{1}{2}J_{i+1}^2\right\}$$
$$+ \frac{1}{2}J_1^2 + \frac{1}{2}J_N^2. \qquad (5)$$

Using Eq. (1) and realizing that $\sum_{i=1}^{N}\{-J_i^2 + \frac{1}{2}J_{i-1}^2 + \frac{1}{2}J_{i+1}^2\} + \frac{1}{2}J_1^2 + \frac{1}{2}J_N^2 = 0$, Eq. (5) becomes

$$E = \sum_{i=1}^{N} J_i\left(n_i - \frac{\phi}{\phi_0}\right). \qquad (6)$$

Inserting J_i from Eq. (4) yields

$$E = \sum_{i=1}^{N}\sum_{j=1}^{N} B_{ij}\left(n_j - \frac{\phi}{\phi_0}\right)\left(n_i - \frac{\phi}{\phi_0}\right) =$$

$$= \sum_{ij} B_{ij}\left(n_i n_j - 2\frac{\phi}{\phi_0}\,n_i + \left(\frac{\phi}{\phi_0}\right)^2\right) \qquad (7)$$

The above expression for the total energy, *E*, is reminiscent of the Ising model for the energy of a spin configuration, having the form $\sum_{ij} J_{ij}S_iS_j - \mu\sum_j h_jS_j$ [25]; n_j, and B_{ij} playing the role of the Ising variable S_j and the exchange energy J_{ij}, respectively. The first term on the right hand side of Eq. (7), $(\sum_{ij} B_{ij}n_in_j)$, represents the interaction between fluxoids, including the self-interactions $\sum_i B_{ii}n_i^2$. The second term $(-2\frac{\phi}{\phi_0}\sum_{ij} n_iB_{ij})$ expresses the interaction between the fluxoids and the effective magnetic field. The third term, $(\frac{\phi}{\phi_0})^2\sum_{ij} B_{ij}$, is a constant, independent of the vorticities and thus may be ignored.

For the matrix $\hat{A}$ given in Eq. (2), $\hat{B} = \hat{A}^{-1}$ is a symmetric matrix with elements [26]:

$$B_{ij} = \frac{(\gamma_1^i - \gamma_2^i)(\gamma_1^{N+1-j} - \gamma_2^{N+1-j})}{(\gamma_1 - \gamma_2)(\gamma_1^{N+1} - \gamma_2^{N+1})}, \text{ for } i \leq j \qquad (8)$$

where $\gamma_{1,2} = (l+1) \pm \sqrt{(l+1)^2 - 1}$. Due to the symmetry of $\hat{B}$, B_{ij} for $i > j$ can be calculated as B_{ji} using Eq. (4). Defining $\eta \equiv \gamma_2/\gamma_1$, and $C \equiv 1/(1-\eta)(1-\eta^{N+1})$, Eq. (8) takes the form

$$B_{ij} = C\gamma_1^{i-j-1}\left(1 - \eta^i\right)\left(1 - \eta^{N+1-j}\right), \text{ for } i \leq j. \qquad (9)$$

γ_1, γ_2, η and C are geometrical factors that depend on the element length *l*. These dependencies are shown in Fig. 2.

As clarified below, *l* determines the degree of coupling between the loops. For $l \gg 1$, the coupling is weak, and for $l \ll 1$ the coupling is strong. These two cases differ significantly from each other and from the intermediate case $l \gtrsim 1$, on which interest is commonly focused. In the following we discuss these three limiting cases:

Case 1: $l \gg 1$. In this case, $C \to 1$, $\eta \to 0$, and the off-diagonal elements of the matrix $\hat{B}$ become negligible as compared to the diagonal elements. Thus, the dependence of J_i on the vorticities of loops, other than the loop *i*, can be neglected (see Eq. 4). In other words, the coupling between the loops is weak and the energy of the ladder is approximately the sum of the energies of separate loops:

$$E = \gamma_1^{-1}\sum_{i=1}^{N}\left(n_i^2 - 2\frac{\phi}{\phi_0}\,n_i + \left(\frac{\phi}{\phi_0}\right)^2\right). \qquad (10)$$

Consequently, as the field increases, all the loops are occupied with fluxoids essentially in unison.

Case 2: $l \gtrsim 1$. In this case, $\eta \ll 1$, $C \approx 1$ and γ_1 approximately equals to the circumference $2(l+1)$ of a single loop. Thus, it is justified to neglect in Eq. (9) powers of η as compared to 1, and approximate B_{ij} as $\gamma_1^{-(|i-j|+1)}$. In this approximation, Eq. (7) becomes
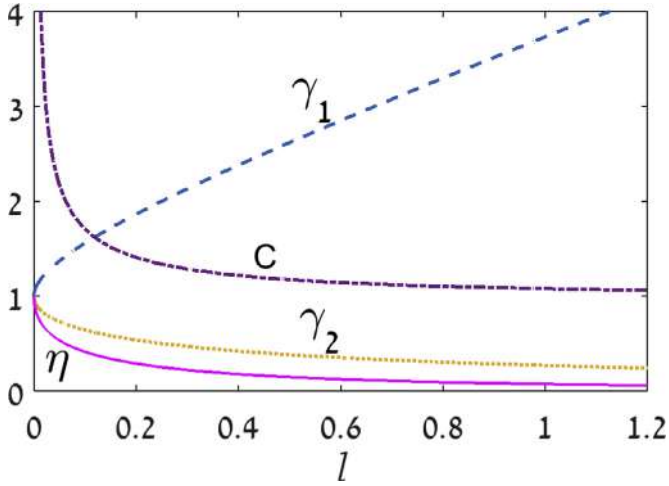
Fig. 2. The geometrical factors γ_1, γ_2, C and η as a function of the ratio l between the loop length and the common width of adjacent loops.

$$E = \sum_{ij} \gamma_1^{-(|i-j|+1)} \left(n_i n_j - 2\frac{\phi}{\phi_0} n_i + \left(\frac{\phi}{\phi_0}\right)^2 \right). \tag{11}$$

The above expression shows that fluxoids can be treated as repulsively interacting objects, with interaction energy that decreases exponentially with their separation in the ladder. In order to minimize the total energy, the repulsive interaction between fluxoids tends to keep them away from each other. The interaction between the fluxoids and the effective magnetic field, represented by the second term in Eq. (11), $(-2\frac{\phi}{\phi_0} \sum_i n_i \sum_j \gamma_1^{-(|i-j|+1)})$, reduces the energy depending on the fluxoids arrangement within the network. It can be shown that the geometric progression factor in this term: $-\sum_j \gamma_1^{-(|i-j|+1)} \propto \cosh(\ln(\gamma_1)(\frac{N+1}{2} - i))$, which is minimal at the center of the ladder ($i = \frac{N+1}{2}$). Thus, to minimize the total energy,

the interaction with the field, tends to drive the fluxoids away from the network edges towards the network's center. As mentioned above, the third term in Eq. (8), $(\frac{\phi}{\phi_0})^2 \sum_{ij} \gamma_1^{-(|i-j|+1)}$, is independent of the vorticities and thus can be ignored. We conclude that while the external magnetic field tends to assemble the fluxoids near the ladder center, the fluxoids repel each other tending to keep themselves apart. Competition between these two opposite interactions determines the equilibrium arrangement of fluxoids in the network as a function of the applied field. The self-interaction term has no role as it has no spatial preference, because in this case the diagonal elements $B_{ii} = \gamma_1^{-1}$ are all the same. Considering the first fluxoid which enters the ladder, it will always appear at the center of the network (or next to it, in a ladder with an even number of loops) as it is affected only by the external field which drives it to the center. As the field increases, a second fluxoid enters the system, pushing the first one out of its central position and both fluxoids arrange themselves in an optimum configuration, keeping apart from each other and away from the network edges. The same principle determines the arrangements of the next fluxoids entering the ladder as the field further increases. Rearrangement of fluxoids in the network continues until the last fluxoid enters at the network center completing one period in which each loop is occupied with one fluxoid. Occupation of the loops in the following periods follows the same pattern.

Case 3: $l \ll 1$. In this case, both γ_1 and η approach 1 and

$$B_{ij} \rightarrow \frac{i(N+1-j)}{N+1} \text{ for } i \leq j. \tag{12}$$

Thus, the repulsive interaction between fluxoids becomes dependent on the product of their locations relative to the ladder's edges. This is in variance with the previous case ($l \gtrsim 1$) in which the interaction between fluxoids decreased exponentially with their relative locations. In addition, contrary to the case $l \gtrsim 1$, where the diagonal elements $B_{ii} = \gamma_1^{-1}$ are all the same, independent of the location i, in the case $l \ll 1$, $B_{ii} = i(N+1-i)/(N+1)$ has a maximum value of $(N+1)/4$ at the center of the ladder (i.e. for $i = (N+1)/2$) and drops parabolicaly to $N/(N+1)$ at the ladder's edges ($i = 1$, and $i = N$). Consequently, the fluxoid self-energy,
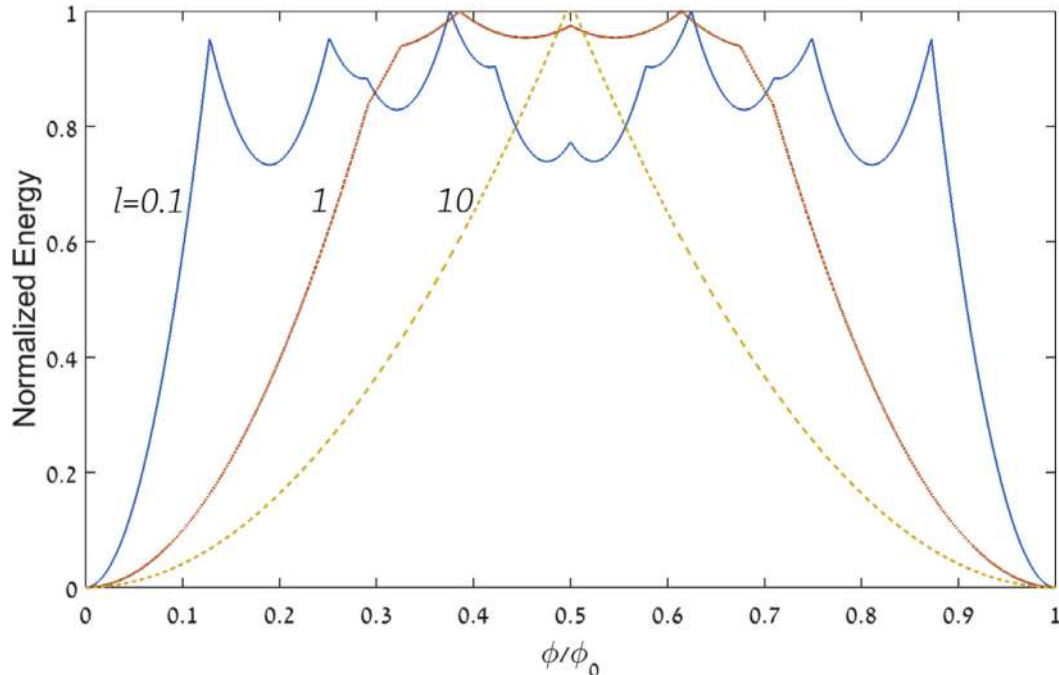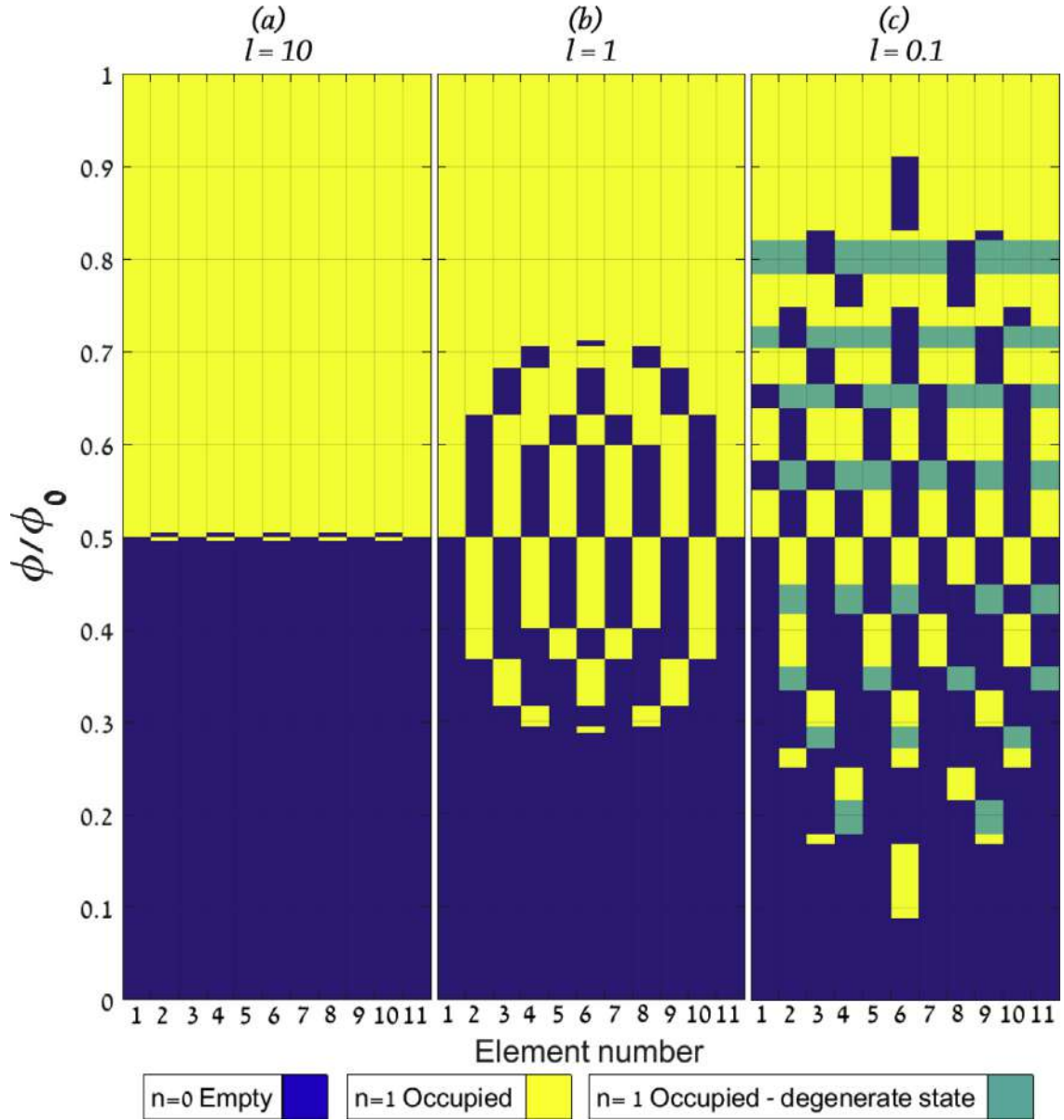

Fig. 3. Normalized energy as a function of the normalized magnetic flux in ladders with 11 loops and different ratios l between the loop length and the common width of adjacent loops.

Fig. 4. Fluxoid configuration as a function of field in ladders with 11 loops, and different ratio $l = 0.1,\ 1$ and 10, between the loop length and the common width of adjacent loops. An empty loop is colored blue, and occupied loop is colored yellow or green. The green color indicates degenerated configurations which are incommensurate with the symmetry of the ladder. (For interpretation of the references to color in this figure legend, the reader is referred to the web version of this article.)

determined by the coefficients B_{ii}, is maximum at the ladder's center and drops towards the ladder's edges.

To examine the role of the self-energy in determining the fluxoids arrangements, it is useful to isolate its contribution to the total energy E. Exploiting the symmetry of $\hat{B}$, the energy E can be written in terms of the diagonal and the lower off-diagonal elements of $\hat{B}$ as follows:

$$E = \sum_{i=1}^{N} B_{ii} n_i^2 + 2 \sum_{i=1}^{N-1} \sum_{j=i+1}^{N} B_{ij} n_i n_j$$
$$- 2 \frac{\phi}{\phi_0} \left[\sum_{i=1}^{N} B_{ii} n_i + \sum_{i=1}^{N-1} \sum_{j=i+1}^{N} B_{ij} \left(n_i + n_j \right) \right]. \tag{13}$$

The first term on the right hand side of Eq. (13) represents the self-interactions of the fluxoids, the second term represents the mutual interactions between fluxoids, and the third term expresses the interaction between the fluxoids and the effective magnetic field. Suppose that a single fluxoid enters the system at a location i_0. To minimize the energy, the location i_0 is determined by a competition between the self-interaction which prefers location at the ladder edges and the interaction with the field which favors location at the ladder's center. Explicitly, the self-interaction is $\frac{i_0(N+1-i_0)}{N+1}$, and the interaction with the field is

$$-2 \frac{\phi}{\phi_0} \left[B_{i_0 i_0} + \sum_{j=i_0+1}^{N} B_{i_0 j} + \sum_{i=1}^{i_0-1} B_{ii_0} \right] = -\frac{\phi}{\phi_0} i_0 (N+1-i_0).$$

The total energy becomes:

$$i_0(N+1-i_0) \left(\frac{1}{N+1} - \frac{\phi}{\phi_0} \right).$$

From this expression it is clear that the self-interaction prevails only if $\phi < \phi_0/(N+1)$. However, in this case the entry of the first fluxoid would increase the energy of the system. A decrease

in the energy requires that $\phi > \phi_0/(N+1)$. Thus, the interaction with the field always prevails, and the first fluxoid appears at the ladder center as in the previous case. Nevertheless, the location dependent self-interaction and the stronger interaction between fluxoids, when $l \ll 1$, give rise to different fluxoid arrangements at higher fields, when more than one fluxoid occupies the ladder. In particular, a larger number of fluxoid configurations are obtained, including different configurations of the same number of fluxoids at different fields. In addition, one obtains degenerated configurations that are incommensurate to the ladder symmetry. These are demonstrated with examples in the following section.

3. Simulations

The simulations described in this section demonstrate the different configurations of fluxoids in ladders with weak, medium and strong coupling between the loops. In each case, the energy of the ladder as a function of the loops vorticities and the external field was calculated using Eq. (7) and the exact expression for the elements B_{ij} (Eq. (8)). For each given field the fluxoid arrangement $(n_1, n_2, \ldots, n_N)$ which minimizes the energy was determined.

The dashed curve in Fig. 3 shows the minimum energy as a function of the normalized flux ϕ/ϕ_0 in a ladder of 11 elements with $l = 10$. This curve exhibits the well-known Little-Parks parabolas of a single loop [2], demonstrating that the loops are essentially decoupled. A diagram of the occupation vs. ϕ/ϕ_0 in the first period is shown in Fig. 4a. It demonstrates that, except for a narrow region near $\phi/\phi_0 = \frac{1}{2}$, all the loops are either empty or occupied with a single fluxoid.

A different picture is obtained when l is reduced to the order of 1. The minimum energy as a function of ϕ/ϕ_0 in the case $l = 1$ is shown by the dotted curve in Fig. 3. Due to the coupling between the loops, the waveform of E vs. ϕ is remarkably changed, showing a broad peak around $\phi_0/2$ and crests at fluxes corresponding to fluxoid entries. The fluxoids arrangements as a function of field is illustrated in Fig. 4b. The first fluxoid enters the sixth loop at the ladder's center at $\phi/\phi_0 = 0.29$. As the field increases a second fluxoid enters ladder, pushing the first one out of its central position and both fluxoids arrange themselves symmetrically in the fourth and eighth loops, keeping apart from each other and away from the network edges. As more fluxoids enter the ladder with increasing field, rearrangement of fluxoids continues until the last fluxoid enters the ladder's center completing one period in which each loop is occupied with one fluxoid. Occupation of the loops in the following periods follows the same pattern.

When l decreases much below 1, the coupling between the loops increases significantly giving rise to a more complex E vs. ϕ curve, as shown by the solid line in Fig. 3 for $l = 0.1$. The additional crests in the $E(\phi)$ curve indicate additional configurations of fluxoids through a period as illustrated in Fig. 4c. It is interesting to note that some of these configurations are incommensurate to the ladder symmetry (marked in green color in Fig. 4c). The first fluxoid enters the ladder's center, as in the previous case. However, with the entry of the second fluxoid, both arrange themselves farther away from each other, in the third and 9th loops, closer to the ladder's edges. With increasing field, both fluxoids rearrange themselves in asymmetric positions, in the fourth and 9th loops. This configuration is degenerated in energy with a configuration where the third and 8th loops are occupied. Rearrangements from symmetric to asymmetric positions also occurs with three and five fluxoids, as shown in Fig. 4c. A 'checkerboard' arrangement is obtained with 5 and 6 fluxoids around $\phi_0/2$. The configurations of 7, 8, 9, 10 and 11 fluxoids are complementary to the configurations of the 4, 3, 2, 1 and zero fluxoids, respectively.

Our analysis of superconducting ladders can be extended to two dimensional superconducting networks. However, the interac-

tion terms between fluxoids, and between them and the external field, become more complicated. In a recent publication [27] we showed numerical results for a 3×3 square network, based on the J^2 model. These numerical-calculations yield 11 different configurations, exceeding the number of loops in the network, due to rearrangement of the same number of fluxoids as the field increases. Among the 11 different configurations, there are 6 degenerated states that are incommensurate to the network symmetry. Calculations of Kato and Sato based on the de-Gennes-Alexander equations for a network yield quite different results [17]. Involving the appearance of anti-fluxoids in the network, their calculations predict 9 configurations all of which are commensurate to the network symmetry. It should be noted, however, that by minimizing the Ginzburg–Landau free energy, asymmetric fluxoid patterns have been reported for a 10×10 network [28]. Experimental work, using, e.g., a scanning SQUID-on-tip [29,30], is required to decide between the predictions of the J^2- and de-Gennes-Alexander models.

4. Summary and conclusions

The fluxoids equilibrium positions in ladders consisting of rectangular loops depend on the ratio l between the loops length and the common width of adjacent loops. For $l \gg 1$ the interaction between fluxoids is weak and, in essence, they occupy the ladder's loops independently as if the loops are decoupled. In ladders with $l \gtrsim 1$, a 'short range' repulsive interactions between fluxoids arise, which decreases exponentially with their relative separation. The fluxoids arrangement is dictated by a competition between their repulsive interaction and their interaction with the external magnetic field which drives them toward the ladder's center. Ladders with $l << 1$ are characterized by a 'long range' interaction between fluxoids, which depends on the product of their locations relative to the ladder's edges. In the competition between this long range interaction and the interaction with the field another factor plays a role, namely the fluxoids self-interaction. Consequently, in such ladders, different fluxoids configurations are obtained. In particular, additional configurations are obtained extending over a wider range of magnetic flux. Some of these configurations include the same number of fluxoids arranged in different positions, some of which are incommensurate to the ladder symmetry.

Finally we note that the basic mechanism governing the fluxoid arrangements in ladders should also apply to two dimensional networks. However, a full extension of our analysis to two dimensional networks remains for a future study. The results of this study could connect to many theoretical and experimental works on films with antidot arrays, which become networks in the limit of large antidots, see e.g. [31].

References

[1] A.O. Caldeira, An Introduction to Macroscopic Quantum Phenomena and Quantum Dissipation, Cambridge University Press, 2014.
[2] M. Tinkham, Introduction to Superconductivity, McGraw-Hill, Inc., 1996.
[3] B. Pannetier, J. Chaussy, R. Rammal, Experimental determination of the (H, T) phase diagram of a superconducting network, Journal de Physique Lettres 44 (1983) 853–858.
[4] B. Pannetier, J. Chaussy, R. Rammal, J. Villegier, Experimental fine tuning of frustration: two-dimensional superconducting network in a magnetic field, Phys. Rev. Lett. 53 (1984) 1845.

[5] J.M. Gordon, A.M. Goldman, J. Maps, D. Costello, R. Tiberio, B. Whitehead, Superconducting-normal phase boundary of a fractal network in a magnetic field, Phys. Rev. Lett. 56 (1986) 2280.

[6] A. Behrooz, M. Burns, D. Levine, B. Whitehead, P. Chaikin, Superconducting phase boundary of aperiodic networks in a magnetic field, Phys. Rev. B 35 (1987) 8396.

[7] J.M. Gordon, A.M. Goldman, B. Whitehead, Dimensionality crossover in superconducting wire networks, Phys. Rev. Lett. 59 (1987) 2311.

[8] F. Nori, Q. Niu, Tc (H) for quasicrystalline micronetworks: Analytical and numerical results, Physica B 152 (1988) 105–112.

[9] C. Chi, P. Santhanam, P. Blöchl, Interacting loop-current model of superconducting networks, J. Low Temp. Phys. 88 (1992) 163–195.

[10] V. Bruyndoncx, C. Strunk, V. Moshchalkov, C. Van Haesendonck, Y. Bruynseraede, Fluxoid quantization effects in superconducting mesoscopic Al multiloop structures, EPL 36 (1996) 449.

[11] D.H. Reich, D.M. Silevitch, C. Chien, D. Davidovic, S. Field, Disorder and correlations in extended superconducting nanostructures, J. Alloys Compounds 303 (2000) 245–251.

[12] A. Burlakov, V. Gurtovoĭ, S. Dubonos, A.V. Nikulov, V. Tulin, Little-parks effect in a system of asymmetric superconducting rings, JETP Lett. 86 (2007) 517–521.

[13] I. Sochnikov, A. Shaulov, Y. Yeshurun, G. Logvenov, I. Božović, Large oscillations of the magnetoresistance in nanopatterned high-temperature superconducting films, Nature Nanotechnol. 5 (2010) 516–519.

[14] I. Sochnikov, A. Shaulov, Y. Yeshurun, G. Logvenov, I. Božović, Oscillatory magnetoresistance in nanopatterned superconducting La 1.84 Sr 0.16 CuO 4 films, Phys. Rev. B 82 (2010) 094513.

[15] I. Sochnikov, I. Božović, A. Shaulov, Y. Yeshurun, Uncorrelated behavior of fluxoids in superconducting double networks, Phys. Rev. B 84 (2011) 094530.

[16] G. Berdiyorov, M. Milošević, M. Latimer, Z. Xiao, W. Kwok, F. Peeters, Large magnetoresistance oscillations in mesoscopic superconductors due to current-excited moving vortices, Phys. Rev. Lett. 109 (2012) 057004.

[17] M. Kato, O. Sato, Magnetic flux structures of finite superconducting networks, Supercond. Sci. Technol. 26 (2013) 033001.

[18] M. Itzler, A. Behrooz, C. Wilks, R. Bojko, P. Chaikin, Commensurate states in disordered networks, Phys. Rev. B 42 (1990) 8319.

[19] C. Reichhardt, C.O. Reichhardt, A Bishop, Commensurate and incommensurate checkerboard charge ordered states, Physica C 460 (2007) 1178–1179.

[20] O.V. Dobrovolskiy, Abrikosov fluxonics in washboard nanolandscapes, Physica C (2016).

[21] R. Gross, A. Marx, D. Einzel, From flux quantization to superconducting quantum bits, J. Superconduct. Novel Magnet. 19 (2006) 331–340.

[22] M.V. Milošević, G.R. Berdiyorov, F.M. Peeters, Fluxonic cellular automata, Appl. Phys. Lett. 91 (2007) 212501.

[23] M. Milošević, F. Peeters, Vortex manipulation in a superconducting matrix with view on applications, Appl. Phys. Lett. 96 (2010) 192501.

[24] P. Chaikin, A. Behrooz, M. Itzler, C. Wilks, B. Whitehead, G. Grest, D. Levine, Studies of quasicrystalline superconducting networks, Physica B 152 (1988) 113–124.

[25] R.T. Giles, F.V. Kusmartsev, Critical fields and devil's staircase in superconducting ladders, Physica B 284 (2000) 1850–1851.

[26] C. Da Fonseca, J. Petronilho, Explicit inverse of a tridiagonal k− Toeplitz matrix, Numerische Mathematik 100 (2005) 457–482.

[27] O.J. Sharon, N. Haham, S. Avner, Y. Yeshurun, Fluxoids behavior in superconducting ladders, in: IOP Conference Series, Proceedings of LT28, Gothenburg, Sweden, 2017.

[28] M. Hayashi, H. Ebisawa, M. Kato, Vortex structures in mesoscopic superconducting network systems, Physica C 426 (2005) 136–140.

[29] D. Vasyukov, Y. Anahory, L. Embon, D. Halbertal, J. Cuppens, L. Neeman, A. Finkler, Y. Segev, Y. Myasoedov, M.L. Rappaport, A scanning superconducting quantum interference device with single electron spin sensitivity, Nature Nanotechnol. 8 (2013) 639–644.

[30] Y. Anahory, J. Reiner, L. Embon, D. Halbertal, A. Yakovenko, Y. Myasoedov, M.L. Rappaport, M.E. Huber, E. Zeldov, Three-junction SQUID-on-tip with tunable in-plane and out-of-plane magnetic field sensitivity, Nano Lett. 14 (2014) 6481–6487.

[31] G. Berdiyorov, M. Milošević, F. Peeters, Vortex configurations and critical parameters in superconducting thin films containing antidot arrays: nonlinear Ginzburg–Landau theory, Phys. Rev. B 74 (2006) 174512.

3.2 Fluxoids behavior in superconducting ladders

Omri J. Sharon, Noam Haham, Avner Shaulov and Yosef Yeshurun

Fluxoids behavior in superconducting ladders

Omri J. Sharon, Noam Haham, Avner Shaulov and Yosef Yeshurun

Department of Physics and Institute of Nano Technology, Bar-Ilan University, 5290002   Ramat-Gan, Israel

omri_s@yahoo.com

Abstract. The nature of the interaction between fluxoids and between them and the external magnetic field is studied in one-dimensional superconducting networks. An Ising like expression is derived for the energy of a network revealing that fluxoids behave as repulsively interacting objects driven towards the network center by the effective applied field. Competition between these two interactions determines the equilibrium arrangement of fluxoids in the network as a function of the applied field. It is demonstrated that the fluxoids configurations are not always commensurate to the network symmetry. Incommensurate, degenerated configurations may be formed even in networks with an odd number of loops.

1. Introduction

The macroscopic quantum nature of superconductivity is manifested in loops, and generally in multiply-connected superconductors, in quantization of the 'fluxoid' defined as: $(4\pi\lambda^2/c)\oint j \cdot dl + \Phi$, where j is the shielding current in a closed loop, λ is the penetration depth, and Φ is the magnetic flux threading the loop [1]. In the early days of superconductivity, it was predicted by Fritz London [2], and later confirmed experimentally by Little and Parks [3], that the fluxoid must be an integer multiple of the flux quantum $\phi_0 = hc/2e$. Fluxoid quantization effects have been studied extensively, both theoretically and experimentally, in a variety of superconducting networks [4-12]. However, most of these studies adopt the mean field approach, providing no intuitive understanding of the interaction between fluxoids and the mechanism governing their arrangement in superconducting networks. The purpose of the present work is to elucidate the nature of the interaction between fluxoids and to clarify the physics behind their arrangements in networks. Analyzing the simplest case of a superconducting one-dimensional network ('ladder'), we show that fluxoids act as repulsively interacting objects dragged towards the ladder center by their interaction with the externally applied field. A competition between these two interactions determines the equilibrium positions of the fluxoids in the network as a function of the applied field. To demonstrate this concept we present calculated results of fluxoid arrangements in several examples of finite 1D and 2D networks.

2. Analysis

Our analysis is based on the "current squared" model (known as the "J^2 model") [6], In which the kinetic energy of the network is calculated as the sum of the squared currents over all the network wires. The number and arrangement of the fluxoids is determined by the requirement of minimum energy.

Consider a superconducting ladder of finite length, consisting of N square loops of unit side, as shown in Figure 1.
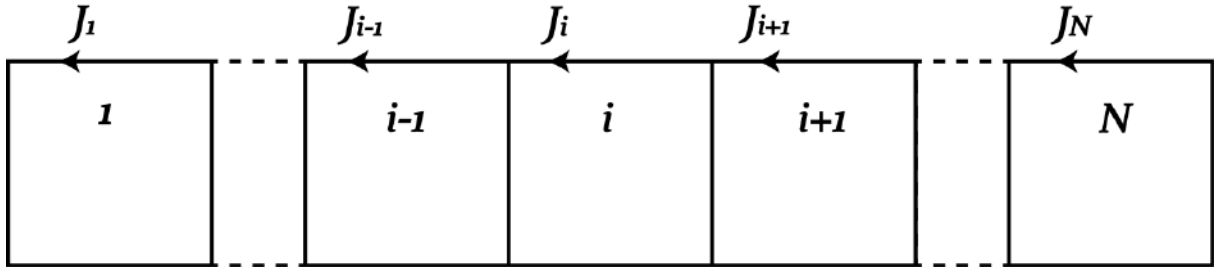
Figure 1: Finite ladder consisting of N square loops.

The fluxoid quantization equation for the loop i reads:

$$4J_i - J_{i-1} - J_{i+1} = n_i - \phi/\phi_0, \tag{1}$$

where n_i is the vorticity of the loop i, ϕ is the flux threading this loop, and by definition $J_i = 0$ for $0 > i$ or $i > N$. For simplicity, the coefficient $4\pi\lambda^2/c$ is taken as 1. According to Eq. (1), the set of the fluxoid quantization equations for all the loops can be written as a matrix equation:

$$\hat{A} \cdot \vec{J} = \vec{n} - \frac{\vec{\phi}}{\phi_0}, \tag{2}$$

where the elements of the matrix $\hat{A}$: $A_{ij} = 4\delta_{i,j} - \delta_{i,j-1} - \delta_{i,j+1}$, and $\delta_{i,j}$ is the Kronecker δ. The current vector $\vec{J}$ can be calculated from Eq. (2) by inversion:

$$\vec{J} = \hat{A}^{-1}(\vec{n} - \frac{\vec{\phi}}{\phi_0}). \tag{3}$$

Denoting the matrix $\hat{A}^{-1}$ as $\hat{B}$, Eq. (3) can be written as a set of equations:

$$J_i = \sum_{j=1}^{N} B_{ij}\left(n_j - \frac{\phi}{\phi_0}\right), \quad i = 1..N. \tag{4}$$

Using the J^2 model, knowledge of J_i allows calculation of the energy E_i of the loop i:

$$E_i = 2J_i^2 + \frac{1}{2}(J_i - J_{i-1})^2 + \frac{1}{2}(J_i - J_{i+1})^2 + \frac{1}{2}J_1^2\delta_{1,i} + \frac{1}{2}J_N^2\delta_{N,i}$$
$$= J_i[3J_i - J_{i-1} - J_{i+1}] + \frac{1}{2}J_{i-1}^2 + \frac{1}{2}J_{i+1}^2 + \frac{1}{2}J_1^2\delta_{1,i} + \frac{1}{2}J_N^2\delta_{N,i},$$

and the total energy E of the network:

$$E = \sum_{i=1}^{N} E_i = \sum_{i=1}^{N}\left\{J_i(3J_i - J_{i-1} - J_{i+1}) + \frac{1}{2}J_{i-1}^2 + \frac{1}{2}J_{i+1}^2\right\} + \frac{1}{2}J_1^2 + \frac{1}{2}J_N^2. \tag{5}$$

Using Eq. (1) and realizing that $\sum_{i=1}^{N}\left\{-J_i^2 + \frac{1}{2}J_{i-1}^2 + \frac{1}{2}J_{i+1}^2\right\} + \frac{1}{2}J_1^2 + \frac{1}{2}J_N^2 = 0$, Eq. (5) becomes

$$E = \sum_{i=1}^{N} J_i\left(n_i - \frac{\phi}{\phi_0}\right). \tag{6}$$

Inserting J_i from Eq. (4) yields

$$E = \sum_{i=1}^{N}\sum_{j=1}^{N} B_{ij}\left(n_j - \frac{\phi}{\phi_0}\right)\left(n_i - \frac{\phi}{\phi_0}\right) = \sum_{ij} B_{ij}\left(n_i n_j - 2\frac{\phi}{\phi_0}n_i + \left(\frac{\phi}{\phi_0}\right)^2\right). \tag{7}$$

The above expression for the total energy, E, is reminiscent of the Ising model for the energy of a spin configuration, having the form $\sum_{ij} J_{ij} S_i S_j$ - $\mu \sum_j h_j S_j$ [13]; n_j, and B_{ij} playing the role of the Ising spin S_j and the exchange interaction term J_{ij}, respectively. The first term on the right hand side of Eq. (7), $\left(\sum_{ij} B_{ij} n_i n_j\right)$, represents the interaction between fluxoids, including the self-interactions $\sum_i B_{ii} n_i^2$. The second term, $\left(-2\frac{\phi}{\phi_0}\sum_{ij} n_i B_{ij}\right)$, expresses the interaction between the fluxoids and the effective magnetic field. The third term, $(\phi/\phi_0)^2 \sum_{ij} B_{ij}$, is constant, independent of the vorticities, and thus may be ignored.

For the matrix $\hat{A}$ given in Eq. (2), $\hat{B} = \hat{A}^{-1}$ is a symmetric matrix with elements [14]:

$$B_{ij} = C\gamma^{i-j-1}\left(1 - \eta^i\right)\left(1 - \eta^{N+1-j}\right), \text{ for } i \leq j. \tag{8}$$

where $\gamma = 2 + \sqrt{3}$, $\eta = (2 - \sqrt{3})/(2 + \sqrt{3})$ and $C = 1/(1 - \eta)(1 - \eta^{N+1})$. Due to the symmetry of $\hat{B}$, B_{ij} for $i > j$ can be calculated as B_{ji} using Eq. (8). Since $\eta \ll 1$, C is approximately 1 and B_{ij} can be approximated as $\gamma^{-(|i-j|+1)}$, for all i and j. Thus Eq. (7) becomes

$$E = \sum_{ij} \gamma^{-(|i-j|+1)}\left(n_i n_j - 2\frac{\phi}{\phi_0}n_i + \left(\frac{\phi}{\phi_0}\right)^2\right) . \tag{9}$$

The above expression shows that fluxoids can be treated as repulsively interacting objects, with interaction energy decreasing exponentially with their separation. In order to minimize the total energy, the repulsive interaction between fluxoids tends to keep them away from each other. On the other hand, the interaction between the fluxoids and the effective magnetic field, represented by the second term in Eq. (9), $\left(-2\phi/\phi_0\sum_i n_i \sum_j \gamma_1^{-(|i-j|+1)}\right)$ tends to drive the fluxoids away from the network edges towards the network's center. This is because the effective magnetic field $-2(\phi/\phi_0)\sum_j \gamma_1^{-(|i-j|+1)} \propto \cosh\left(\ln(\gamma_1)\left((N + 1)/2 - i\right)\right)$ is minimum at the center of the ladder ($i = (N + 1)/2$). Thus, while the external magnetic favors assembling the fluxoids near the ladder center, the fluxoids repel each other tending to keep themselves apart. Competition between these two opposite interactions determines the equilibrium arrangement of fluxoids in the network as a function of the applied field.

Considering the first fluxoid which enters the ladder, it always appears at the center of the network (or next to it, in a ladder with an even number of loops) as it is affected only by the external field which drives it to the center. As the field increases, a second fluxoid appears, pushing the first one out of its central position and both fluxoids arrange themselves in an optimum configuration around the center, keeping apart from each other and away from the network edges. The same principle determines the arrangements of the next fluxoids entering the ladder as the field further increases.

Our analysis of superconducting ladders can be extended to two dimensional superconducting networks. The basic idea that the fluxoid arrangements are determined by a competition between the fluxoid repulsive interaction and their interaction with the applied field, remains the same. However, computations of these interactions, and the resulting fluxoid equilibrium configurations in two dimensional networks become more complicated. The occupation process in 1D and 2D superconducting networks are demonstrated in the following section.

3. Simulations

As an example, we present calculated results for ladders with 7, 8 and 9 loops. In each case, the energy of the ladder, as a function of the loops vorticities and the external field, was calculated using Eq. (7) and the exact expression for the elements B_{ij} (Eq. 8). For each given field the fluxoid arrangement $(n_1, n_2, \ldots, n_N)$ which minimizes the energy was determined.

The solid, dashed, dashed-dotted curves in Figure 2 show the minimum energy as a function of the normalized flux ϕ/ϕ_0 in ladders with 7,8 and 9 loops, respectively. The crests in each curve indicate a change in the fluxoids configurations in the ladder. Thus, in the ladders with 7,8 and 9 elements the total number of configurations is 7,8 and 9, respectively. It is interesting to note that the number of configurations is not necessarily equal to the number of elements. For example, in ladders with rectangular loops attached along their long side, a change of the applied field can cause rearrangement of the same number of fluxoids, giving rise to an access number of configurations [15].
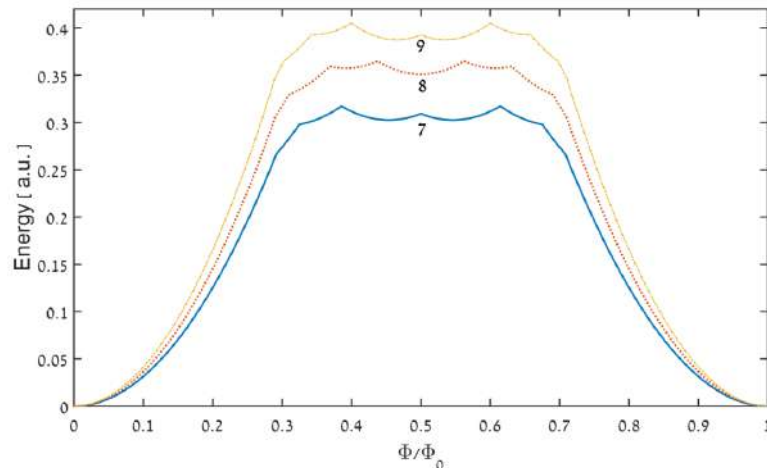

Figure 2: Energy as a function of the normalized magnetic flux in ladders with 7, 8 and 9 loops.
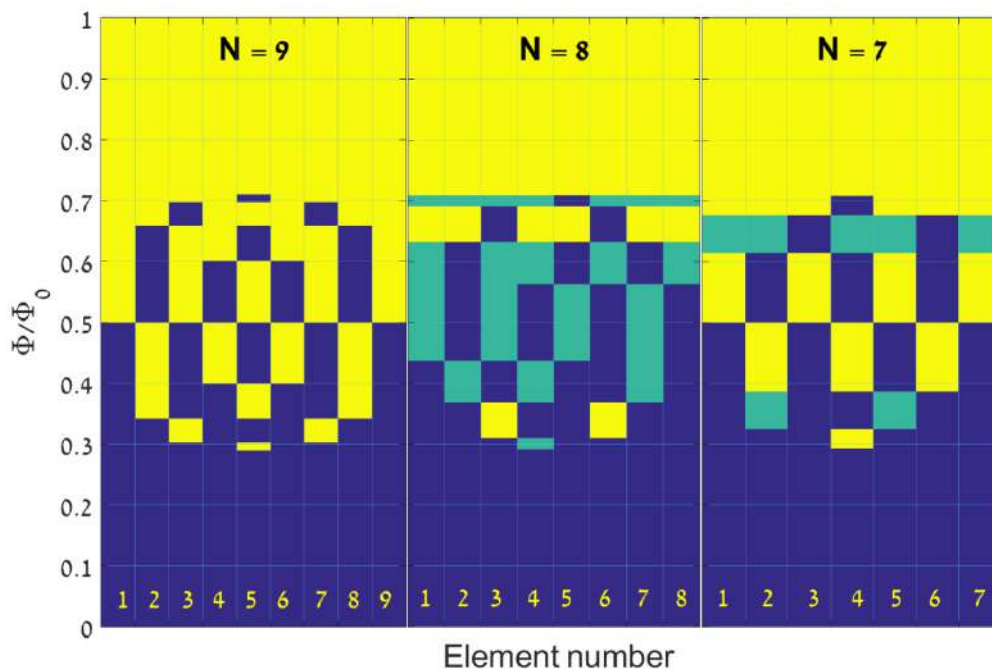

Figure 3: Fluxoid configuration as a function of magnetic flux in ladders with 7, 8 and 9 loops, in the first period. An empty loop is colored dark blue, and occupied loop is colored yellow or green. The green color indicates degenerated configurations which are incommensurate with the symmetry of the ladder.

The fluxoids arrangements as a function of field are illustrated in Figure 3. An empty loop is colored blue, and occupied loop is colored yellow or green. The green color indicates degenerated

configurations which are incommensurate with the symmetry of the ladder. The ladders with 7 and 9 loops demonstrate the general rule that when the number of loops is odd, the first fluxoid always occupies the loop at the ladder's center. In ladders with an even number of loops, the first fluxoid occupies a degenerated state on either side of the center, as demonstrated by the ladder with 8 loops. As the field increases, a second fluxoid enters the ladder, pushing the first one out of its position and both fluxoids arrange themselves in an optimum configuration, keeping apart from each other and away from the network edges. In the ladder with 9 loops, this configuration conforms the symmetry of the ladder, however, this is not the case in the ladders with 7 and 8 elements. As more fluxoids enter the ladder with increasing field, rearrangement of fluxoids continues until the last fluxoid enters the ladder's center completing one period in which each loop is occupied with one fluxoid. Occupation of the loops in the following periods follows the same pattern.

Figure 4 illustrates calculated results for a 3x3 square network, based on the J^2 model. Note that the first fluxoid appears in the central loop of the network, as in a ladder. Also note that the number of different configurations (11) exceeds the number of loops in the network, due to rearrangement of the same number of fluxoids as the field increases. This situation occurs in configurations of 3 and 6 fluxoids. Among the 11 different configurations, there are 6 degenerated states that are incommensurate to the network symmetry (marked in green in Fig. 4). The degenerated configurations are obtained by applying the symmetry operations of the network. Thus, two degenerated configurations correspond to N=2,7, and four degenerated configurations correspond to each configuration with N=3,6.

We note that calculations based on the de-Gennes-Alexander equations for a network yield quite different results [16]. For example, following the appearance of the first fluxoid at the network central loop, the second fluxoid appears at the same loop creating a double fluxoid at the network center. This configuration has a higher energy than that the configuration of two separated fluxoids derived from the $'J^2$ model' (see Fig. 4). Involving the appearance of anti-fluxoids in the network, the calculation based on the de-Gennes-Alexander equations, predicts 9 configurations all of which are commensurate to the network symmetry. It should be noted, however, that by minimizing the Ginzburg–Landau free energy, asymmetric fluxoid patterns have been reported for a 10x10 network [17]. Finally we note that in our calculations based on the J^2 model, the fluxoid configurations are temperature independent, as the only temperature dependent factor in this model is $4\pi\lambda^2/c$ which scales the current density, and the square of this factor scales the energy.
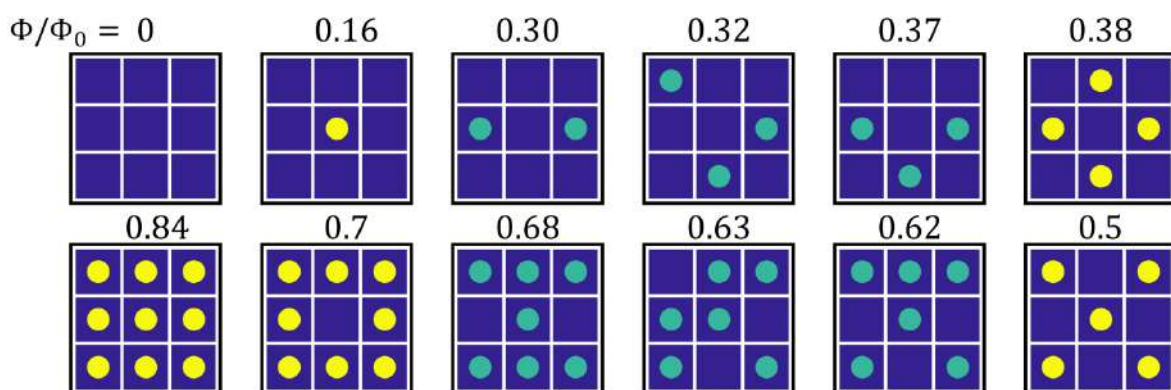

Figure 4: Fluxoid configurations in 3x3 square network calculated in the framework of the $'J^2$ model'. An empty loop is colored dark blue, and occupied loop is colored yellow or green. The green color indicates degenerated configurations which are incommensurate with the symmetry of the ladder.

4. Summary and conclusions

An Ising-like expression derived for the energy of fluxoids in a 1D superconducting network reveals that the fluxoids act as repulsively interacting objects with an interaction energy that decreases exponentially with their relative separation. In this expression, the effective magnetic field drives the fluxoids toward the network center. The competition between these two interactions determines the equilibrium configuration of the fluxoids in the ladders. These configurations may be incommensurate to the symmetry of the ladder, in ladders with even as well as odd number of loops. Fluxoids in 2D networks follow a similar pattern, i.e. they repel each other and are driven to the center by the applied field.

References
[1]　Tinkham M 1996 *Introduction to superconductivity* 2nd edition: McGraw-Hill, Inc.
[2]　London F 1948 On the Problem of the Molecular Theory of Superconductivity *Physical Review* **74** 562-73
[3]　Parks R and Little W 1964 Fluxoid quantization in a multiply-connected superconductor *Physical Review* **133** A97
[4]　Pannetier B, Chaussy J, Rammal R and Villegier J 1984 Experimental fine tuning of frustration: Two-dimensional superconducting network in a magnetic field *Physical review letters* **53** 1845
[5]　Behrooz A, Burns M, Levine D, Whitehead B and Chaikin P 1987 Superconducting phase boundary of aperiodic networks in a magnetic field *Physical Review B* **35** 8396
[6]　Chaikin P, Behrooz A, Itzler M, Wilks C, Whitehead B, Grest G and Levine D 1988 Studies of quasicrystalline superconducting networks *Physica B: Condensed Matter* **152** 113-24
[7]　Gordon J M, Goldman A M and Whitehead B 1987 Dimensionality crossover in superconducting wire networks *Physical review letters* **59** 2311
[8]　Chi C, Santhanam P and Blöchl P 1992 Interacting loop-current model of superconducting networks *Journal of low temperature physics* **88** 163-95
[9]　Bruyndoncx V, Strunk C, Moshchalkov V, Van Haesendonck C and Bruynseraede Y 1996 Fluxoid quantization effects in superconducting mesoscopic Al multiloop structures *EPL (Europhysics Letters)* **36** 449
[10]　Reich D H, Silevitch D M, Chien C, Davidovic D and Field S 2000 Disorder and correlations in extended superconducting nanostructures *Journal of Alloys and Compounds* **303** 245-51
[11]　Burlakov A, Gurtovoĭ V, Dubonos S, Nikulov A V and Tulin V 2007 Little-parks effect in a system of asymmetric superconducting rings *JETP Letters* **86** 517-21
[12]　Sochnikov I, Shaulov A, Yeshurun Y, Logvenov G and Božović I 2010 Large oscillations of the magnetoresistance in nanopatterned high-temperature superconducting films *Nature Nanotechnology* **5** 516-9
[13]　Giles R T and Kusmartsev F V 2000 Critical fields and devil's staircase in superconducting ladders *Physica B: Condensed Matter* **284** 1850-1
[14]　Da Fonseca C and Petronilho J 2005 Explicit inverse of a tridiagonal k− Toeplitz matrix *Numerische Mathematik* **100** 457-82
[15]　Sharon O J, Haham N, Shaulov A A and Yeshurun Y 2017 Fluxoids configurations in finite superconducting networks *Unpublished*
[16]　Kato M and Sato O 2013 Magnetic flux structures of finite superconducting networks *Superconductor Science and Technology* **26** 33001-26
[17]　Hayashi M, Ebisawa H and Kato M 2005 Vortex structures in mesoscopic superconducting network systems *Physica C: Superconductivity* **426** 136-40

3.3 Current-induced SQUID behavior of superconducting Nb nano-rings

Omri J. Sharon, Avner Shaulov, Jorge Berger, Amos Sharoni, and Yosef Yeshurun

SCIENTIFIC REP⚙RTS

Current-induced SQUID behavior of superconducting Nb nano-rings

Omri J. Sharon[1], Avner Shaulov[1], Jorge Berger[2], Amos Sharoni[1] & Yosef Yeshurun[1]

The critical temperature in a superconducting ring changes periodically with the magnetic flux threading it, giving rise to the well-known Little-Parks magnetoresistance oscillations. Periodic changes of the critical current in a superconducting quantum interference device (SQUID), consisting of two Josephson junctions in a ring, lead to a different type of magnetoresistance oscillations utilized in detecting extremely small changes in magnetic fields. Here we demonstrate current-induced switching between Little-Parks and SQUID magnetoresistance oscillations in a superconducting nano-ring without Josephson junctions. Our measurements in Nb nano-rings show that as the bias current increases, the parabolic Little-Parks magnetoresistance oscillations become sinusoidal and eventually transform into oscillations typical of a SQUID. We associate this phenomenon with the flux-induced non-uniformity of the order parameter along a superconducting nano-ring, arising from the superconducting leads ('arms') attached to it. Current enhanced phase slip rates at the points with minimal order parameter create effective Josephson junctions in the ring, switching it into a SQUID.

Small-size SQUIDs attract considerable interest for investigations of local magnetic signals, measuring, e.g., dynamics and pinning of single vortices[1,2] and local superfluid density in superconductors[3], ferromagnetic patches at the $LaAlO_3/SrTiO_3$ interface[4], quantum magnetization reversal of ferromagnetic nanoparticles[5] and single molecule magnets[6]. A few designs of small SQUIDs without Josephson junctions have been proposed, based on mesoscopic superconducting loops[7], asymmetric superconducting rings[8], inhomogeneous superconductors[9], constrictions in the superconducting rim[10], interrupted mesoscopic normal loop in contact with two superconducting electrodes[11], and a combination of superconducting and metallic contact banks[12]. SQUIDs without Josephson junctions may offer advantages in simplicity of fabrication, and, under certain conditions, a steeper dependence of the measured quantities on the magnetic flux[8]. The present study may offer a different approach in designing a SQUID without Josephson junctions by switching a nano-ring with two arms into a SQUID using a large enough bias current. The potential application of such a SQUID will be discussed elsewhere. Here we focus on the fundamentally important observation of current-induced switching between Little-Parks and SQUID magnetoresistance oscillations in Nb nano-rings.

Niobium amorphous films, 40 nm thick, were deposited from a Nb target on silicon substrates via DC-magnetron sputtering. The films were patterned into square rings (side 340 nm, rim's width 55 nm) with two arms (65 nm wide, 250 nm long) as shown in Fig. 1. For signal amplification, a string consisting of a serial connection of 260 such rings was measured. Details of the sputtering and patterning processes are described in the *Methods* Section. Measurements were performed near the superconducting transition temperature for bias currents between 10 nA and 10 μA, employing a commercial Physical Properties Measurements System (PPMS, Quantum-Design).

Figure 2 shows the temperature dependence of the resistance of a single ring with two arms measured at zero applied magnetic field. The curve corresponding to the lowest measuring current exhibits a sharp transition at $T_c \sim 7.2$ K with a width $\lesssim 0.1$ K. As the current increases, the R(T) curves are shifted to lower temperatures, as expected. The right inset to Fig. 2 shows the temperature dependence of the sample resistance over an extended temperature range, between room temperature and 4 K, using measuring current of 10 nA.

Figure 3 shows typical magnetoresistance oscillations measured at T = 7.1 K, representing three different types of waveforms obtained for different measuring currents. At low currents (1 μA and below) classical Little-Parks oscillations[13] are obtained, exhibiting parabolic shape with *upward* cusps at odd multiples of $\Phi_0/2$, and a field-period of ~170 Oe, corresponding to the area of a single ring (~$1.2 \cdot 10^{-9}$ cm²). For higher currents, in the range ~2–3 μA, the cusps disappear and the oscillations become sinusoidal. As the current further increases to 4 μA, the waveform drastically changes, exhibiting *downward* cusps at multiples of Φ_0, typical of the

[1]Department of Physics and Institute of Nano Technology, Bar-Ilan University, 5290002 Ramat-Gan, Israel. [2]Department of Physics and Optical Engineering, Ort Braude College, 21982 Karmiel, Israel. Correspondence and requests for materials should be addressed to Y.Y. (email: yosiyeshurun@gmail.com)
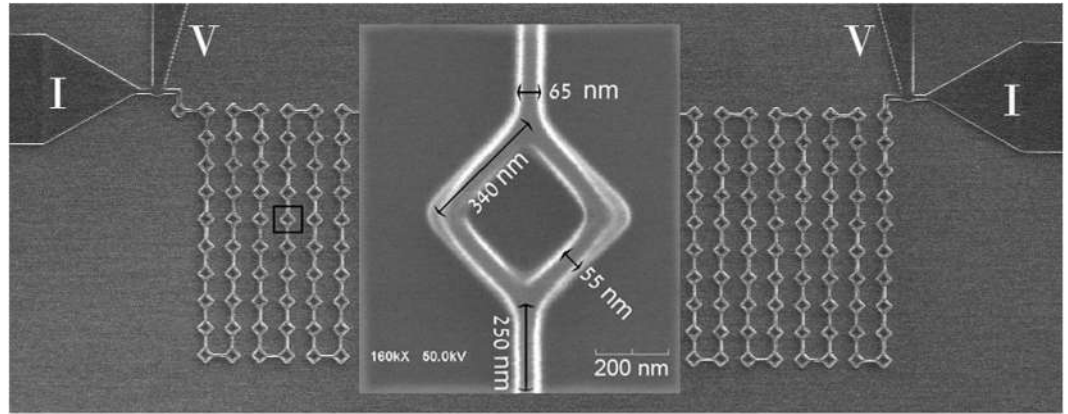
Figure 1. A Scanning Electron Microscope (SEM) image of a single ring with two arms. The background shows the serially connected rings with the current and voltage leads.
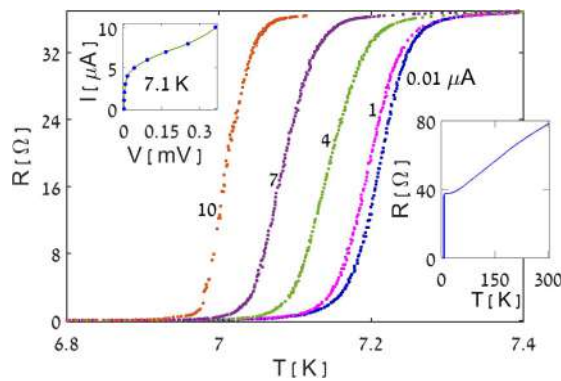
Figure 2. Resistance of a single ring with two arms versus temperature measured with different bias currents. Right inset: Temperature dependence of the resistance in an extended temperature range for I = 10 nA. Left inset: I-V curve measured at 7.1 K in zero field.

magnetoresistance response of a SQUID biased with a current that is equal to its maximum supercurrent[14]. The data of Fig. 3 can thus be well interpreted as indicating a current induced switching of the ring into a SQUID. Similar results were obtained in a narrow temperature range between 7 and 7.15 K. However, the current required to obtain the SQUID response sharply increased with decreasing temperature, such that below 7 K it reached a level beyond the limit of our system. In addition, we performed measurements at constant currents varying the temperature between 6.5 and 7.2 K. These measurements showed that SQUID like magnetoresistance oscillations can also be obtained by increasing the temperature biasing the sample at a high current.

To better illustrate the current-induced switching between Little-Parks and SQUID magnetoresistance oscillations, we add in Fig. 3 guide to the eye solid curves through the data points, based on theoretical predictions for the various types of magnetoresistance oscillations, ΔR. The theoretical curves are superimposed on the measured monotonous background. The lowest curve (1 μA) in Fig. 3 describes typical Little-Parks parabolic oscillations (see, e.g. Figure 4.5 in ref. 15):

$$\Delta R_{LP} \propto \left(n - \frac{\Phi}{\Phi_0}\right)^2; \quad \left(n - \frac{1}{2}\right)\Phi_0 \leq \Phi \leq \left(n + \frac{1}{2}\right)\Phi_0, \; n = 0, \pm 1, \pm 2, \dots. \tag{1}$$

The intermediate curves (2 and 3 μA), correspond to the Little-Parks oscillations in a ring with two symmetric Josephson junctions (i.e., a SQUID), calculated on the basis of the J² model[16]. According to this model, the magnetoresistance oscillations in a single superconducting loop follow the field dependence of the square of the screening current I_s. Thus, the linear field dependence of I_s in a simple ring gives rise to parabolic oscillations. However, in a SQUID the screening current is sinusoidal, $|I_s| = I_c |\sin(\pi\Phi/\Phi_0)|$, where I_c is the critical current of each of the Josephson junctions forming the SQUID[17]. Accordingly, the Little-Parks oscillations in a SQUID are expected to be sinusoidal:

$$\Delta R_{LP-SQUID} \propto \sin^2\left(\frac{\pi\Phi}{\Phi_0}\right). \tag{2}$$
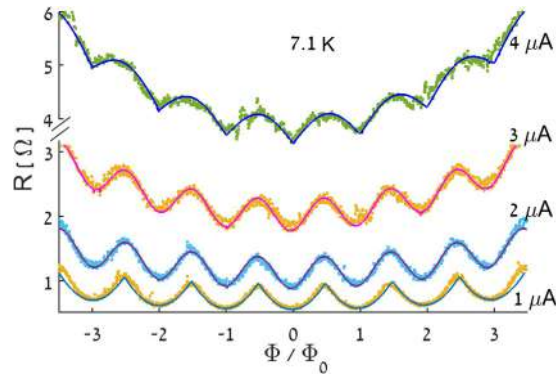
Figure 3. Magnetoresistance of a single ring for different bias currents. Measurements performed at $T = 7.1\,K$ with currents between $1\,\mu A$ and $4\,\mu A$ are described as a function of the magnetic flux, Φ, normalized to the quantum flux, Φ_0, taking the ring area as $1.2 \cdot 10^{-9}\,cm^2$. The guide to the eye solid curves through the data points describe classical Little-Parks parabolic oscillations ($1\,\mu A$ curve), Little-Parks sinusoidal oscillations in a SQUID (2 and $3\,\mu A$ curves) and typical SQUID oscillations ($4\,\mu A$ curve), Eqs (1), (2) and (4), respectively, superimposed on monotonic backgrounds.

Note that in a conventional SQUID it is assumed that the rim width is larger than the superconducting penetration depth, λ, and, therefore, the Little-Parks effect is unobservable. However, in our case, as is virtually the case in all nano-rings, the rim width is smaller than λ. Thus, magnetoresistance oscillations due to Little-Parks effect, Eq. (2), are expected in such SQUIDs near T_c.

The upper solid curve in Fig. 3, corresponding to $4\,\mu A$, is based on the formula for the average voltage across a SQUID in the dissipative regime,

$$V = (R_s/2)\{I^2 - [2I_c \cos(\pi\Phi/\Phi_0)]^2 \}^{1/2}, \tag{3}$$

where R_s is the junction's shunt resistance and I_c is the critical current of each of the Josephson junctions (see Eq. 6.48 in Ref. 15). Assuming that the external current $I = 2I_c$, one obtains:

$$\Delta R_{SQUID} \propto \left[1 - \cos^2\left(\frac{\pi\Phi}{\Phi_0}\right)\right]^{1/2} = \left|\sin\left(\frac{\pi\Phi}{\Phi_0}\right)\right|. \tag{4}$$

The agreement between the calculated curves and the data shown in Fig. 3 supports our scenario of current-induced switching of a superconducting nano-ring with two arms into a SQUID.

The data of Fig. 3 indicate that the crossover from a ring to a SQUID occurs for currents around $2\,\mu A$, where the parabolic Little-Parks oscillations transform to sinusoidal oscillations. As noted above, the bias current of $\sim 4\,\mu A$ corresponds to the SQUID response for external current that equals the maximum supercurrent of the SQUID, $I_m(\Phi = 0) = 2I_c$. Indeed, the I-V curve measured at 7.1 K in zero field (see left inset to Fig. 2) shows an abrupt voltage increase around this current. It should be noted that the bias current of $4\,\mu A$ includes the current ($\sim 2\,\mu A$) needed to transform the ring into a SQUID. Thus, the maximum supercurrent of the SQUID, $I_m(0)$, is approximately $2\,\mu A$. The dependence of I_m on Φ can be deduced from the data of Fig. 3, using Eq. (3). The results are shown in Fig. 4 together with the theoretical $I_m(\Phi)$ in a conventional SQUID (solid line). The theoretical curve is superimposed on the bias current I_0 required for the creation of our SQUID:

$$I_m = I_0 + 2I_c|\cos(\pi\Phi/\Phi_0)|. \tag{5}$$

In deriving $I_m(\Phi)$, the background was subtracted and the junction's shunt resistance for a single SQUID was estimated as $R_S = 2.3\,\Omega$, corresponding to twice the measured resistance of the SQUID at $\Phi_0/2$. The oscillatory behavior of the critical current above a bias current of $2\,\mu A$ seems to compare quite well with that of a real SQUID with two Josephson junctions (solid curve in Fig. 4). Note, however, that our current-induced SQUID does not show the plateau behavior of $I_m(\Phi)$ around integer flux quanta as proposed in Refs 7 and 18.

The current induced switching of a superconducting nano-ring with two arms into a SQUID can be understood considering the non-uniform order parameter along the ring in such a structure when a magnetic field is applied[19–23]. Based on the Ginzburg-Landau equations, de-Gennes[19] and Alexander[20] showed that two minima of the order parameter are generated at equal distances from the connection points of the arms to the ring[20,21]. An intuitive way to understand this result is by starting with a ring with a single arm. As the arm is not affected by the magnetic flux, the order parameter along the ring has a maximum at the connection point and a minimum at the antipodal point. This minimum drops to zero at the onset of superconductivity when the flux becomes equal to a half flux quantum, $\Phi = \Phi_0/2$. When two symmetrical arms are connected to a ring, the order parameter is maximum at the connection points and minimum at equal distances from these points[20,21]. Solving the nonlinear Ginzburg-Landau equations, Fink *et al.*[18] predicted that the maximum supercurrent in a ring with two arms of size comparable to the coherence length, depends periodically on Φ in a way similar to a classical SQUID.
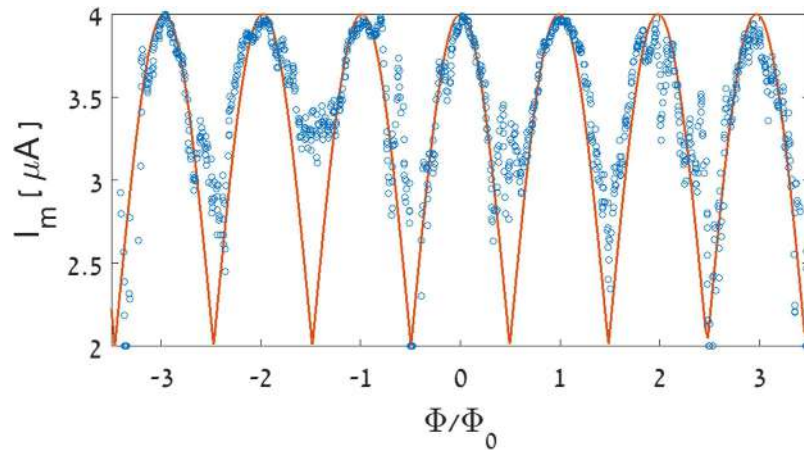
Figure 4. The maximum supercurrent I_m of the current-induced SQUID as a function of the normalized flux. The solid curve describes the theoretical $I_m(\Phi)$ in a conventional SQUID superimposed on the bias current I_0 required for the creation of the SQUID, Eq. (5). The junction's shunt resistance R_S is taken as $2.3\,\Omega$.

Experimental confirmation of this prediction was demonstrated in Al mesoscopic rings using current-voltage measurements[7]. The previous studies[7,22] emphasized the role of the geometrical parameters of the ring and did not consider the role of the bias current in inducing the SQUID behavior. Our magnetoresistance measurements indicate that the geometry alone is insufficient to produce a SQUID without the involvement of large enough bias current. This is evident from the classical parabolic Little-Parks oscillations observed at low bias current (lowest curve in Fig. 3). As explained above, formation of a SQUID at these low bias currents would result in sinusoidal rather than parabolic Little-Parks oscillations. Such sinusoidal oscillations are observed only when the bias current is increased to $\sim2\,\mu A$.

The role of the bias current in inducing a SQUID behavior can be associated with current-induced phase slips[24]. Currents above $I_m(\Phi)$ generate a voltage drop across the SQUID. Due to the position dependence of the voltage, the phase of the order parameter changes at different rates in different places, leading to phase slips that are more effective at the points with weakest superconductivity in the circuit. Phase slips at these points further reduce the order parameter down to a level required for the creation of effective Josephson junctions. Note that the current passes asymmetrically through some of the loops sitting at the right and left sides of the array, see Fig. 1. However, as shown in refs 8 and 25, except for skewness the behavior of an asymmetric loop is similar to that of a symmetric loop.

For the creation of the Josephson junctions within the range of a single Φ_0, the weak links must be limited to a length scale comparable to the coherence length, $\xi(T)$. Furthermore, for the phase slips to be effective, the rim's cross-section should be of order $\xi^2(T)$. These requirements are satisfied at temperatures close to T_c where $\xi(T) = \xi_0(1 - T/T_c)^{-1/2} = 340$ nm at $T = 7.1$ K, taking the zero temperature coherence length $\xi_0 = 37$ nm[10]. Finally, we note that the possibility of coupling of the response of neighboring rings due to non-local effects is excluded because the distance between neighboring rings is an order of magnitude larger than ξ_0. Non-locality between neighboring rings due to the magnetic field generated by the rings is also excluded, since close to T_c the screening currents are negligibly small.

In conclusion, we have demonstrated that a superconducting nano-ring with two arms can be switched into a SQUID by externally applied bias current. The SQUID behavior was demonstrated by the current induced transformation of the Little-Parks magnetoresistance oscillations from parabolic into sinusoidal oscillations and eventually into oscillations typical of a SQUID. The formation of a SQUID is attributed to the combined effects of current induced phase slips and non-uniform order parameter along the ring caused by the superconducting arms. We note that such superconducting structures comprising a ring with two arms are common in nano-fabrication in which the arms serve as leads to the ring. Such superconducting nano-structures may be utilized as field sensitive nano-devices without artificial Josephson junctions.

Methods

Niobium thin films were deposited from a Nb target (99.95%, ACI Alloys) on silicon substrates with $1\,\mu m$ of thermal silicon oxide via DC-magnetron sputtering. Sputtering was performed in 2 mTorr Ar pressure, at room temperature and a rate of 1.8 Å/s, to a total thickness of 40 nm. Subsequently, the Nb films were spin-coated with about 200 nm of Poly(methyl ethacrylate) (PMMA) 950 A4 resist (Microchem Corp.) and baked on a hot-plate at 180 °C for 120 seconds.

Masks were made using Electron-Beam Lithography by overexposing the PMMA and causing the PMMA polymers to be cross-linked as described in[26,27]. The Nb was etched with Reactive Ion Etching (RIE) using SF_6. The full procedure is described in[28]. Electrical contacts were made by wire bonding of 25 um thick aluminum wires directly to the Nb.

References

1. Finkler, A. *et al.* Self-aligned nanoscale SQUID on a tip. *Nano Letters* **10,** 1046–1049 (2010).
2. Embon, L. *et al.* Probing dynamics and pinning of single vortices in superconductors at nanometer scales. *Scientific reports* **5,** 1–9 (2015).
3. Luan, L. *et al.* Local measurement of the superfluid density in the pnictide superconductor Ba $(Fe_{1-x}Co_x)_2As_2$ across the superconducting dome. *Physical Review Letters* **106,** 067001 (2011).
4. Kalisky, B. *et al.* Scanning probe manipulation of magnetism at the LaAlO3/SrTiO3 heterointerface. *Nano Letters* **12,** 4055–4059 (2012).
5. Wernsdorfer, W. *et al.* Macroscopic quantum tunneling of magnetization of single ferrimagnetic nanoparticles of barium ferrite. *Physical Review Letters* **79,** 4014 (1997).
6. Suzuki, Y. *et al.* Propagation of avalanches in $Mn_{12-acetate}$: Magnetic Deflagration. *Physical Review Letters* **95,** 147201 (2005).
7. Moshchalkov, V., Gielen, L., Dhallé, M., Van Haesendonck, C. & Bruynseraede, Y. Quantum interference in a mesoscopic superconducting loop. *Nature* **361,** 617–620 (1993).
8. Burlakov, A., Gurtovoi, V., Il'in, A., Nikulov, A. V. & Tulin, V. Superconducting quantum interference device without Josephson junctions. *JETP letters* **99,** 169–173 (2014).
9. Il'ichev, E., Zakosarenko, V., Tishinin, D., Tulin, V. & Jacobsen, C. Radio-frequency properties of inhomogeneous superconductors in low magnetic fields (SQUIDs). *Superconductor Science and Technology* **8,** 180 (1995).
10. Troeman, A. G. *et al.* NanoSQUIDs based on niobium constrictions. *Nano Letters* **7,** 2152–2156 (2007).
11. Wei, J., Cadden-Zimansky, P. & Chandrasekhar, V. Observation of large h/2e and h/4e oscillations in a proximity dc superconducting quantum interference device. *Applied Physics Letters* **92,** 102502 (2008).
12. Berger, J. Proposal for a stationary micro-SQUID. *arXiv preprint arXiv:1508.05177* (2015).
13. Little, W. & Parks, R. Observation of quantum periodicity in the transition temperature of a superconducting cylinder. *Physical Review Letters* **9,** 9 (1962).
14. Clarke, J. & Braginski, A. I. (Editors). *The SQUID Handbook, Volume I: Fundamentals and Technology of SQUIDs and SQUID Systems.* (Wiley VCH Verlag GmbH & Co. KGaA, Weinheim, 2006).
15. Tinkham, M. Introduction to Superconductivity: (Dover Books on Physics)(Vol i) pp. 172–174 (2004).
16. Grest, G. S., Chaikin, P. M. & Levine, D. Commensurate states on incommensurate lattices. *Physical Review Letters* **60,** 1162 (1988).
17. Rose-Innes, A. C. & Rhoderick, E. H. Introduction to Superconductivity, 2nd edition. (Pergamon Press, New York, 1978).
18. Fink, H., Grünfeld, V. & López, A. Quantum-interference device without Josephson junctions. *Physical Review B* **35,** 35 (1987).
19. de Gennes, P.-G. Suspensions colloïdales dans un mélange binaire critique. *C. R. Acad. Sci. B* **292,** 279, 9 (1981).
20. Alexander, S. Superconductivity of networks. A percolation approach to the effects of disorder. *Physical Review B* **27,** 1541 (1983).
21. Rammal, R., Lubensky, T. & Toulouse, G. Superconducting networks in a magnetic field. *Physical Review B* **27,** 2820 (1983).
22. Berger, J. & Rubinstein, J. *Connectivity and superconductivity.* Vol. 62 (Springer Science & Business Media, 2000).
23. Kato, M. & Sato, O. Magnetic flux structures of finite superconducting networks. *Superconductor Science and Technology* **26,** 33001–33026 (2013).
24. Sivakov, A. *et al.* Josephson behavior of phase-slip lines in wide superconducting strips. *Physical Review Letters* **91,** 267001 (2003).
25. Burlakov, A., Gurtovoi, V., Dubonos, S., Nikulov, A. V. & Tulin, V. Little-parks effect in a system of asymmetric superconducting rings. *JETP Letters* **86,** 517–521 (2007).
26. Teh, W., Liang, C.-T., Graham, M. & Smith, C. G. Cross-linked PMMA as a low-dimensional dielectric sacrificial layer. *Journal of Microelectromechanical Systems* **12,** 641–648 (2003).
27. Teh, W., Luo, J., Liang, C.-T. & Smith, C. in *MEMS/NEMS* 504–552 (Springer, 2006).
28. Zhong, Q., Cao, W., Li, J., Zhong, Y. & Wang, X. *Study of dry etching process using SF_6 and CF_4/O_2 for $Nb/Nb_xSi_{1-x}/Nb$ Josephson-junction fabrication.* Paper presented at Conference on Precision Electromagnetic Measurements: CPEM, Washington, DC. Precision Electromagnetic Measurements, 2012 Conference on, pp 46–47: IEEE. (doi: 10.1109/CPEM.2012.6250653) (2012 July 1–6).

Acknowledgements

Author Contributions

O.J.S. designed and performed the experiment. Avner Shaulov and Y.Y. analyzed the data and wrote the manuscript. Amos Sharoni prepared and characterized the Nb films and wrote the relevant Methods section. J.B. assisted in theoretical aspects and reviewed the manuscript.

Additional Information

Competing financial interests: The authors declare no competing financial interests.

How to cite this article: Sharon, O. J. *et al.* Current-induced SQUID behavior of superconducting Nb nano-rings. *Sci. Rep.* **6,** 28320; doi: 10.1038/srep28320 (2016).

3.4 Little-Parks oscillations in superconducting ring with Josephson junctions

Omri J. Sharon, Amos Sharoni, Jorge Berger, Avner Shaulov, and Yosef Yeshurun

Little-Parks oscillations in superconducting ring with Josephson junctions

Omri J. Sharon[1], Amos Sharoni[1], Jorge Berger[2], Avner Shaulov[1], and Yosi Yeshurun[1]

[1] Department of Physics and Institute of Nano Technology, Bar-Ilan University, 5290002 Ramat-Gan, Israel

[2] Department of Physics, Ort Braude College, 21982 Karmiel, Israel

omri_s@yahoo.com

Abstract. Nb nano-rings connected serially by Nb wires exhibit, at low bias currents, the typical parabolic Little-Parks magnetoresistance oscillations. As the bias current increases, these oscillations become sinusoidal. This result is ascribed to the generation of Josephson junctions caused by the combined effect of current-induced phase slips and the non-uniformity of the order parameter along each ring due to the Nb wires attached to it. This interpretation is validated by further increasing the bias current, which results in magnetoresistance oscillations typical of a SQUID.

1. Introduction

The Little-Parks magnetoresistance oscillations in superconducting rings have been extensively studied both theoretically and experimentally, see e.g. [1-13]. However, quite frequently the observed oscillations' waveform deviates from the predicted parabolic oscillations, exhibiting sinusoidal-like oscillations, see e.g. [2-4]. Such deviations can be related to a distribution of the ratio ξ/R in a wide ring [2] (ξ is the coherence length and R is the radius of the ring), or to a size distribution of rings in a network [3]. In this article we propose an alternative explanation associated with the existence of Josephson junctions (JJ) in a ring. The existence of such junctions is highly probable in superconducting nano-rings with superconducting leads ('arms') attached to them. Such superconducting structures comprising a ring with two arms are common in nano-fabrication in which the arms serve as leads to the ring. As shown by de-Gennes [14] and Alexander [15] the arms cause a non-uniform order parameter along the ring with two minima at equal distances from the connection points of the arms to the ring. In the presence of large enough bias-current, enhanced phase slips at these minima can generate Josephson junctions in the ring [16]. In this paper we show that in such a ring with Josephson junctions, the Little-Parks (LP) oscillations should become sinusoidal. We demonstrate this effect in Nb nano-rings by showing that the parabolic Little-Parks oscillations at low bias currents are switched into sinusoidal oscillations by increasing the bias current.

2. Experimental

E-beam lithography was used to fabricate Nb square loops (340x340 nm^2) connected serially by 66 nm wide Nb wires, see right panel of Figure 1. The ring rim (~57 nm) is of the order of the zero

temperature coherence length in Nb, ξ_0 = 40 nm. For details of the fabrication process see Ref. [16]. Magnetoresistance measurements were performed using a commercial system (PPMS, Quantum-Design).

3. Results

Current-induced switching of the classical LP parabolic oscillations into sinusoidal ones is demonstrated in the left panel of Figure 1 which shows typical magnetoresistance oscillations measured at T = 7.1 K. At low currents (1 µA and below) parabolic LP oscillations are obtained [1], exhibiting upward cusps at odd multiples of $\Phi_0/2$, and a field-period of ~ 170 Oe, corresponding to the area of a single ring (~$1.2 \cdot 10^{-9}$ cm^2). For higher currents, (2 - 3 µA), the cusps disappear and the oscillations become sinusoidal. As we argue below, this change results from generation of Josephson junctions in the rings. A clear manifestation of the existence of these junctions is obtained by further increasing the current to 4 µA, yielding oscillations with downward cusps at multiples of Φ_0, typical of the magnetoresistance response of a SQUID biased with a current that is equal to its maximum critical current [17].
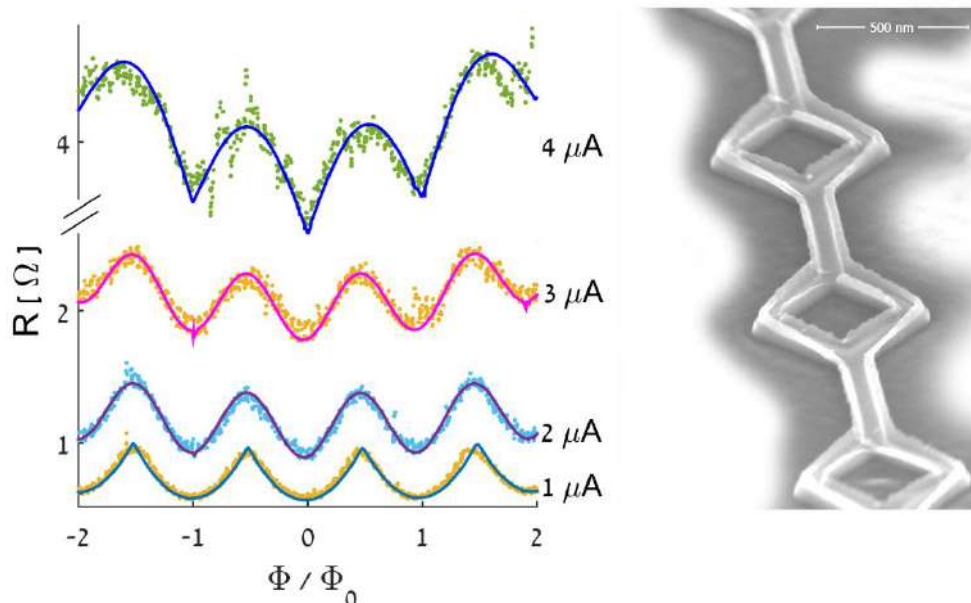

Figure 1. Left panel: Magnetoresistance of a single Nb ring measured at T = 7.1 K with currents between 1 and 4 µA. The magnetic flux, Φ, is normalized to the quantum flux, Φ_0, and calculated for a ring area of $1.2 \cdot 10^{-9}$ cm^2. The solid curves through the data points are guide to the eye. Right panel: A scanning electron microscope image of the Nb rings.

4. Discussion

We begin by considering the effect of a single arm on a ring. As the arm is not affected by the magnetic flux, the order parameter along the ring has a maximum at the connection point and a minimum at the antipodal point. This minimum drops to zero when the flux becomes equal to a half flux quantum, $\Phi = \Phi_0/2$ [18, 19]. When two symmetrical arms are connected to a ring, the order parameter is maximum at the connection points and minimum at equal distances from these points [18, 19]. Current-induced phase slips at these minima further reduce the order parameter down to a level required for the creation of effective Josephson junctions.

We recall that screening current in a ring without Josephson junctions is linear with the magnetic flux, with discontinuities at odd multiplications of $\Phi_0/2$:

$$(2)\ I_s^{LP-JJ} = I_c \sin(\pi\Phi/\Phi_0)\cos(\pi n)\ ; \ \left(n-\frac{1}{2}\right)\Phi_0 \leq \Phi \leq \left(n+\frac{1}{2}\right)\Phi_0, n = 0, \pm 1, \pm 2, ...$$

as shown by the dashed line in Figure 2. Consequently, the magnetoresistance, which is proportional to the kinetic energy I_s^2 [20-22] is parabolic (see the dashed line in Figure 3). However, for a ring with Josephson junctions of critical current I_c, the dependence of the screening current $I_s^{(LP-JJ)}$ on Φ/Φ_0 is [23]:

$$(2)\ \ I_s^{LP-JJ} = I_c \sin(\pi\Phi/\Phi_0)\cos(\pi n)\ ; \ \left(n-\frac{1}{2}\right)\Phi_0 \leq \Phi \leq \left(n+\frac{1}{2}\right)\Phi_0, n = 0, \pm 1, \pm 2, ...$$

as described by the solid line in Figure 2. As a result, the magnetoresistance is sinusoidal, as shown by the solid line in Figure 3. The switching of the magnetoresistance waveform from parabolic to sinusoidal in our data can, therefore, be ascribed to the generation of Josephson junctions in the ring due to the combined effects of current induced phase slips and non-uniform order parameter along the ring caused by the superconducting arms. The existence of the Josephson junctions in the ring is clearly manifested by the SQUID-like magnetoresistance oscillations, with cusps down, obtained when the current is increased to 4 μA (see Fig. 1). At this current the magnetoresistance oscillations result from the flux dependence of the critical current of the SQUID rather than by oscillation of the critical temperature due to oscillations of the screening current.

Note that in a conventional SQUID it is assumed that the rim width is larger than the superconducting penetration depth, λ, and, therefore, the Little-Parks effect is unobservable. However, in our case, as is usually the case in most nano-rings, the rim width is smaller than λ. Thus, magnetoresistance oscillations due to Little-Parks effect, Eq. (2), are expected in such SQUIDs near Tc.
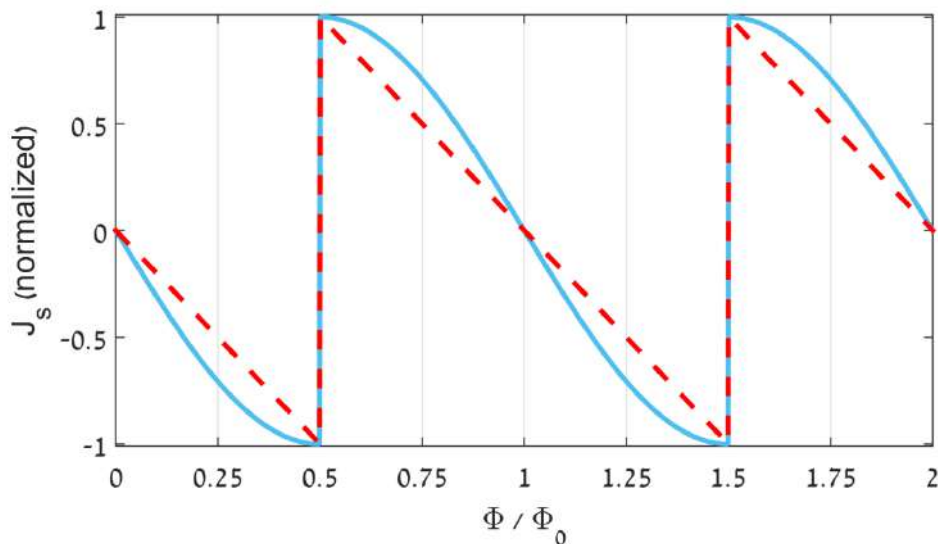

Figure 2. Flux dependence of the screening current in homogeneous ring and in a ring with Josephson junctions (dashed and solid lines, respectively).
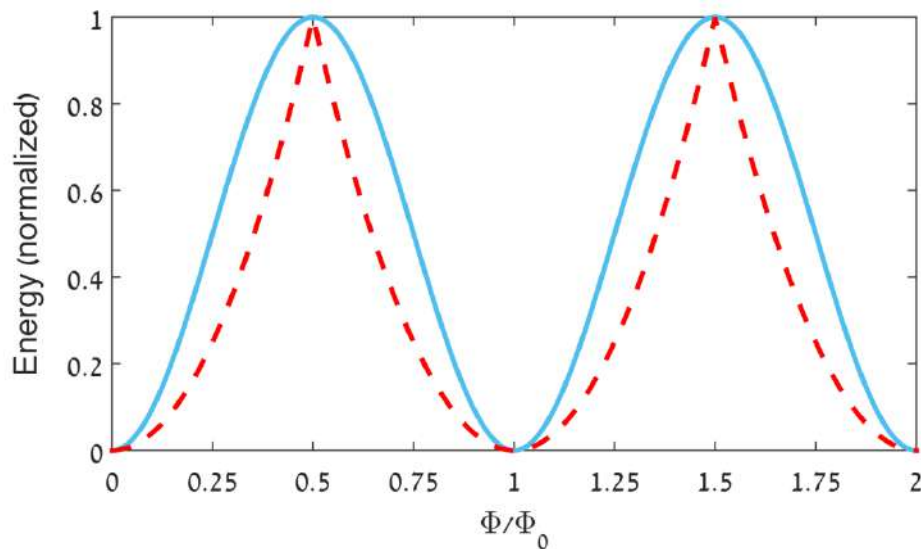
Figure 3. Flux dependence of the superconducting kinetic energy in homogeneous ring and in a ring with Josephson junctions (dashed and solid lines, respectively).

5. Summary and Conclusion

Little-Parks oscillations can transform from parabolic to sinusoidal when a Josephson junction is generated in the superconducting loop. We demonstrated that such an effect can be induced by external current in Nb nano-rings with two arms. Moreover, we demonstrated that such a ring exhibits SQUID-like magnetoresistance oscillations when large enough bias current is applied.

References
[1]   Little W and Parks R 1962 Observation of quantum periodicity in the transition temperature of a superconducting cylinder *Physical Review Letters* **9** 9
[2]   Carillo F, Papari G, Stornaiuolo D, Born D, Montemurro D, Pingue P, Beltram F and Tafuri F 2010 Little-Parks effect in single nanoscale $YBa_2Cu_3O_{6+x}$ rings *Physical Review B* **81** 054505
[3]   Sochnikov I, Shaulov A, Yeshurun Y, Logvenov G and Božović I 2010 Large oscillations of the magnetoresistance in nanopatterned high-temperature superconducting films *Nature Nanotechnology* **5** 516-9
[4]   Gammel P, Polakos P, Rice C, Harriott L and Bishop D 1990 Little-Parks oscillations of T_c in patterned microstructures of the oxide superconductor $YBa_2Cu_3O_7$: Experimental limits on fractional-statistics-particle theories *Physical Review B* **41** 2593
[5]   Israeloff N, Yu F, Goldman A and Bojko R 1994 Nonlocal conductance of small superconducting loops in the paraconductive regime *Physica B: Condensed Matter* **203** 454-9
[6]   Vodolazov D Y, Golubović D, Peeters F and Moshchalkov V 2007 Enhancement and decrease of critical current due to suppression of superconductivity by a magnetic field *Physical Review B* **76** 134505

[7]   Snyder S, Dunn T, Erickson M, Kinney J, Lee Y, Nelson J and Goldman A 2013 High-resistance state of phase coherent nanoscale thin-film Al superconducting nanorings in magnetic fields *Physical Review B* **87** 144503

[8]   Burlakov A, Gurtovoĭ V, Dubonos S, Nikulov A V and Tulin V 2007 Little-parks effect in a system of asymmetric superconducting rings *JETP Letters* **86** 517-21

[9]   Gurtovoi V, Ilin A, Nikulov A and Tulin V 2010 Weak dissipation does not result in the disappearance of the persistent current *Low Temperature Physics* **36** 974-81

[10]   Michotte S, Lucot D and Mailly D 2010 Fluxoid quantization in the critical current of a niobium superconducting loop far below the critical temperature *Physical Review B* **81** 100503

[11]   Berdiyorov G, Milošević M and Peeters F 2010 Vortices induced in a superconducting loop by asymmetric kinetic inductance and their detection in transport measurements *Physical Review B* **81** 144511

[12]   Burlakov A, Gurtovoi V, Ilin A, Nikulov A and Tulin V 2012 Possibility of persistent voltage observation in a system of asymmetric superconducting rings *Physics Letters A* **376** 2325-9

[13]   Moshchalkov V, Gielen L, Dhallé M, Van Haesendonck C and Bruynseraede Y 1993 Quantum interference in a mesoscopic superconducting loop *Nature* **361** 617-20

[14]   de Gennes P-G 1981 and C. R. Acad. Sci. Ser. B 292, 9 (1981) Suspensions colloïdales dans un mélange binaire critique *C. R. Acad. Sci. B* **292** 279

[15]   Alexander S 1983 Superconductivity of networks. A percolation approach to the effects of disorder *Physical Review B* **27** 1541

[16]   Sharon O J, Shaulov A, Berger J, Sharoni A and Yeshurun Y 2016 Current-induced SQUID behavior of superconducting Nb nano-rings *Scientific Reports* **6**

[17]   Clarke J and Braginski A I, (Editors) 2006 *The SQUID Handbook, Volume I: Fundamentals and Technology of SQUIDs and SQUID Systems*: Wiley VCH Verlag GmbH & Co. KGaA, Weinheim)

[18]   Kato M and Sato O 2013 Magnetic flux structures of finite superconducting networks *Superconductor Science and Technology* **26** 33001-26

[19]   Rammal R, Lubensky T and Toulouse G 1983 Superconducting networks in a magnetic field *Physical Review B* **27** 2820

[20]   Behrooz A, Burns M, Levine D, Whitehead B and Chaikin P 1987 Superconducting phase boundary of aperiodic networks in a magnetic field *Physical Review B* **35** 8396

[21]   Chaikin P, Behrooz A, Itzler M, Wilks C, Whitehead B, Grest G and Levine D 1988 Studies of quasicrystalline superconducting networks *Physica B: Condensed Matter* **152** 113-24

[22]   Itzler M, Behrooz A, Wilks C, Bojko R and Chaikin P 1990 Commensurate states in disordered networks *Physical Review B* **42** 8319

[23]   Rose-Innes A. C. and Rhoderick E. H. 1978 *Introduction to Superconductivity, 2nd edition*: Pergamon Press New York

3.5 Flux-periodicity crossover from *h/2e* to *h/e* in aluminum nano-loops

C. Espy, O. J. Sharon, J. Braun, R. Garreis, F. Strigl, A. Shaulov, P. Leiderer, E. Scheer, Y. Yeshurun

Flux-periodicity crossover from *h/2e* to *h/e* in aluminium nano-loops

C. Espy[1], O. J. Sharon[2], J. Braun[1], R. Garreis[1], F. Strigl[1], A. Shaulov[2], P. Leiderer[1], E. Scheer[1],*, Y. Yeshurun[2]

[1]Department of Physics, University of Konstanz, 78457 Konstanz, Germany
[2]Department of Physics and Institute of Nano Technology and Advanced Materials, Bar-Ilan University, 5290002 Ramat-Gan, Israel
*Elke.scheer@uni-konstanz.de

Abstract. We study the magnetoresistance of aluminium 'double-networks' formed by connecting the vertexes of nano-loops with relatively long wires, creating two interlaced subnetworks of small and large loops (SL and LL, respectively). Far below the critical temperature, Aharonov-Bohm like quantum interference effects are observed for both the LL and the SL subnetworks. When approaching T_c, both exhibit the usual Little-Parks oscillations, with periodicity of the superconducting flux quantum $\Phi_0=h/2e$. For one sample, with a relatively large coherence length, ξ, at temperatures very close to T_c, the Φ_0 periodicity of the SL disappears, and the waveform of the first period is consistent with that predicted recently for loops with a size $a < \xi$, indicating a crossover to $2\Phi_0$ periodicity.

1. Introduction

In a multiply connected superconductor, the fluxoid, defined as the sum of the magnetic flux and the line integral of the screening current, is quantized in units of $\Phi_0 = h/2e$, where the *2e* is a hallmark of electron pairing in the superconductor. As a direct consequence of this fluxoid quantization, periodic oscillations of the critical temperature T_c as a function of magnetic field, known as the Little-Parks effect manifest themselves as oscillations of the magnetoresistance (MR) close to T_c. The amplitudes of the critical temperature, ΔT_c, and the magnetoresistance oscillations, ΔR, are related by the slope of the resistance *vs.* temperature, $R(T)$: $\Delta R \approx (dR/dT)\Delta T_c$ [1].

Theoretical studies [2] have predicted that in superconducting nano-loops with a length-scale $a < \xi$ the dominant periodicity is *h/e* rather than *h/2e*. The same theories predict that for high-T_c superconductors (HTS) with d-wave symmetry, the *h/e* periodicity is also expected for $a \gtrsim \xi$. Recent experiments ([3, 4]) failed to identify the *h/e* component in HTS, probably because ξ_0 in these materials is only ~2 nm and, therefore, $a >> \xi$ in most of the temperature range.

In the present study we focus on aluminium, a low-T_c superconductor with a relatively large bulk coherence length ($\xi_0 = 1.6$ μm). In nanostructures made of diffusive thin films the coherence length is reduced due to the finite mean free path, and simultaneously the penetration depth λ_L is enhanced. Typical values of ξ in these aluminium nanostructures lie in the range of 100 to 200 nm. Close to T_c, the coherence length $\xi(T)$ diverges, allowing in principle to meet the criterion $a < \xi$ in nanostructures with circumferences in the order of several hundred nanometres. On the other hand, the critical field of

bulk Al amounts to only 10 mT, giving a strong limitation for the number of Little-Parks oscillations (LPO) that can be observed. In reduced dimension, *i.e.* when the lateral dimensions are in the order of the penetration depth λ_L, the critical field B_c may increase to a few hundred mT. Taking these considerations together, we fabricated 'double-networks' [3], see figure 1, with small loops of order of 400 x 400 nm^2, connected by wires of ~ 1600 nm length. An applied field of ~ 10 mT corresponds to a flux of *h/2e* through the small loops.
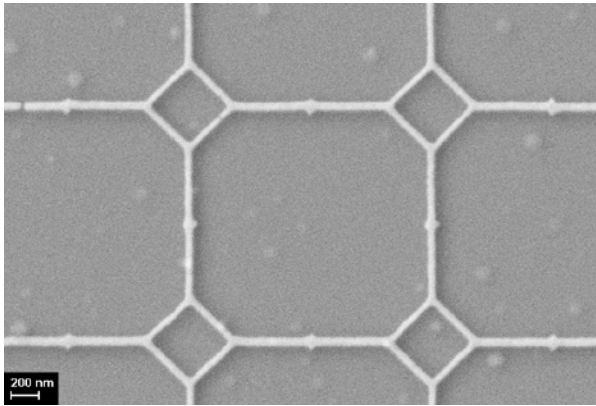
Figure 1. Scanning electron micrograph of an Al double-network (sample 1) with large (small) loop side length 1.71 µm (426 nm), line width $w = 50 \pm 5$ nm, thickness $d = 30$ nm.

2. Experimental

2.1. Sample fabrication

We use a lift-off electron beam lithography process in which Al is electron-beam evaporated onto a cooled, pre-patterned, oxidized Si substrate. The lithographic mask is then removed in warm acetone. The width of the lines is around 60 nm, the film thickness amounts to 30 nm. The arrays consist of roughly 10 x 10 loops. The samples feature normal state resistance of $R_n = 20 - 40$ Ω.

2.2. Transport measurements

Due to the pronounced temperature dependence of the LPO, particular care is taken to stabilize the cryostat temperature during the magnetic field sweeps. We use a combination of a carefully calibrated resistive thermometer to determine the absolute temperature and a capacitive sensor for keeping it constant within ± 1 mK around the set-point temperature. The set temperature spacing is adapted to the steepness of the $R(T)$ curves and amounts to a few mK around T_c. Before starting the magnetoresistance sweeps the temperature is allowed to stabilize for several minutes.

The cryostat is equipped with home-made high-frequency filtered cables to record the four-point differential resistance dV/dI by biasing a DC bias current that is kept smaller than 500 nA superimposed with a small AC current in lock-in technique. We simultaneously measured the resistance $R = V/I$ which shows qualitatively the same but more noisy data than the dV/dI. The low temperature critical current of the samples amounts to 50 - 250 µA. Close to T_c, where the LPO are maximal, the zero-field critical current still amounts to more than 2 µA.

The magnetic field is applied perpendicular to the sample plane using a superconducting solenoid. For each temperature, measurements are performed at a sweep rate of ~ 5 mT/min. For each temperature we record a sweep with increasing and decreasing field, as a control for constant temperature throughout a sweep, and in order to be able to correct for small field offsets. The field range is adapted to the critical field at the set temperature.

Table 1. Dimensions and transport characteristics of the two samples presented in this article. LL: large loops, SL small loops. w: line width from electron micrographs, w_{fit}: line width from fit to eq. (1), ξ: coherence length from fit to eq. (1), ξ_{cal}: coherence length from fit to eq. (2), T_c: critical temperature, I_c: critical current at 300 mK, B_c: critical field extrapolated to $T = 0$ from the dV/d$I(B)$ measurements, R_n: normal resistance measured above B_c. For sample 2 the fits have been performed with the low-bias data shown in figure 3.

| Sample No.	SL size (nm)	LL size (nm)	w (nm)	w_{fit} (nm)	ξ_{cal} (nm)	ξ (nm)	T_c (mK)	I_c (µA)	B_c (mT)	R_n (Ω)
1	426±10	1710±30	50±10	50±5	118±24	102±10	1408±5	55±5	194±10	33.2±1
2	324±10	1540±30	66±10	61±5	114±19	137±15	1457±5	240±10	152±10	23.3±1

3. Results

3.1. Critical temperature, critical field and coherence length

Figure 2 a) shows differential MR, dV/d$I(B)$, curves in the temperature range 380 - 1600 mK, recorded on sample 1 with 426 nm side length of the small loops and 1.71 µm of the large loops (see table 1 for sample dimensions). From the set of dV/d$I(B)$ curves we construct the envelope of the $B_c(T)$ phase boundary (without the oscillatory part) from which we deduce the coherence length, ξ, and T_c using the relation [7]

$$T_c(B) = T_c \left[1 - \frac{\pi^2}{3} \left(\frac{w_{fit} \xi B}{\Phi_0} \right)^2 \right], \qquad (1)$$

where w_{fit} is the width of the wire. For comparison we also estimate the coherence length from the low temperature critical field, $B_c(0)$ assuming a thin slab in magnetic field resulting in the relation [10]:

$$\xi_{cal} = \sqrt{3}\Phi_0/(\pi w B_c(0)) \qquad (2)$$
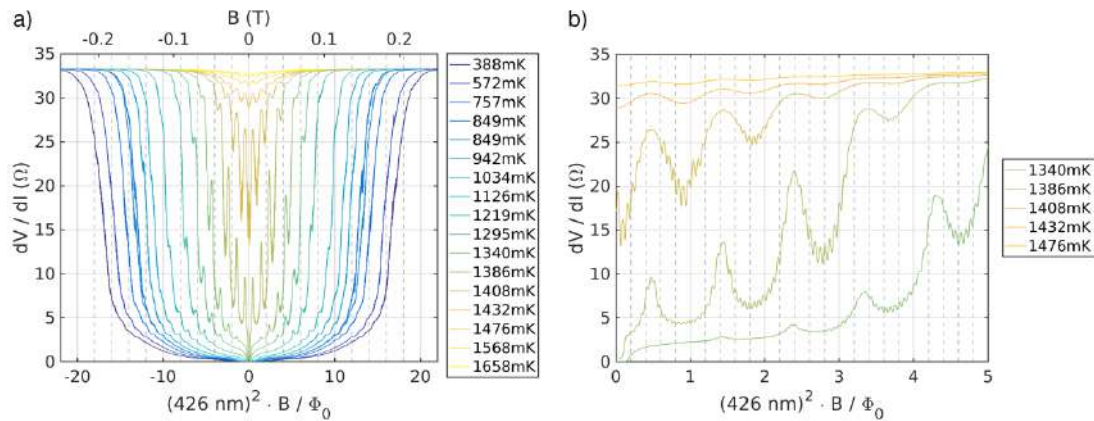
Figure 2. a) dV/d$I(B)$ curves of sample 1 covering the whole field range and the whole temperature range from 388 mK (dark blue) to 1658 mK (yellow), b) Zoom into the positive field direction of selected data from panel a) close to T_c.

The loop sizes have been determined by inspection of the electron micrographs and are additionally deduced from the observed flux periodicity assuming square-shaped loops. The numerical values for the various parameters are given in table 1. The values for T_c correspond well with the position of the $R(T) = R_n/2$ in the temperature curves as well as with the dV/d$I(B)$ curve at which the largest oscillation amplitude is observed. Also, both estimates for the coherence length agree with each other

within ~ 20% for both samples, supporting the suitability of the simplified models. Taking the average value of these two estimates, we find that for sample 1 (2) the ratio between the coherence length and the SL edge length a amounts to $\xi/a \sim 0.26$ (0.39). Thus, we expect the transition to the h/e periodicity being more likely to be observable in sample 2.

3.2. Little Parks effect

Figure 2 b) zooms into the positive field direction close to T_c. Figure 3 shows $dV/dI(B)$ data for sample 2 with SL size of 324 nm and LL size of 1.54 µm. For both samples and at all temperatures we observe symmetric periodic oscillations of $dV/dI(B)$ corresponding to $h/2e$ oscillations of the small loops (SL) and of the large loops (LL).
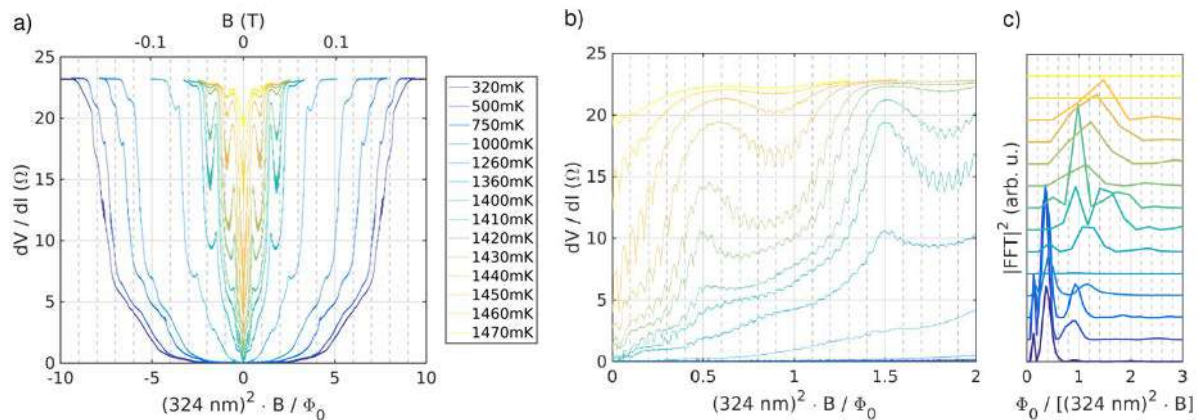
Figure 3. a) Selected $dV/dI(B)$ traces of sample 2. b) Same curves as in a) for a reduced range in positive field direction. c) FFT of the $dV/dI(B)$ data shown in a).

Closer inspection reveals for both samples a gradual change of the LL oscillations from a cusp-up form (typical of LPO) at low temperature, through a sinusoidal behaviour at intermediate temperature, into a cusp-down (SQUID-like) shape at higher temperatures. A similar crossover, induced by the bias current rather than by temperature, was reported by Sharon *et al.* for Nb chains of rings [5]. The effect is most pronounced at low fields when the flux through the SL is still smaller than $\Phi_0/2$. The amplitude of the LL oscillations vanishes at somewhat smaller temperatures than the SL oscillations. Both observations suggest that the coherence in the LLs is not fully developed and that weak links exist that act as Josephson junctions. Furthermore the amplitude of the LL oscillations is locally suppressed at odd multiples of $\Phi_0/2$ of the SLs. At these flux values the ring current in the SL is maximal. Hence, the suppression of the LL amplitude can be understood as an interruption of the ring current in the LLs. Similar observations were made in Al nanostructures consisting of several loops sharing the same strands [6, 7]. This observation is related to the Little-Parks-de Gennes effect [8] which describes the destruction and restauration of superconductivity in multiply connected superconductors around odd multiples of $\Phi_0/2$ [9].

3.3. Little-Parks effect of small loops and transition to h/e periodicity

We now turn to discuss the SL oscillations. These also show the typical cusp-up behaviour well below T_c and a sinusoidal shape close to T_c. This shape transition is most pronounced in sample 2 and is marked by a broadening and a shift of the resistance maximum at $\Phi_0/2$ to larger fields. The Fast Fourier Transform (FFT) of the data (see figure 3 c)) reveals that besides the usual $h/2e$ component also an $h/3e$ component is present which starts to dominate close to T_c. The $h/3e$ component indicates a modulation of the amplitude of the regular $h/2e$ LPO. We interpret these findings as an onset of the transition to h/e which is expected for very small loop sizes. Due to the limited field range that covers

only slightly more than one period of the *h/e*, the fundamental *h/e* component cannot be seen in the FFT, but rather a higher harmonic of it, *i.e.* the *h/3e* component.

To investigate this observation further we performed dV/dI(B) measurements on sample 2 under relatively high bias current of 2.1 µA. With this bias the apparent T_c is somewhat smaller than in the low bias data. Two examples of differential resistance curves, one with low and one with high bias, are plotted in figure 4 a). In the high-bias data the oscillations appear more pronounced and dV/dI(B) exceeds R_n around $\Phi = \Phi_0/2$ and close to B_c(T). In these field ranges also irregular oscillations are visible although the LPOs are washed out in the low bias data. Both observations are consequences of the non-linear current-voltage characteristics in this range and the differential measurement scheme. We checked that the absolute resistance remains everywhere smaller than R_n.
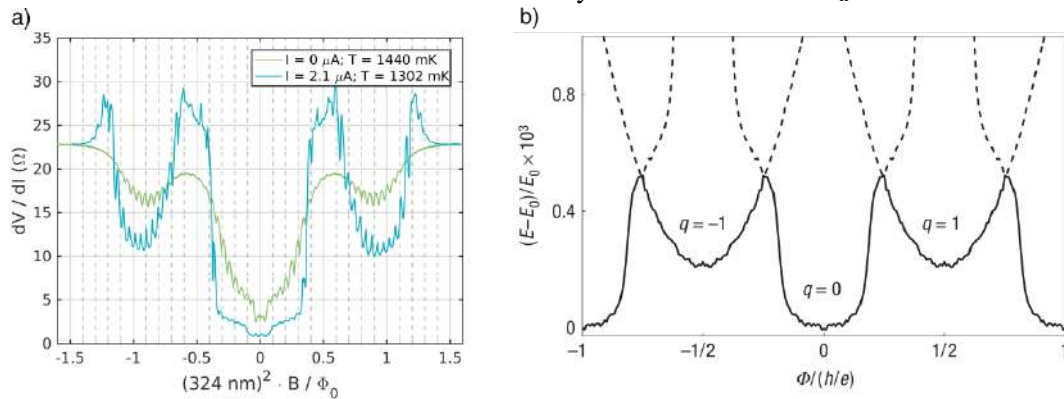
Figure 4. a) Comparison of differential resistance *vs.* B curves of sample 2 with zero DC bias current and with finite DC bias current (2.1 µA) close to T_c. b) Energy vs. flux for a superconducting loop with $a < \xi$, showing the modulation of the odd LPOs. Reprinted with permission from MacMillan Publishers Ltd: Nature Physics [2], copyright 2008. In this right figure Φ is described in units of $\Phi_0 = h/e$.

For both curves, the shape of the central dip (at $\Phi = 0$) is much different from that of the side dips (at $\Phi = \Phi_0$), implying that the Little-Parks $h/2e$ periodicity is broken. On the other hand, these data show a striking similarity to the theoretical calculations of Loder *et al.* [2] predicting *h/e* periodicity, as depicted in figure 4 b). Note that in this figure the flux is plotted in units of *h/e*. Unfortunately, we observe only one period as the field required to observe more periods exceeds the critical field, $B_c(0)$, of this sample. Nevertheless, the nearly parabolic shape of the side minima and the distorted shape of the parabola centred at $\Phi = 0$ may serve as a fingerprint of the predicted *h/e* periodicity. Note that the theoretical prediction (right panel) describes the oscillation in the energy while the experimental results (left) describe the differential resistance. The two, however, are related since both are directly related to ΔT_c [10]. The similarity with the theoretical curve is most apparent for the high-bias dV/dI curve. This suggests that under these measurement conditions, *i.e.* when the system is driven close to the transition to the normal state, the relation between differential resistance and energy is most direct.

3.4. Aharonov-Bohm effect in small loops

Finally we note that the temperature dependence of the amplitude of the SL oscillations is non-monotonous. As figure 3 c) shows, at low temperature, $T < {\sim}1000$ mK, we observe *h/e* and *h/2e* oscillations of the small loops that almost disappear for intermediate temperatures, ${\sim}1000$ mK $< T < {\sim}1200$ mK. Above 1200 mK dominantly the *h/2e* and *h/3e* components corresponding to the Little-Parks effect appear. We attribute the low-temperature oscillations to quantum interference effects, *i.e.* the Aharonov–Bohm effect, indicating that also the phase coherence length of the quasiparticles, L_Φ, in this range is in the order of the perimeter of the SLs or larger. When increasing the temperature,

inelastic scattering sets in that reduces L_Φ [11]. For completeness we mention that we do not observe such non-monotonous behaviour for the LL oscillations, indicating that L_Φ is always smaller than the perimeter of the LLs.

4. Conclusions

Summarizing, we have presented magnetoresistance data in interlaced networks comprising small and large loops made of aluminium. We observe the interplay between the magnetoresistance oscillations in these two subsets of loops. In particular, the $\Phi_0 = h/2e$ periodic Little-Parks oscillations of the large loops are modulated by the flux conditions in the small loops. For a sample with high ratio between coherence length and loop size we observe an onset of the transition from the conventional $h/2e$ to an h/e periodicity, as predicted for long coherence length. A full experimental verification of the theory requires measurements of more than one period. However, the relatively low critical field of aluminium, and the large period of small loops, presently impedes achieving this condition. Further improvements of the sample design and material quality are currently underway to overcome this limitation.

References

[1] Little W, Parks R 1962 *Phys. Rev. Lett*. **9** 9.
[2] Loder F, Kampf A P, Kopp T, Mannhart J, Schneider, C W, Barash, Y S 2008 *Nature Phys* **4** 112.
[3] Sochnikov I, Shaulov A, Yeshurun Y, Logvenov G, Božović I 2010 *Nature Nanotechnol*. **5** 516.
[4] Carillo F, Papari G, Stornaiuolo D, Born D, Montemurro D, Pingue P, Beltram F, Tafuri F 2010 *Phys. Rev. B* **81** 054505.
[5] Sharon O J, Shaulov A, Berger J, Sharoni A, Yeshurun Y 2016 *Sci. Rep*. **6** 28320.
[6] Bruyndoncx V, Strunk C, Moshchalkov V V, van Haesendonck C, Bruynseraede Y 1996 *Europhys. Lett*. **36** 449.
[7] Strunk C, Bruyndoncx V, Moshchalkov V V, Van Haesendonck C, Bruynseraede Y Jonckheere R 1996 *Phys. Rev. B* **54** R12701.
[8] de Gennes P G, 1981 *C. R. Acad. Sci. Ser. B* **292** 9, and *ibid. *292** 279.
[9] Staley N E, Liu Y 2012 *Proc. Nat. Acad. Sci* **109** 14819.
[10] Tinkham M 1996 *Introduction to Superconductivity* McGraw-Hill New York.
[11] Washburn S, Webb R A 1986, *Adv. Phys*. **35** 375.

3.6 Current-Induced Crossover of Flux Periodicity from *h/2e* to *h/e* in Superconducting Nb Nano-Ring

Omri J. Sharon, Avner Shaulov, Jorge Berger, Amos Sharoni, Richard Berkovits and Yosef Yeshurun

Current-Induced Crossover of Flux Periodicity from *h*/2*e* to *h*/*e* in a Superconducting Nb Nano-Ring

Omri Sharon,*,[†] Avner Avraham Shaulov,[†] Jorge Berger,[‡] Amos Sharoni,[†] Richard Berkovits,[†] and Yosef Yeshurun[†]

[†]Department of Physics and Institute of Nano Technology, Bar-Ilan University, 5290002 Ramat-Gan, Israel
[‡]Department of Physics and Optical Engineering, Ort Braude College, 21982 Karmiel, Israel

Ⓢ Supporting Information

ABSTRACT: Magnetoresistance measurements in a granular Nb nanoring reveal current-induced crossover between two distinct quantum coherence effects. At low bias currents, Cooper-pair coherence is manifested by Little−Parks oscillations with flux periodicity of *h*/2*e*. At high bias currents, magnetoresistance oscillations with flux periods of *h*/*e* are observed and interpreted as Aharonov−Bohm oscillations, reflecting the phase coherence of individual quasi-particles. The model explaining these data views the ring as a chain of superconducting grains weakly coupled by tunnel junctions. Low bias currents allow coherent tunneling of Cooper pairs between the grains. Increasing the current above the critical current of all the junctions creates a quasi-particles conduction channel along the ring, allowing for quantum interference of quasi-particles.

KEYWORDS: *Superconductivity, nanorings, quantum interference, Little−Parks effect, Aharonov−Bohm effect*
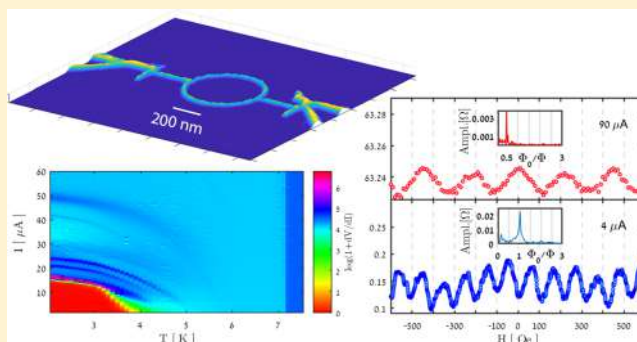
Quantum phase coherence and interference effects, commonly associated with superconductors,[1] are also observed in mesoscopic normal metals at low temperatures so that the scattering of electrons is almost entirely elastic.[2] Such effects are experimentally manifested in magnetoresistance (MR) measurements, in which the resistance of a superconducting or a metal ring is measured as a function of the magnetic flux threading it. Mesoscopic normal-metal rings with narrow rims exhibit the Aharonov−Bohm MR oscillations with a flux period of *h*/*e*,[3] whereas superconducting rings exhibit MR oscillations with a flux period of *h*/2*e*, 2*e* being the hallmark of the electron pairing. In the present work we show a crossover of the flux periodicity in a granular Nb mesoscopic ring, from *h*/2*e* at low bias currents to *h*/*e* at higher currents in a range below the depairing current. This crossover is explained by viewing the granular ring as a chain of superconducting islands weakly coupled by tunnel junctions. The *h*/2*e* flux periodicity is associated with the Little−Parks effect in a ring consisting of Josephson junctions in the zero voltage state.[4] The magnetoresistance oscillations with a flux period of *h*/*e* are interpreted as an Aharonov−Bohm effect arising from phase coherence of quasi-particles flowing in the resistive channel created by the Josephson junctions in the voltage state.

Thin Nb films were grown by magnetron sputtering on SiO₂ substrates. X-rays diffraction (XRD) and reflection (XRR) measurements revealed granularity with grains size between 10 and 12 nm. Nb rings were patterned on these films using e-

beam lithography followed by reactive ion etching (RIE). Altogether, seven samples with the same diameter (500 nm) and different rim sizes (20−80 nm) were measured. The effect reported below was observed in three samples with the lowest rim size. Here we report representative results obtained in one of these samples, with a diameter of 500 nm, and a rim's width and thickness of 23 and 20 nm, respectively. Figure 1 shows a scanning electron microscopy (SEM) image of this sample. Transport and magnetoresistance measurements were performed by employing a commercial physical properties measurements system (PPMS, Quantum-Design) for temperatures 3−10 K and bias currents between 1 and 128 μA.

Figure 2a shows the temperature dependence of the ring resistance for several measuring currents. A sharp drop of the resistance is apparent at $T_c \sim 7.2$ K for all the measuring currents, followed by a current-dependent broad transition. For increasing the measuring current up to 32 μA, superconductivity along the ring is gradually destroyed. For currents between 32 and 128 μA, a remarkable behavior is observed at low temperatures, namely, a decrease of the resistance with increasing temperature. The observed temperature and current dependence of the resistance become clear by viewing the granular ring as a chain of Josephson coupled superconducting
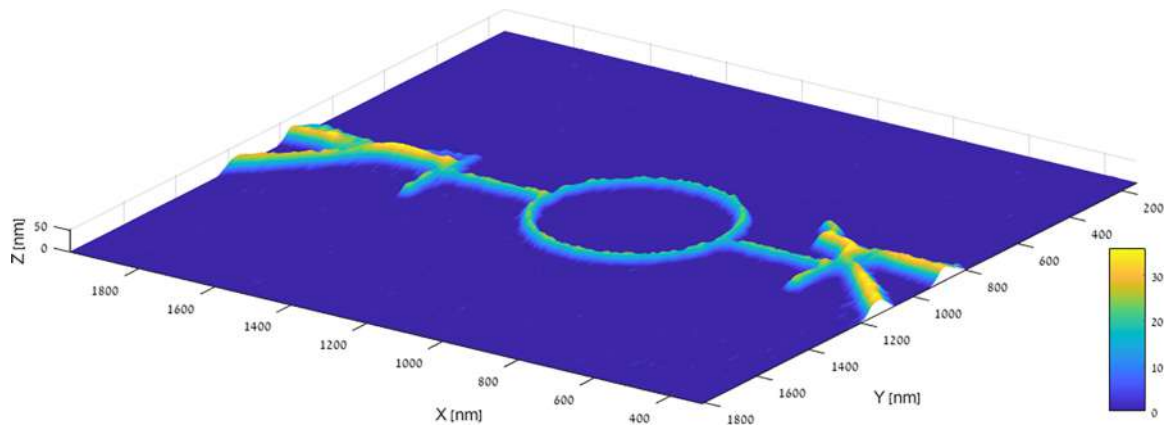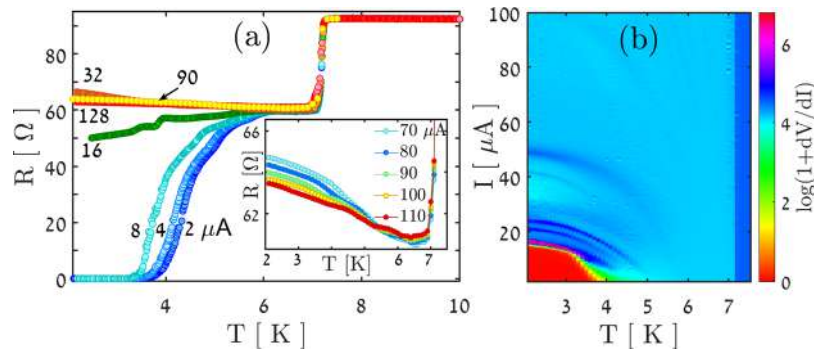
Figure 1. SEM image of the Nb ring with a diameter of 500 nm and rim's width and thickness of 23 and 20 nm, respectively.


Figure 2. (a) Temperature dependence of the ring resistance for the indicated measuring currents. Inset: $R(T)$ for bias currents between 70 and 110 μA. (b) Color encoded diagram of the differential resistance, dV/dI, in the current−temperature plane. The dark arcs indicate the temperature dependence of the critical current of the different Josephson junctions in the ring.

islands. The initial sharp drop at ∼7.2 K to approximately 65% of the normal resistance indicates the onset of super-conductivity in the isolated superconducting islands within the ring. The broad transition for low bias currents (2−8 μA) is associated with gradual achievement of Josephson coupling between the superconducting islands, eventually driving the ring into a zero resistance state. In the intermediate current range (represented by the 16 μA in the figure), part of the Josephson junctions in the ring switch into the voltage state, resulting in nonvanishing resistance. This resistance saturates for larger currents, represented by the curves for 32−128 μA in the figure, indicating that *all* the Josephson junctions in the ring are in the voltage state. In this state, a continuous resistive channel associated with the quasi-particle current along the ring is established.[5] The quasi-particles are generated either by thermal excitations or due to breaking up of Cooper pairs by the current. The excited quasi-particles in each junction can tunnel already at voltages smaller than the gap voltage, resulting in a finite resistance, $R_{sg}(T)$, known as the "subgap resistance". The magnitude of $R_{sg}(T)$ is determined by the amount of excited quasi-particles and is given by $R_{sg}(T) = (n_{total}/n(T,I_b))R_N$, where n_{total} is the total density of electrons in the normal state, $n(T,I_b)$ is the density of the excited quasi-particles at temperature T and bias current I_b, and R_N is the normal resistance of the Josephson junction.[5] For a constant bias current, R_{sg} decreases with temperature as $n(T)$ increases. As the bias current increases, R_{sg} drops and its decrease with temperature becomes more moderate, indicating that the generation of the quasi-particles is dominated by the current. These effects are visible in the $R(T)$ data of Figure 2a for high

bias currents, and more clearly in the inset to this figure. It is important to note that even for the largest measuring current the grains are still superconducting as the depairing current density, $J_{dp} = \frac{\Phi_0}{2\pi\mu_0\lambda^2\xi} = 1.5 \times 10^8$ A/cm^2, is an order of magnitude larger than the density of the largest bias current in our experiment. This, in fact, is also evident from the large drop of the resistance at 7.1 K, only a small part of which can be attributed to the effect of the superconducting electrodes. Furthermore, this large drop is followed by an almost constant resistance down to low temperatures, excluding an influence of the proximity effect caused by the electrodes. We note that the above value for J_{dp} estimated for bulk Nb, may be an overestimate for Nb films. As reported in ref 6, the depairing current density in Nb films may be as low as ∼4 × 10^7 A/cm^2 at 3.5 K. However, even this low estimate is significantly larger than the current where the crossover to h/e periodicity is observed.

A further support to our view of the granular Nb ring as a chain of Josephson junctions with distributed critical currents is obtained from the $I−V$ curves shown in Figure S-1 in the Supporting Information. The $I−V$ curves are characterized by several voltage steps at different current values. These are clearly seen especially at low temperatures. A voltage step occurs when the current reaches the value of the critical current of a single or a group of Josephson junctions in the chain. To provide an even clearer picture, we show here, in Figure 2b, a color encoded diagram of dV/dI in the current−temperature plane. Voltage steps in this diagram are visible as a
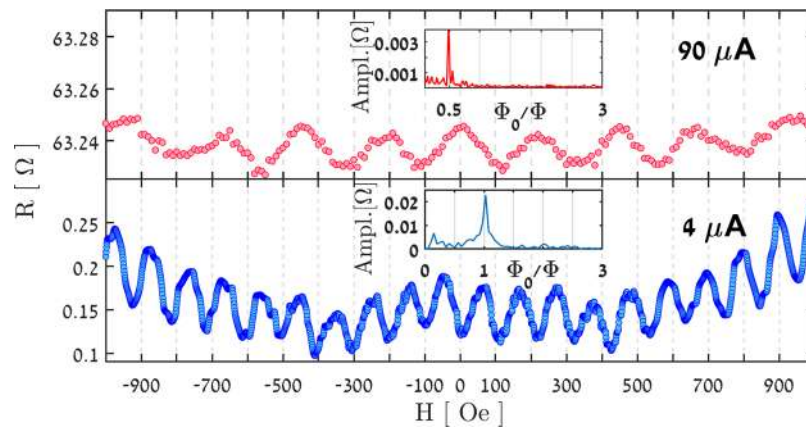
Figure 3. Magnetoresistance oscillations in the Nb ring at 3.5 K, for bias currents of 4 and 90 μA, lower and upper panels, respectively. Note the doubling of the flux periodicity from 105 to 210 Oe, corresponding to a crossover of the flux periodicity from $h/2e$ to h/e, respectively. Insets show the Fourier transform of the data.

set of dark arcs that reflect the temperature dependence of the critical currents of the involved Josephson junctions.

Low current magnetoresistance measurements $(1-12\ \mu$A) at temperatures between 3.5 and 3.9 K, exhibit oscillations with a field periodicity of $\sim$105 G, corresponding to flux periodicity of $h/2e$ for our ring of area $\sim$2 $\times$ 10^5 nm^2. Typical magnetoresistance data, at 3.5 K and a current of 4 μA, are shown in Figure 3 (lower panel). The inset to this figure shows the Fourier transform of the data, demonstrating domination of the $h/2e$ periodicity.

A dramatic change in the flux periodicity to h/e is observed as the measuring current is increased to a range of 75–110 μA. Figure 3 (upper panel) demonstrates the h/e periodicity obtained at 3.5 K with current of 90 μA. The Fourier transform in the inset demonstrates domination of the h/e periodicity. Figure 4 shows the amplitude of the h/e oscillations as a function of the bias current. Interestingly, the amplitude is a nonmonotonic function of I_b, exhibiting a peak around I_b = 90 μA.
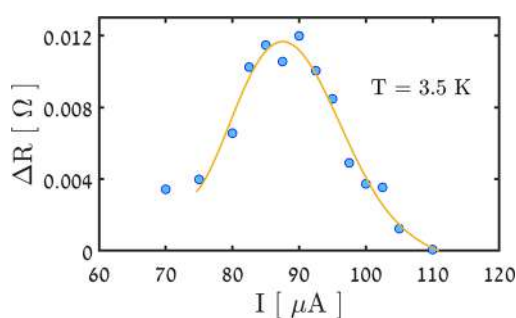
Figure 4. Current dependence of the h/e amplitude near zero field. The error in the amplitude is estimated to be of order 10%. The solid line is a guide to the eye.

The current-induced flux periodicity crossover is explained based on our view of the granular ring as a chain of Josephson coupled superconducting islands. As evident from the $R(T)$ data of Figure 2, the $h/2e$ magnetoresistance oscillations of Figure 3 (lower panel) were measured in the superconducting state where all the Josephson junctions comprising the ring are in a zero voltage state. It is, therefore, natural to associate these oscillations with the Little–Parks effect in the Nb ring, indicating coherence of electron pairs along the whole ring.[4,7]

The existence of Josephson junctions in the ring is expected to modify the waveform of the oscillations to sinusoidal instead of parabolic.[8] Indeed, the observed waveform is closer to sinusoidal rather than to parabolic, as apparent from the Fourier analysis shown in the inset to the lower panel of Figure 3.

The h/e oscillations of Figure 3 (upper panel) appear in the temperature and current range (see Figure 2) where each Josephson junction in the ring is in the voltage state; i.e., the bias current is larger than the critical current of each of the junctions. In this state, a resistive, conduction channel of quasi-particles is established along the ring. Thus, it is plausible to associate the h/e oscillations with the Aharonov–Bohm effect arising from interference of phase coherent quasi-particles flowing along the two branches of the ring consisting of Josephson junctions. Phenomena related to the Aharonov–Bohm effect in condensed matter were observed in the past in various metallic[2] and nonmetallic systems (see, e.g., refs 9–16). The present work demonstrates the effect for the first time in a ring consisting of Josephson junctions.

In view of a lack of a theory for Aharonov–Bohm oscillations in such a unique granular ring, it is instructive to compare the amplitude of the h/e oscillations obtained in this ring (see upper panel of Figure 3) to the amplitude expected for a normal Nb ring of the same size. This will provide an upper bound for the Aharonov–Bohm amplitude expected in our Nb granular ring. For a metal in zero voltage, the phase coherence length can be calculated from[17] $L_\phi(T) = \sqrt{D\tau_\phi}$, where D is the diffusion coefficient and $\tau_\phi = \frac{\tau_{e-e}\tau_{e-ph}}{\tau_{e-e} + \tau_{e-ph}}$ is the time between inelastic collisions. Here τ_{e-e} and τ_{e-ph} are the times between electron–electron and electron–phonon collisions, respectively. For Nb at 3.5 K, $D = 3.5 \times 10^{-3}$ m^2/s, the inelastic electron–electron collision rate estimated from ref 18 is $\frac{1}{\tau_{e-e}} = 2 \times 10^8$ s^{-1}, and the electron–phonon collisions rate estimated from ref 19 is $\frac{1}{\tau_{e-ph}} = 1.7 \times 10^8$ s^{-1}. The average time between inelastic collisions is thus $\tau_\phi = 2.6$ ns. These yield $L_\phi = 3\ \mu$m, which is larger than the size of our Nb ring. Inserting this value in the relation[20] $\Delta G_{h/e} = \frac{e^2}{h}\frac{L_T}{\pi r}\sqrt{\frac{L_\phi}{\pi r}}e^{-\pi r/L_\phi}$, using a thermal length $L_T = \sqrt{\frac{D\hbar}{k_B T}} = 87$ nm, we find $\Delta R \approx$

$R^2\Delta G = 0.026\ \Omega$. Obviously, the value of L_ϕ calculated above, using the bulk values for diffusivity and scattering times, is much larger than that expected for our granular ring. Thus, one would expect a much lower value of ΔR for our ring. Surprisingly, the experimentally measured ΔR in our granular sample is comparable to the calculated one for a bulk Nb. This points to an enhanced Aharonov–Bohm effect in our granular ring, which consists of decoupled superconducting grains. The enhancement effect can also be deduced from the fact that the Aharonov–Bohm effect in our experiment is observed at relatively high voltages, whereas the calculations above were made for zero voltage. Clearly, as the voltage increases, L_ϕ, and consequently ΔR, should decrease because the rate of inelastic collisions increases with the electron energy.[21] We thus may conclude that our measured oscillations amplitude is, in fact, much larger than expected for a metallic Nb ring of the same size under the same voltage. This enhancement may be attributed to the reduced density of quasi-particles in the ring consisting of Josephson junctions as compared to the density of electrons in a metallic ring. A lower value of the quasi-particle density reduces the rate of inelastic collisions and thus increases L_ϕ. Note that enhancement of the Aharonov–Bohm effect, however of different origin, was reported in metallic rings with superconducting "mirrors".[22,23]

The amplitude, ΔR, of the h/e oscillations shown in Figure 4, exhibits a nonmonotonic behavior as a function of the bias current. This can be explained as resulting from two competing processes. As the current increases, the number of quasi-particles increases, leading to a larger amplitude. However, a larger bias current is associated with a larger voltage and a larger energy of the quasi-particles, leading to a larger rate of electron–electron collisions and consequently to a reduced length of phase coherence.

As mentioned above, the crossover to the Aharonov–Bohm h/e flux periodicity was observed in three samples with the lowest rim size. This is expected in light of the work of Webb et al.[24] who showed that a clear Aharonov–Bohm h/e periodicity may be observed in rings having an area much larger than the area covered by the rims. When this condition is not fulfilled, an Aharonov–Bohm $h/2e$ periodicity appears that can hardly be distinguished from the Little–Parks $h/2e$ periodicity. Current dependence of the magnetoresistance oscillations obtained in the three samples can hardly be compared as they differ widely, probably due to different granular structure of these samples.

A further support for our interpretation of the h/e periodicity as the Aharonov–Bohm effect is found in measurement of the magnetoresistance as a function of the bias current at a constant magnetic field. As noted by Webb et al.,[25] if the voltage developed across the sample is changed, the interference properties are also affected. This leads to voltage-dependent fluctuations in the conductance that are similar to effects seen when the vector potential is changed. Such an effect is demonstrated in Figure S-2 in the Supporting Information. Oscillations of the differential resistance are clearly observed as a function of the bias current in the same region for which the Aharonov–Bohm oscillations are observed.

We close our discussion by noting that in the intermediate current range, between 15 and 45 μA, magnetoresistance oscillations are not observed. In a current range between 50 and 75 μA there is an indication for a flux periodicity close to $3\Phi_0$, a phenomenon that requires further investigation.

Magnetoresistance data in these current ranges are shown in Figures S-3b,c in the Supporting Information. The Supporting Information also includes magnetoresistance data for the whole range in which the h/e periodicity is observed (Figure S-3d,e). We note that no change in the phase of the h/e oscillations is observed in this current range. The phase shift reported in ref 26 was obtained in normal metals in a range of relatively low currents (0–6.8 μA). The absence of an observable phase shift in our experiment could well be related to the unique structure of our sample and to the relatively small variations of the current in a much higher range.

We also note that the existence of Cooper pairs does not necessarily imply an $h/2e$ periodicity. For example, an h/e flux periodicity was predicted for s-wave nanorings with a size *smaller* than the coherence length, ξ_0.[27] Experimental efforts to detect the h/e periodicity in nanorings were partially successful.[28,29] Clearly, the physical origin of the h/e periodicity observed in our Nb ring is different, as the size of the ring is much larger than the coherence length ($\xi_0 \approx 40$ nm).

In conclusion, this work demonstrates two distinct quantum coherence effects in a single Nb ring. A Little–Parks effect, which manifests coherence of Cooper pairs, gives rise to a flux periodicity of $h/2e$ at low bias currents. The Aharonov–Bohm effect resulting from phase coherence of quasi-particles gives rise to a flux periodicity of h/e at high bias current. To the best of our knowledge, this is the first demonstration of the Aharonov–Bohm effect in a ring of Josephson junctions, resulting from phase coherence of quasi-particles tunneling between superconducting islands. The data indicate an enhancement of this effect as compared to the effect in metallic rings. This is attributed to the reduced density of quasi-particles in the superconducting islands which gives rise to a larger phase coherence length.

■ ASSOCIATED CONTENT

Ⓢ Supporting Information

The Supporting Information is available free of charge on the ACS Publications website at DOI: 10.1021/acs.nanolett.8b03617.

> $I–V$ curves for the Nb ring in the temperature range 2.5–7.5 K, differential resistance as a function of the bias current at zero magnetic field, and magnetoresistance oscillations in different current regimes (2–150 μA) (PDF)

■ AUTHOR INFORMATION

Corresponding Author

*O. Sharon. E-mail: omri_s@yahoo.com. Mobile phone: +972507416679.

ORCID Ⓘ

Omri Sharon: 0000-0003-0158-4119
Amos Sharoni: 0000-0003-3659-0818

Notes

The authors declare no competing financial interest.

■ ACKNOWLEDGMENTS

■ REFERENCES

(1) Tinkham, M. *Introduction to superconductivity*, 2nd ed.; Dover Publ.: New York, 2004.

(2) Imry, Y. *Introduction to mesoscopic physics*; Oxford University Press, 2002.

(3) Washburn, S.; Webb, R. A. *Adv. Phys.* **1986**, *35*, 375.

(4) Little, W.; Parks, R. *Phys. Rev. Lett.* **1962**, *9*, 9.

(5) Gross, R.; Marx, A.; Deppe, F. *Applied superconductivity: Josephson effect and superconducting electronics*; Walter de Gruyter, 2016.

(6) Rusanov, A. Y.; Hesselberth, M.; Aarts, J. *Phys. Rev. B: Condens. Matter Mater. Phys.* **2004**, *70*, 024510.

(7) Sochnikov, I.; Shaulov, A.; Yeshurun, Y.; Logvenov, G.; Božović, I. *Nat. Nanotechnol.* **2010**, *5*, 516.

(8) Sharon, O. J.; Sharoni, A.; Berger, J.; Shaulov, A.; Yeshurun, Y. *J. Phys.: Conf. Ser.* **2018**, *969*, 012047.

(9) Chakraborty, T.; Manaselyan, A.; Barseghyan, M. *J. Phys.: Condens. Matter* **2017**, *29*, 075605.

(10) Cho, S.; Dellabetta, B.; Zhong, R.; Schneeloch, J.; Liu, T.; Gu, G.; Gilbert, M. J.; Mason, N. *Nat. Commun.* **2015**, *6*, 7634.

(11) Fuhrer, A.; Lüscher, S.; Ihn, T.; Heinzel, T.; Ensslin, K.; Wegscheider, W.; Bichler, M. *Nature* **2001**, *413*, 822.

(12) Hong, S. S.; Zhang, Y.; Cha, J. J.; Qi, X.-L.; Cui, Y. *Nano Lett.* **2014**, *14*, 2815.

(13) Lorke, A.; Luyken, R. J.; Govorov, A. O.; Kotthaus, J. P.; Garcia, J.; Petroff, P. M. *Phys. Rev. Lett.* **2000**, *84*, 2223.

(14) Sangalli, D.; Marini, A. *Nano Lett.* **2011**, *11*, 4052.

(15) Wang, L.; Gutiérrez-Lezama, I.; Barreteau, C.; Ubrig, N.; Giannini, E.; Morpurgo, A. F. *Nat. Commun.* **2015**, *6*, 8892.

(16) Yao, Y.; Elborg, M.; Kuroda, T.; Sakoda, K. *J. Phys.: Condens. Matter* **2017**, *29*, 385301.

(17) Palenskis, V. *World J. Condens. Matter Phys.* **2013**, *3*, 73.

(18) Huibers, A.; Switkes, M.; Marcus, C.; Campman, K.; Gossard, A. *Phys. Rev. Lett.* **1998**, *81*, 200.

(19) Kaplan, S.; Chi, C.; Langenberg, D.; Chang, J.-J.; Jafarey, S.; Scalapino, D. *Phys. Rev. B* **1976**, *14*, 4854.

(20) Pierre, F.; Birge, N. O. *Phys. Rev. Lett.* **2002**, *89*, 206804.

(21) Linke, H.; Omling, P.; Xu, H.; Lindelof, P. *Superlattices Microstruct.* **1996**, *20*, 441.

(22) Petrashov, V.; Antonov, V.; Delsing, P.; Claeson, R. *Phys. Rev. Lett.* **1993**, *70*, 347.

(23) Courtois, H.; Gandit, P.; Mailly, D.; Pannetier, B. *Phys. Rev. Lett.* **1996**, *76*, 130.

(24) Webb, R. A.; Washburn, S.; Umbach, C.; Laibowitz, R. *Phys. Rev. Lett.* **1985**, *54*, 2696.

(25) Webb, R. A.; Washburn, S.; Umbach, C. *Phys. Rev. B: Condens. Matter Mater. Phys.* **1988**, *37*, 8455.

(26) Häussler, R.; Scheer, E.; Weber, H. B.; Löhneysen, H. v. *Phys. Rev. B: Condens. Matter Mater. Phys.* **2001**, *64*, 085404.

(27) Loder, F.; Kampf, A.; Kopp, T.; Mannhart, J.; Schneider, C.; Barash, Y. S. *Nat. Phys.* **2008**, *4*, 112.

(28) Espy, C.; Sharon, O.; Braun, J.; Garreis, R.; Strigl, F.; Shaulov, A.; Leiderer, P.; Scheer, E.; Yeshurun, Y. JOP *J. Phys.: Conf. Ser.* **2018**, *969*, 012063.

(29) Carillo, F.; Papari, G.; Stornaiuolo, D.; Born, D.; Montemurro, D.; Pingue, P.; Beltram, F.; Tafuri, F. *Phys. Rev. B: Condens. Matter Mater. Phys.* **2010**, *81*, 054505.

Supporting Information for

"Current-Induced Crossover of Flux Periodicity from *h/2e* to *h/e*

**in Superconducting Nb Nano-Ring"**

Omri Sharon[1], Avner Avraham Shaulov[1], Jorge Berger[2],
Amos Sharoni[1], Richard Berkovits[1] and Yosef Yeshurun[*,1]

*[1] Department of Physics and Institute of Nano Technology, Bar-Ilan University, 5290002
Ramat-Gan, Israel*
*[2] Department of Physics and Optical Engineering, Ort Braude College,
21982 Karmiel, Israel*

* *yeshurun@mail.biu.ac.il* mobile phone: *+972544810575*

I-V Curves at different temperatures
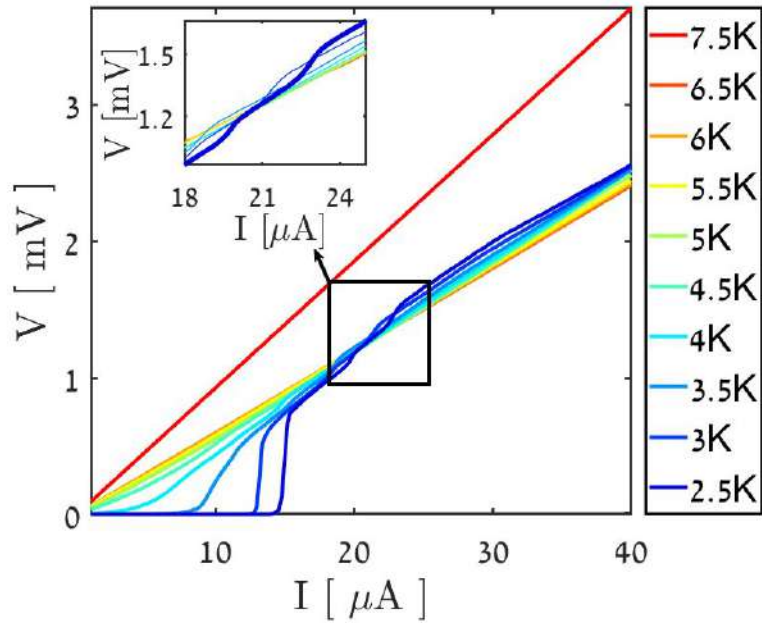
**Figure S-1.** *I-V* curves for the Nb ring in the temperature range 2.5 − 7.5 K. These curves are characterized by several voltage steps at different current values, clearly seen especially at low temperatures, see inset. These data provide a strong support to the view of the granular Nb ring as a chain of Josephson junctions with distributed critical currents. A voltage step occurs when the current reaches the value of the critical current of a single or a group of Josephson junctions in the chain.

Differential resistance as a function of the bias current.
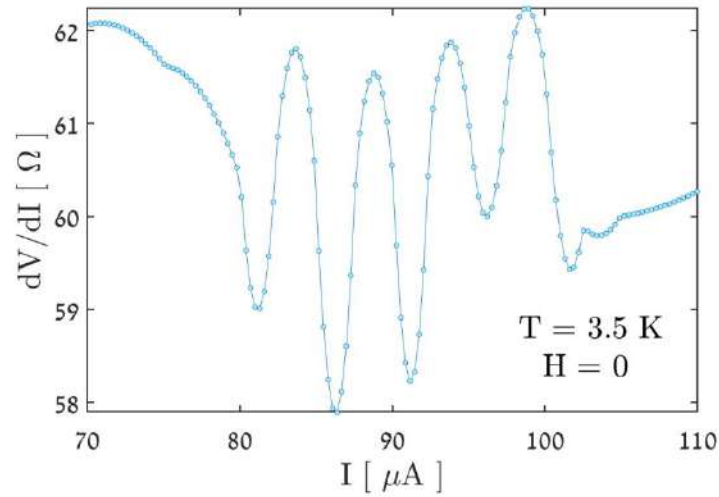
Figure S-2. Differential resistance as a function of the bias current at zero magnetic field. As noted by Webb *et al.* (PRB 37, 8455 (1988)), if the voltage developed across the sample is changed, the interference properties are also affected. This leads to voltage-dependent fluctuations in the conductance that are similar to effects seen when the vector potential is changed. Oscillations of the differential resistance as a function of the bias current are clearly observed in the Figure, in the same region for which the Aharonov-Bohm oscillations are observed.

Magnetoresistance at different bias current ranges.

(a)

(b)

(c)

(d)

(e)

(f)
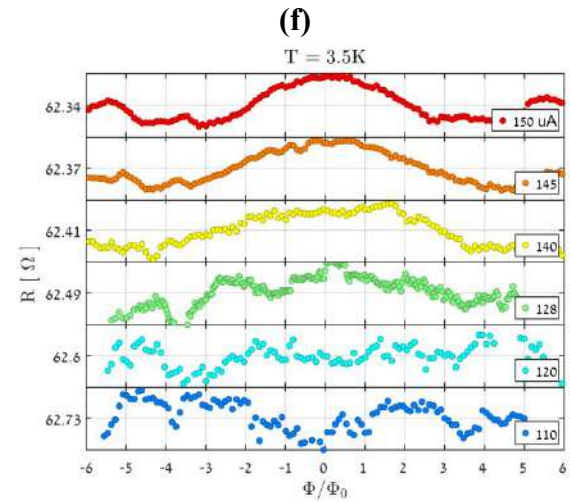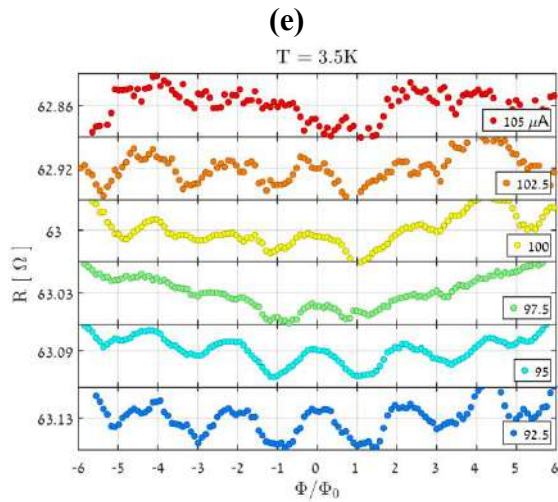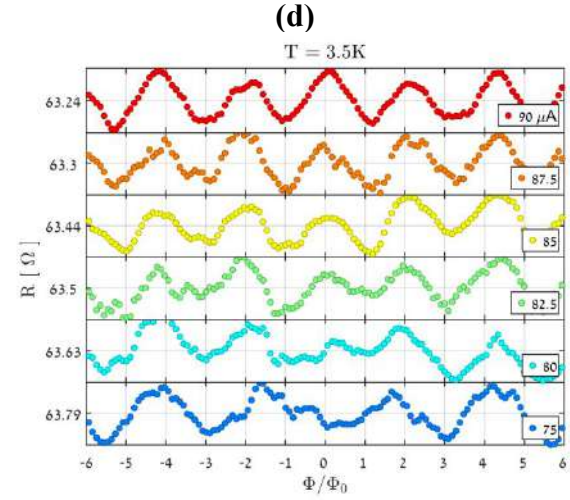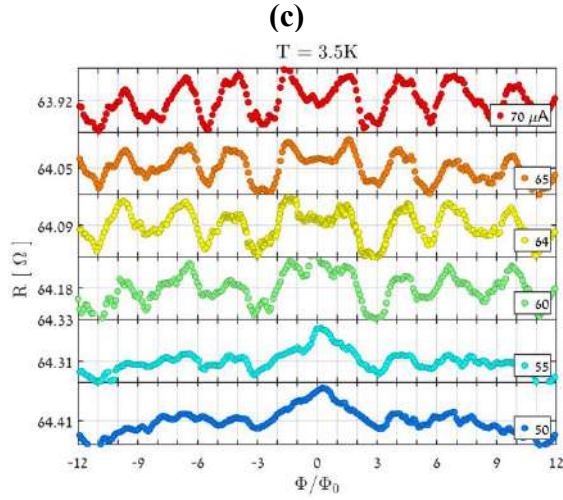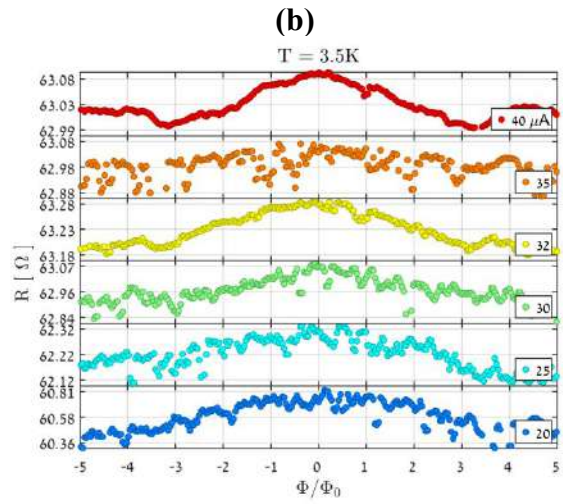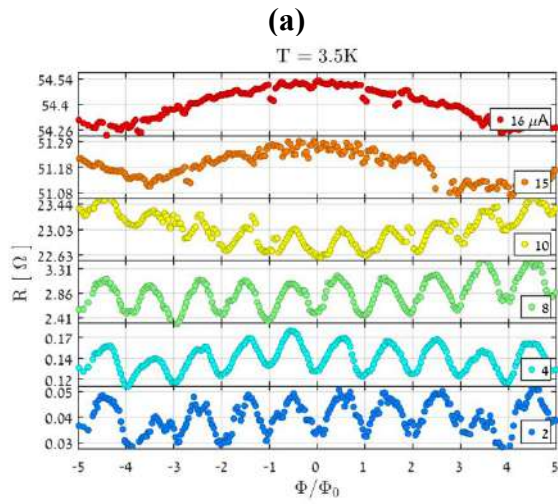
Figure S-3. Magnetoresistance oscillations in different current regimes.
a. Low current regime, showing *h/2e* magnetic flux periodicity (2-10 µA).
b. These oscillations disappear as the bias current increases beyond this range.
c. In the intermediate current regime (60-70 µA), unexplained oscillations with a period of ¬*3h/2e* appear.
d-e. In the high current regime (75-105 µA) magnetoresistance oscillations with period of *h/e* are observed.
f. In the very high current regime (120-150 µA), all oscillations are washed out.

4   Summary and Conclusions

Our study of fluxoid quantization in superconducting nano-loops and nano-networks revealed novel phenomena, mainly those associated with the effects of a bias current. These include current induced SQUID behavior in a superconducting ring without Josephson junctions and current-induced crossover of flux periodicity from *hc/2e* to *hc/e*. In addition, we analyzed the behavior of fluxoid occupation in 1- and 2-dimentional networks, revealing the nature of interaction between fluxoids.

We have demonstrated that a superconducting nano-ring with two arms can be switched into a SQUID by externally applied bias current. The SQUID behavior was demonstrated by the current induced transformation of the Little-Parks magnetoresistance oscillations from parabolic into sinusoidal oscillations and eventually into oscillations typical of a SQUID. The formation of a SQUID is attributed to the combined effects of current induced phase slips and non-uniform order parameter along the ring caused by the superconducting arms. We note that such superconducting structures comprising a ring with two arms are common in nano-fabrication in which the arms serve as leads to the ring. Such superconducting nano-structures may be utilized as field sensitive nano-devices without artificial Josephson junctions.

Our measurements in a current carrying granular Nb ring revealed two distinct coherent quantum effects. A Little-Parks effect, which manifests coherence of Cooper pairs, gives rise to a flux periodicity of *hc/2e* at low bias currents. Aharonov-Bohm effect resulting from phase coherence of quasi-particles gives rise to a flux periodicity of *hc/e* at very high bias current, but still below the depairing current. To the best of our knowledge, this is the first demonstration of the Aharonov-Bohm effect in a ring of Josephson junctions, resulting from phase coherence of quasi-particles tunneling between superconducting islands. The data indicate an enhancement of this effect as compared to the effect in metallic rings. This is attributed to the reduced density of quasi-particles in the superconducting islands which gives rise to a larger phase coherence length.

In a joint effort with Prof. Dr. Elke Scheer group from Konstanz we searched for the theoretically predicted *hc/e* periodicity in loops smaller than the superconducting

coherence length. In this study we focused on aluminum, a low-T_c superconductor with relatively large bulk coherence length (ξ_0=1.6 μm). Magnetoresistance measurements in an aluminum double network with large (small) loop side length of 1.71 μm (426 nm) have shown an indication for the predicted *hc/e* periodicity. Namely, the waveform of the first period was consisted with that predicted for loops with size smaller than the coherence length. Nevertheless, only one period of the oscillations could be observed because the relatively low critical field of aluminum, and the large period of small loops, impeded observation of more periods. Further improvements of the sample design and material quality are required to overcome this limitation.

In an effort to elucidate the nature of the interaction between fluxoids and the physics behind their arrangements in networks, we pursued a theoretical work analyzing 1D and 2D finite networks based on the 'current squared' model. An Ising-like expression was derived for the energy of a network revealing that fluxoids behave as repulsively interacting objects driven towards the network's center by the effective applied field. The competition between these two interactions determines the equilibrium configuration of fluxoids in the networks as a function of the applied field. We showed that distinctive repulsive interactions between fluxoids are obtained depending on the ratio l between the loop's length and the common width of adjacent loops. A 'short range' and a 'long range' interactions obtained for $l \geq 1$ and $l \ll 1$, respectively, give rise to remarkably different fluxoid configurations. We also demonstrated that the fluxoids configurations are not always commensurate to the network's symmetry. Incommensurate degenerated configurations may be formed even in networks with an odd number of loops. We demonstrated these concepts with calculated results of fluxoid arrangements in several examples of finite 1D and 2D networks.

In conclusion, our studies provided a deeper insight into the behavior of superconducting nano loops and networks, shedding light on the different mechanisms underlying the various flux periodicities and fluxoid configurations in these systems. Unlike previous studies, this thesis has focused on the influence of high bias current (close but still below the depairing current) on the behavior of nano multiply connected superconductors. Our studies expanded the knowledge in this field and exposed new

phenomena that were never observed before. These may lead to the development of new concepts in the growing research area aiming at exploiting superconductors in nano-circuits.

5 References

[1] F. London, On the Problem of the Molecular Theory of Superconductivity, Physical Review, 74 (1948) 562-573.

[2] V. Moshchalkov, H. Vloeberghs, M. Dhallé, G. Neuttiens, C. Van Haesendonck, Y. Bruynseraede, R. Jonckheere, Anomalous Little-Parks oscillations and field enhanced superconductivity in mesoscopic loops, Physica Scripta, 1992 (1992) 226.

[3] D. Davidović, S. Kumar, D.H. Reich, J. Siegel, S. Field, R. Tiberio, R. Hey, K. Ploog, Correlations and disorder in arrays of magnetically coupled superconducting rings, Physical review letters, 76 (1996) 815.

[4] X. Zhang, J.C. Price, Susceptibility of a mesoscopic superconducting ring, Physical Review B, 55 (1997) 3128.

[5] S. Pedersen, G. Kofod, J. Hollingbery, C. Sørensen, P. Lindelof, Dilation of the giant vortex state in a mesoscopic superconducting loop, Physical Review B, 64 (2001) 104522.

[6] D.Y. Vodolazov, F. Peeters, S. Dubonos, A. Geim, Multiple flux jumps and irreversible behavior of thin Al superconducting rings, Physical Review B, 67 (2003) 054506.

[7] A. Burlakov, V. Gurtovoĭ, S. Dubonos, A.V. Nikulov, V. Tulin, Little-parks effect in a system of asymmetric superconducting rings, JETP Letters, 86 (2007) 517-521.

[8] A. Kanda, B. Baelus, D. Vodolazov, J. Berger, R. Furugen, Y. Ootuka, F. Peeters, Evidence for a different type of vortex that mediates a continuous fluxoid-state transition in a mesoscopic superconducting ring, Physical Review B, 76 (2007) 094519.

[9] N.C. Koshnick, H. Bluhm, M.E. Huber, K.A. Moler, Fluctuation superconductivity in mesoscopic aluminum rings, Science, 318 (2007) 1440-1443.

[10] G. Berdiyorov, S. Yu, Z. Xiao, F. Peeters, J. Hua, A. Imre, W. Kwok, Effect of sample geometry on the phase boundary of a mesoscopic superconducting loop, Physical Review B, 80 (2009) 064511.

[11] J.A. Bert, N.C. Koshnick, H. Bluhm, K.A. Moler, Fluxoid fluctuations in mesoscopic superconducting rings, Physical Review B, 84 (2011) 134523.

[12] B. Pannetier, J. Chaussy, R. Rammal, J. Villegier, Experimental fine tuning of frustration: Two-dimensional superconducting network in a magnetic field, Physical review letters, 53 (1984) 1845.

[13] A. Behrooz, M. Burns, D. Levine, B. Whitehead, P. Chaikin, Superconducting phase boundary of aperiodic networks in a magnetic field, Physical Review B, 35 (1987) 8396.

[14] J.M. Gordon, A. Goldman, Magnetoresistance measurements on fractal wire networks, Physical Review B, 35 (1987) 4909.

[15] P. Chaikin, A. Behrooz, M. Itzler, C. Wilks, B. Whitehead, G. Grest, D. Levine, Studies of quasicrystalline superconducting networks, Physica B: Condensed Matter, 152 (1988) 113-124.

[16] M. Tinkham, D.W. Abraham, C. Lobb, Periodic flux dependence of the resistive transition in two-dimensional superconducting arrays, Physical Review B, 28 (1983) 6578.

[17] V.M. Vinokur, T.I. Baturina, M.V. Fistul, A.Y. Mironov, M.R. Baklanov, C. Strunk, Superinsulator and quantum synchronization, Nature, 452 (2008) 613.

[18] T.I. Baturina, V. Vinokur, A.Y. Mironov, N. Chtchelkatchev, D. Nasimov, A. Latyshev, Nanopattern-stimulated superconductor-insulator transition in thin TiN films, EPL (Europhysics Letters), 93 (2011) 47002.

[19] D.S. Hopkins, D. Pekker, P.M. Goldbart, A. Bezryadin, Quantum interference device made by DNA templating of superconducting nanowires, Science, 308 (2005) 1762-1765.

[20] D. Pekker, A. Bezryadin, D.S. Hopkins, P.M. Goldbart, Operation of a superconducting nanowire quantum interference device with mesoscopic leads, Physical Review B, 72 (2005) 104517.

[21] B. Pannetier, J. Chaussy, R. Rammal, Experimental determination of the (H, T) phase diagram of a superconducting network, Journal de Physique Lettres, 44 (1983) 853-858.

[22] J.M. Gordon, A.M. Goldman, J. Maps, D. Costello, R. Tiberio, B. Whitehead, Superconducting-normal phase boundary of a fractal network in a magnetic field, Physical review letters, 56 (1986) 2280.

[23] J.M. Gordon, A.M. Goldman, B. Whitehead, Dimensionality crossover in superconducting wire networks, Physical review letters, 59 (1987) 2311.

[24] F. Nori, Q. Niu, Tc (H) for quasicrystalline micronetworks: Analytical and numerical results, Physica B: Condensed Matter, 152 (1988) 105-112.

[25] C. Chi, P. Santhanam, P. Blöchl, Interacting loop-current model of superconducting networks, Journal of low temperature physics, 88 (1992) 163-195.

[26] V. Bruyndoncx, C. Strunk, V. Moshchalkov, C. Van Haesendonck, Y. Bruynseraede, Fluxoid quantization effects in superconducting mesoscopic Al multiloop structures, EPL (Europhysics Letters), 36 (1996) 449.

[27] D.H. Reich, D.M. Silevitch, C. Chien, D. Davidovic, S. Field, Disorder and correlations in extended superconducting nanostructures, Journal of Alloys and Compounds, 303 (2000) 245-251.

[28] I. Sochnikov, A. Shaulov, Y. Yeshurun, G. Logvenov, I. Božović, Large oscillations of the magnetoresistance in nanopatterned high-temperature superconducting films, Nature Nanotechnology, 5 (2010) 516-519.

[29] I. Sochnikov, A. Shaulov, Y. Yeshurun, G. Logvenov, I. Božović, Oscillatory magnetoresistance in nanopatterned superconducting La 1.84 Sr 0.16 CuO 4 films, Physical Review B, 82 (2010) 094513.

[30] I. Sochnikov, I. Božović, A. Shaulov, Y. Yeshurun, Uncorrelated behavior of fluxoids in superconducting double networks, Physical Review B, 84 (2011) 094530.

[31] G. Berdiyorov, M. Milošević, M. Latimer, Z. Xiao, W. Kwok, F. Peeters, Large magnetoresistance oscillations in mesoscopic superconductors due to current-excited moving vortices, Physical review letters, 109 (2012) 057004.

[32] M. Kato, O. Sato, Magnetic flux structures of finite superconducting networks, Superconductor Science and Technology, 26 (2013) 033001.

[33] M. Itzler, A. Behrooz, C. Wilks, R. Bojko, P. Chaikin, Commensurate states in disordered networks, Physical Review B, 42 (1990) 8319.

[34] C. Reichhardt, C.O. Reichhardt, A. Bishop, Commensurate and incommensurate checkerboard charge ordered states, Physica C: Superconductivity, 460 (2007) 1178-1179.

[35] W. Little, R. Parks, Observation of quantum periodicity in the transition temperature of a superconducting cylinder, Physical Review Letters, 9 (1962) 9.

[36] R. Parks, W. Little, Fluxoid quantization in a multiply-connected superconductor, Physical Review, 133 (1964) A97.

[37] F. Carillo, G. Papari, D. Stornaiuolo, D. Born, D. Montemurro, P. Pingue, F. Beltram, F. Tafuri, Little-Parks effect in single nanoscale YBa 2 Cu 3 O 6+ x rings, Physical Review B, 81 (2010) 054505.

[38] P. Gammel, P. Polakos, C. Rice, L. Harriott, D. Bishop, Little-Parks oscillations of T c in patterned microstructures of the oxide superconductor YBa 2 Cu 3 O 7: Experimental limits on fractional-statistics-particle theories, Physical Review B, 41 (1990) 2593.

[39] P.-G. de Gennes, Suspensions colloïdales dans un mélange binaire critique, C. R. Acad. Sci. B, 292 (1981 and C. R. Acad. Sci. Ser. B 292, 9 (1981)) 279.

[40] S. Alexander, Superconductivity of networks. A percolation approach to the effects of disorder, Physical Review B, 27 (1983) 1541.

[41] H. Fink, V. Grünfeld, A. López, Quantum-interference device without Josephson junctions, Physical Review B, 35 (1987) 35.

[42] Y.S. Barash, Low-energy subgap states and the magnetic flux periodicity in d-wave superconducting rings, Physical review letters, 100 (2008) 177003.

[43] V. Juričić, I.F. Herbut, Z. Tešanović, Restoration of the Magnetic h c/e-Periodicity in Unconventional Superconductors, Physical review letters, 100 (2008) 187006.

[44] F. Loder, A. Kampf, T. Kopp, J. Mannhart, C. Schneider, Y.S. Barash, Magnetic flux periodicity of h/e in superconducting loops, Nature Physics, 4 (2008) 112.

[45] V. Vakaryuk, Universal Mechanism for Breaking the h c/2 e Periodicity of Flux-Induced Oscillations in Small Superconducting Rings, Physical review letters, 101 (2008) 167002.

[46] T.-C. Wei, P.M. Goldbart, Emergence of h/e-period oscillations in the critical temperature of small superconducting rings threaded by magnetic flux, Physical Review B, 77 (2008) 224512.

[47] J.-X. Zhu, H. Quan, Magnetic flux periodicity in a hollow d-wave superconducting cylinder, Physical Review B, 81 (2010) 054521.

[48] F. Tafuri, J. Kirtley, D. Born, D. Stornaiuolo, P. Medaglia, P. Orgiani, G. Balestrino, V. Kogan, Dissipation in ultra-thin current-carrying superconducting bridges; evidence for quantum tunneling of Pearl vortices, EPL (Europhysics Letters), 73 (2006) 948.

[49] S. Washburn, R.A. Webb, Aharonov-Bohm effect in normal metal quantum coherence and transport, Advances in Physics, 35 (1986) 375-422.

[50] Y. Aharonov, D. Bohm, Significance of electromagnetic potentials in the quantum theory, Physical Review, 115 (1959) 485.

[51] A. Huibers, M. Switkes, C. Marcus, K. Campman, A. Gossard, Dephasing in open quantum dots, Physical review letters, 81 (1998) 200.

[52] Y. Imry, Introduction to mesoscopic physics, Oxford University Press on Demand, 2002.

[53] T. Chakraborty, A. Manaselyan, M. Barseghyan, Irregular Aharonov–Bohm effect for interacting electrons in a ZnO quantum ring, Journal of Physics: Condensed Matter, 29 (2016) 075605.

[54] S. Cho, B. Dellabetta, R. Zhong, J. Schneeloch, T. Liu, G. Gu, M.J. Gilbert, N. Mason, Aharonov–Bohm oscillations in a quasi-ballistic three-dimensional topological insulator nanowire, Nature communications, 6 (2015) 7634.

[55] A. Fuhrer, S. Lüscher, T. Ihn, T. Heinzel, K. Ensslin, W. Wegscheider, M. Bichler, Energy spectra of quantum rings, Nature, 413 (2001) 822.

[56] S.S. Hong, Y. Zhang, J.J. Cha, X.-L. Qi, Y. Cui, One-dimensional helical transport in topological insulator nanowire interferometers, Nano letters, 14 (2014) 2815-2821.

[57] A. Lorke, R.J. Luyken, A.O. Govorov, J.P. Kotthaus, J. Garcia, P.M. Petroff, Spectroscopy of nanoscopic semiconductor rings, Physical review letters, 84 (2000) 2223.

[58] D. Sangalli, A. Marini, Anomalous Aharonov–Bohm gap oscillations in carbon nanotubes, Nano letters, 11 (2011) 4052-4057.

[59] L. Wang, I. Gutiérrez-Lezama, C. Barreteau, N. Ubrig, E. Giannini, A.F. Morpurgo, Tuning magnetotransport in a compensated semimetal at the atomic scale, Nature communications, 6 (2015) 8892.

[60] Y. Yao, M. Elborg, T. Kuroda, K. Sakoda, Excitonic Aharonov–Bohm effect in QD-on-ring nanostructures, Journal of Physics: Condensed Matter, 29 (2017) 385301.
[61] W. Teh, J. Luo, C.-T. Liang, C. Smith, Crosslinked PMMA as a Low-Dimensional Dielectric Sacrificial Layer for MEMS/NEMS and Quantum Nanostructures Fabrication, in: MEMS/NEMS, Springer, 2006, pp. 504-552.

תקציר

ההבנה של תופעת מוליכות-העל בקנה מידה ננוסקופי חשובה הן מן הבחינה הבסיסית והן מן הבחינה היישומית. המחקר הבסיסי תורם להבנה של תופעות המתרחשות רק בעולם הננו והחשיבות המעשית נובעת מהפוטנציאל של מבנים ננומטרים מוליכי-על לשימוש בהתקנים חדשניים. עבודה זו מתמקדת בחקר ההתנהגות הקוונטית של טבעות ורשתות מוליכות-על בסקאלה ננומטרית. היא מורכבת מארבעה נושאי מחקר עיקריים: (א) עבודה ניסיונית בה חקרנו את התלות בזרם של המגנטו-התנגדות במערך טורי של ננו-טבעות עשויות ניוביום, (ב) עבודה ניסיונית בה ביצענו מדידות מגנטו-התנגדות בטבעות מוליכות-על בודדות העשויות ניוביום וגילינו תנודות מחזורית במגנטו-התנגדות, גם בזרמים גבוהים הקרובים לזרם ששובר את זוגות הקופר (depairing current), (ג) מצאנו אינדיקציות ניסיוניות לתחזית תיאורטית שצופה מחזוריות hc/e של השטף המגנטי ברשתות אלומיניום מוליכות-על, כאשר הטבעות הקטנות ברשתות אלו הן בקנה מידה ננו-מטרי – עבודה זו נעשתה בשיתוף פעולה עם קבוצתה של פרופ' שיר מאוניברסיטת קונסטאנץ בגרמניה, (ד) עבודה תיאורטית של סידור פלאקסואידים ברשתות סופיות העשויות ממוליכות-על. עבודות אלו חשפו תופעות חדשות ותובנות הקשורות להתנהגות ננו-טבעות ורשתות מוליכות על.

עבודת המחקר הראשונה מדגימה התנהגות של סקוויד (SQUID) שנשלטת ע"י הזרם בננו-טבעות ניוביום מוליכות-על ללא צמתי ג'וספסון. מדידות מגנטו-התנגדות בטבעות אלו הראו שכאשר אנו מגבירים את זרם המדידה, ההתנהגות הפרבולית המחזורית של המגנטו-התנגדות המתאימה לאפקט Little-Parks הופכת סינוסיאודלית, ובזרמים גבוהים יותר הופכת להיות בעלת התנהגות האופיינית לסקוויד. אנו משייכים את התופעה הזאת לכך שבחשיפה לשדה מגנטי, פרמטר הסדר בטבעת הופך להיות לא אחיד לאורך היקפה של הטבעת. הדבר נובע מחיבור חוטים מוליכי-על לצורך הולכת זרם המדידה לטבעת. זרם המדידה מגביר את הקצב של תופעת החלקת-הפאזה (phase-slip) בנקודות בהן פרמטר הסדר הוא הנמוך ביותר וכך יוצר בצורה אפקטיבית צמתי ג'וספסון בנקודות אלו והופך את הטבעת לסקוויד.

בעבודת המחקר השנייה מדדנו טבעת בודדת העשויה ניוביום גרגרי (granular) בטווח רחב של זרמים. מדידותינו חשפו מעבר תלוי-זרם בין שתי תופעות קוונטיות הקשורות לקוהרנטיות של פונקצית הגל אך שונות לחלוטין זו מזו. גם כאן, בזרמים נמוכים הקוהרנטיות של זוגות קופר מושפעת מאפקט -Little Parks ומדדנו מחזוריות של $hc/2e$ במדידות המגנטו-התנגדות של הטבעת. בזרמים גבוהים מאד, אם כי עדיין נמוכים יותר מהזרם בו נשברים זוגות הקופר, ראינו מחזוריות של hc/e במדידות המגנטו-התנגדות. אנחנו מפרשים מחזוריות זו כנובעת מאפקט-אהרונוב בוהם שמתגלה בקוהרנטיות של הפאזה של קווזי-חלקיקים בודדים. אנחנו רואים את הטבעת כשרשרת של גרגרים מוליכי-על שמקושרים בצורה חלשה אחד לשני ע"י צמתי מנהור בין הגרגרים. הגדלת הזרם מעל לזרם הקריטי של כל הצמתים יוצר ערוץ הולכה של קווזי-חלקיקים לאורך ענפי הטבעת כך שמתאפשרת התאבכות קוונטית של הקווזי חלקיקים.

המחזוריות של *hc/2e* בשטף המגנטי הנמדד במגנטו-התנגדות של טבעות מוליכות-על נחשבת לחותמת של זיווג האלקטרונים לזוגות במוליכי-על וכהוכחה הניצחת לקיומם של זוגות קופר. עם זאת, עבודות תיאורטיות מהשנים האחרונות הראו שבטבעות מוליכות-על הקטנות מאורך הקוהרנטיות צפויה מחזוריות של *hc/e* בשטף-המגנטי. בניסיון לאשש את התחזית הזאת בצורה ניסיונית, הכנו רשתות המורכבות ממנו-טבעות אלומיניום ומדדנו את המגנטו-התנגדות של טבעות אלה. הבחירה של אלומיניום בתור מוליך-העל הייתה מבוססת על אורך הקוהרנטיות הגדול שלו. במחקר השלישי הזה אותו אנו מציגים, העבודה נעשתה בשיתוף פעולה הדוק עם פרופ' ד"ר אלקה שיר מאוניברסיטת קונסטאנץ בגרמניה. במסגרת שיתוף הפעולה הכנו את הטבעות והשתתפנו במדידות ובפרשנותן. אינדיקציה למעבר למחזוריות של *hc/e* נראתה בצורת הגל של מדידות המגנטו-התנגדות באחד הדגמים, בו ראינו את המחזור הראשון דומה מאוד לתחזית התיאורטית. אולם, לא יכולנו למדוד יותר ממחזור אחד בגלל השדה הקריטי הנמוך יחסית של אלומיניום.

אפקטים של קוויינטוט הפלאקסואיד (Fluxoid Quantization) נחקרו בעבר באופן נרחב, גם בצורה תיאורטית וגם ניסיונית במגוון רשתות מוליכות-על. עם זאת, רוב העבודות האלו שמו דגש על המעבר בין מצב מוליך-על למצב נורמלי ולא התחשבו בסידור הפלאקסואידים ברשת כפונקציה של השדה המגנטי. המספר המצומצם של עבודות שכן התחשבו בסידור הפלאקסואידים הציגו תוצאות ניסיוניות או חישובים של הסידור בסוגי רשתות שונים, אך לא הביאו שום הבנה אינטואיטיבית של הפיזיקה מאחורי הסידור. בעבודת המחקר הרביעית שלנו, אנחנו מנתחים בצורה תיאורטית את סידור הפלאקסואידים ברשתות סופיות העשויות מוליכי-על בעזרת המודל המקשר בין זרמי הפלאקסואיד לאנרגיה של המערכת (J^2 model). הניתוח שלנו הניב ביטוי דמוי מודל Ising לאנרגיה הכללית של המערכת כפונקציה של מספר הפלאקסואידים ומיקומם ברשת והשדה המגנטי שהרשת נמצאת בו. ביטוי זה סיפק הסבר אינטואיטיבי של המנגנון השולט על סידור הפלאקסואידים ברשתות סופיות. הדבר המיוחד שגילינו הוא שאפשר להתייחס לפלקסואידים כאובייקטים הנדחים אחד מהשני ואשר נדחפים למרכז הרשת ע"י השדה המגנטי. בהתבסס על הניתוח הזה המחושבנו, בעזרת גראפים ואיורים ועל"י סימולציות, סידורים שונים של פלאקסואידים בסוגים שונים של רשתות.

המחקרים שלנו שופכים אור על המנגנונים השונים העומדים בבסיסם של מחזורי השטף השונים ובסידור הפלקסואידים בננו-לולאות וברשתות מוליכות-על. הבנת הפיזיקה שמאחורי תופעות אלו עשויה להוביל לפיתוח מושגים חדשים בתחום המחקר ההולך וגדל שמטרתו ניצול מוליכי-על לייצור מעגלים חשמליים ננו-מטריים.

תוכן עניינים

עבודה זו נעשתה בהדרכתם של

פרופ' יוסף ישורון ופרופ' אבנר שאולוב

מן המחלקה לפיזיקה של בר-אילן.

אפקטים קוונטיים
בטבעות וברשתות ננומטריות מוליכות-על

חיבור לשם קבלת התואר "דוקטור לפילוסיפיה"

מאת

עמרי י. שרון

המחלקה לפיזיקה

הוגש לסנט של אוניברסיטת בר-אילן

רמת גן   תשרי, תשע"ט